Republic of Iraq
Ministry of Higher Education and Scientific Research
University of Misan/Collage of Engineering
Department of Civil Engineering

Numerical Analysis for Shear Strength of Ultra High Performance Concrete Tapered Beams

By

Aqeel Abdul Ridha Jbarah

B.Sc. civil engineering, 2019

A THESIS

Submitted in Partial Fulfillment of the
Requirements for the Degree of
Master of Science/Master of Structural Engineering
(in Civil Engineering)

Advisor Name: Assist. Prof. Dr. Nasser Hakeem Tu'ma

بِسْمِ اللَّهِ الرَّحْمَنِ الرَّحِيمِ

”يَرْفَعِ اللَّهُ الَّذِينَ آمَنُوا مِنْكُمْ وَالَّذِينَ أُوتُوا الْعِلْمَ دَرَجَاتٍ وَاللَّهُ بِمَا تَعْمَلُونَ خَبِيرٌ“

سورة المجادلة آية 11

صَدَق اللّه الْعَلِيُّ الْعَظِيْم

Numerical Analysis for Shear Strength of Ultra High Performance Concrete Tapered Beams

By Aqeel Abdul Ridha Jbarah

Thesis Advisor: Assist. Prof. Dr. Nasser Hakeem Tu'ma

An Abstract of the Thesis Presented

in Partial Fulfillment of the Requirements for the

Degree of Master of Science/Master of Structural Engineering

(in Civil Engineering)

August/ 2023

ABSTRACT

Non-prismatic reinforced concrete beam of is an optimal beam and has special importance. The tapered configuration is a specific mechanism could be utilized in structural engineering to get optimum material investment. This study is introduced to verify the structural confidence of the recently developed tapered beam of new trends in plane tapered using a numerical analysis by "ABAQUS program" which included a wide spectrum of variables that relate to various structural aspects.

The current study investigates of tapered beams of Ultra-High Performance Concrete (UHPC) with using steel fiber 2% by volume. These non-prismatic beams introduced a new approach of the production of UHPC to be used as an alternative to traditional concrete. Tensile of concrete plays an important role in improving different resistance, especially the shear strength. Many factors that effect on the UHPC behavior due to the presence of steel fibers and their different failure patterns, as well as the distribution mechanism within the concrete matrix.

The comparison of numerical results with the available experimental results, in range of ultimate shear strength, load-displacement relationships; showed a good agreement. Proposed rates ranged from 0.96 to 1.07. Besides, parametric study is concerned with many structural parameters such that crown length, scale factor, steel reinforcement ratio (longitudinal and transversal), shear span to effect depth, longitudinal openings (location and size), boundary condition. Results obtained from numerical

modeling indicated a significant reduction in weight of beam with longitudinal openings along the span. Six different ratios of shear span to effective depth ratio (a/d) have been studied, with numerical prediction that increasing the (a/d) reduces shear strength. For the boundary conditions, the simply supported shows a very close shear strength estimation is obtained in the case of fixed conditions. It noted that the increase in the longitudinal reinforcement ratio from longitudinal reinforcement ratio 2.73 to 3.01 results in a 14% increase in ultimate shear strength. This may be due to the increase of the dowel action component and therefore increased shear strength. When increased the transverse reinforcement ratio, more cracks occurred with a smaller openings width was noticed. There is a significant effect on the mid-span deflection as the increase was observed by 79% and 148% on taking over compared to the model TR845. There was change in pattern of failure mode from shear failure mode to flexural-shear failure mode. The models were designed to shear strength failure so the models were designed without stirrups. When the scale factor 2.4 was increased, an increase in shear strength was observed at 348%. While, the increasing of crown's length from 0 to 200 mm led to an increase in shear strength by 10%.

SUPERVISOR CERTIFICATION

I certify that the preparation of this thesis entitled "Numerical Analysis for Shear Strength of Ultra High Performance Concrete Tapered Beams" was presented by "**Aqeel Abdul Ridha Jbarah**", and prepared under my supervision at The University of Misan, Department of Civil Engineering, College of Engineering, as a partial fulfillment of the requirements for the degree of Master of Science in Civil Engineering (Structural Engineering).

Signature:

Assist. Prof. Dr. Nasser Hakeem Tu’ma

Date: 28/12/2023

In view of the available recommendations, I forward this thesis for discussion by the examining committee.

Signature:

Assist. Prof. Dr. Murtada Abass A. Alrubaie

(Head of Civil Eng. Department)

Date: 28/12/2023

ACKNOWLEDGEMENTS

In the name of Allah.

All my thanks for Allah who led me during my way to complete this work.

I would like to express my cordial thanks and deepest gratitude to my supervisor **Assist. Prof. Dr. Nasser Hakeem Tu'ma** whom I had the honor of being under his supervision, for his advice, help, and encouragement during the course of this study.

I would like to extend my thanks to **Prof. Dr. Abbas Oda Dawood** Dean of the college of engineering, **Assist. Prof. Dr. Murtada Abass Alrubaie** Head of civil engineering department, **Assist. Prof. Dr. Fatin I. Mussa** and to all my Teachers in my college.

EXAMINING COMMITTTEE'S REPORT

We certify that we, the examining committee, have read the thesis titled **(Numerical Analysis for Shear Strength of Ultra High Performance Concrete Tapered Beams)** which is being submitted by (**Aqeel Abdul Ridha Jbarah**), and examined the student in its content and in what is concerned with it, and that in our opinion, it meets the standard of a thesis for the degree of Master of Science in Civil Engineering (Structures).

Signature:

Assist. Prof. Dr. Nasser Hakeem Tu'ma

(Supervisor)

Date: 28/12/2023

Signature: Signature:

Name: Prof. Dr. Sa'ad Fahad Resan Prof. Dr. Samoel Mahdi Saleh

(Chairman) (Member)

Date: 28/12/2023 Date: 28/12/2023

Signature:

Name: Name: Assist. Prof. Dr. Murtada Abass Alrubaie

(Member)

Date: 28/12/2023

Approval of the College of Engineering:

Signature:

Prof. Dr. Abbas Oda Dawood

Dean, College of Engineering

Date: 28/12/2023

DEDICATION

I dedicate this work to whom stood beside me and took care of me over the years, to my

Parents,

sisters,

Brother,

and close friend

To all those who supported and helped me, made the difficult easy, present my effort to them with all of my respect and appreciation.

TABLE OF CONTENTS

LIST OF TABLES

LIST OF FIGURES

LIST OF SYMBOLES

Symbol	Description	Unit
σ^{ah}	Ambient hydrostatic stress state	MPa
P and V	Any applied force on the structure	kN
fc´	Compressive strength of concrete cylinder	MPa
f_t	Concrete strength in tension	MPa
f'c	Concrete ultimate uniaxial compressive strength	MPa
[*D*]	Constitutive matrix	
f_{cr}, ε_{cr}	Cracking stress and strain	MPa
[*L*]	Differential operator matrix	
u,v,w	Displacement components in x,y and z coordinates	mm
{*U*}	Displacement vector	
D.I	Ductility index	None
Me	Elastic moment strength	MPa
$[K]_e$	Element stiffness matrix	
ψ	Energy dissipation	None
W_{ext}, W_{int}	External and internal work	kN
I_1	First stress invariant	MPa
F	Function of principal state $(\sigma_{xp}, \sigma_{yp}, \sigma_{zp})$	MPa
x,y,z	Global coordinate	None
α	Haunch angle with horizontal line	Degree
σh	Hydrostatic stress	MPa
[*J*]	Jacobian matrix	

$\{f\}$	Load vector	
ζ , η	Local coordinates	None
$[N]$	Matrix of shape functions	
L_f	Middle uniform region	mm
E	Modulus of elasticity	MPa
Ec	Modulus of elasticity of concrete	MPa
Es	Modulus of elasticity of reinforcing bars	MPa
f_r	Modulus of rupture of concrete	MPa
{a}	Nodal displacement vector	
ε	Normal strain	mm/mm
(σ)	Normal stress	MPa
B_t , β_c	Opened and closed shear transfer coefficient	None
$[K]$	Overall stiffness matrix	
ν	Poisson's ratio	
σxp	Principal stress in the x – direction.	MPa
σyp	Principal stress in the y – direction.	MPa
σzp	Principal stress in the z – direction.	MPa
J_2	Second deviatoric stress invariant	MPa
γ	Shear strain	mm/mm
τ	Shear stress	MPa
β	Shear transfer coefficient	None
L	Span length of the beam	mm
f_u	Steel ultimate tensile strength	MPa
ε_o	Strain at ultimate compressive stress $f'c$	mm/mm

$\{\varepsilon\}$	Strain vector	
$[B]$	Strain-displacement matrix	
Rs	Strength rating	None
$\{\sigma\}$	Stress vector	
$[T]$	Transformation matrix	
$[A]^{T}$	Transpose of matrix [A]	
fcb	Ultimate biaxial compressive strength	MPa
f_1	Ultimate compressive strength for a state of biaxial compression superimposed on hydrostatic stress state	MPa
f_2	Ultimate compressive strength for a state of uniaxial compression superimposed on hydrostatic stress state	MPa
P_u	Ultimate load	kN
Mu	Ultimate moment strength	MPa
ε_u	Ultimate strain	mm/mm
f_t	Ultimate uniaxial tensile strength of concrete	MPa
F^a	Vector of applied loads	
fy	Yielding stress of steel reinforcement	MPa

LIST OF ABBREVIATIONS

AASHTO	American Association of State Highway and Transportation Officials.
ACI	American Concrete Institute
CFRP	Carbon Fiber Reinforced Polymer
EC2	Euro Code2
FE	Finite Element
FEA	Finite Element Analysis
FRP	Fiber-Reinforced polymer
FRPRC	Fiber-Reinforced polymer Reinforced Concrete
GFRP	Glass Fiber Reinforced Polymer
HPC	High Performance Concrete
HPFRCC	High Performance Fiber Reinforced Cement Composite.
HRWRA	High-Range Water Reducers Admixture.
HSC	High Strength Concrete.
JSCE	Japan Society of Civil Engineers.
N. A	Neutral Axis
PVC	Poly vinyl Chloride.
RC	Reinforced Concrete
RCC	Reinforced Cement Concrete
RPC	Reactive Powder Concrete
RTS	Residual Tensile Stress
SCC	Self-Compacting Concrete
SF	Silica Fume.
UHPC	Ultra-high-performance concrete

CHAPTER ONE: INTRODUCTION

1.1 General

Tapered beam is a type of a non-prismatic beam that has varying depth and/or width along span. This type of geometry widely utilized in the continuous and simply supported bridges, portal frames, cantilevers and buildings with midrise framed. Such beams could reduce structures weight and contribution in the appearance from aesthetic viewpoint.

1.2 Reinforcement Concrete Beam of Non-prismatic Sections

Engineers design the structures in such a way that structural systems execute their jobs satisfactorily while also being cost effective. This aids in the selection of the appropriate type of sections that are both economical and safe for construction. Beams are a common for carrying and transferring loads. A meticulous approach to design may result in good serviceability and cost optimization of the structure. Prismatic beams are often utilized for medium span and bending forces. Furthermore, with the increased depth there is considerable decrease in headroom. As a result, in such cases, non-prismatic beams are an appealing choice [1].

The non-prismatic reinforced concrete (RC) beam is a unique case in structural engineering because it has variable depth throughout the beam section and lacks sufficient information in structural codes. This can put structural engineers in a challenge to predict how this beam will react under specific types of loads or with different geometrical variables and strengthening existence [2].

Non-prismatic beams can be classified based on the variation of depth [3]:

1. Tapered beams or Hunched beams: beams that have a linear variation in cross-section along their length. Hunched beams have greater depth near the support,

sufficient to resist the applied shear forces, and less depth at the center, sufficient to resist the applied bending moment. Tapered beams have the depth in the center with increase if the load applied is large or the amount of reinforcement used is insufficient and lake in shear at support.

2. Curved beams: beams with a parabolic or curvilinear cross-section that varies along the length. This change could occur in either the horizontal or the vertical plane. These beams have the structural advantage of being able to carry torsional moments as well as others capacities.

1.2.1 Advantage and Disadvantage of Reinforcement Concrete Beam of Non-prismatic Section

The Reinforced concrete beam of the tapered section provides the following advantages compared with prismatic beams[4] **:**

1. Reducing construction weight for a given lateral stiffness.
2. More efficient use of concrete and steel reinforcement.
3. Eased placement of various facilities or equipment types (electrical, sewage, air conditioning etc.)
4. Aesthetic reason.

Despite the wide spread now days of this type of beams and some advantages that engineers can obtain, there are some difficulties that occur in the modeling of non-prismatic beams, which can lead to inaccurate predictions and thus performing optimization operation. On the other hand, the higher construction costs, such as a high-quality worker in construction and special molds, caused unfavorable in a common structural solution in building[5]. Also, there are some code available such as ACI318-14 [6] and BS-5400-1 [7] not covering this type of beams. the designers in this field must rely on some experience and provision [5].

1.2.2 Applications of Reinforcement Concrete Beam of Non-prismatic Section

Non- prismatic beams are an important issue in structural engineering, not only for their versatile application in engineering structures, because of their unique ability to simulate different types of material or geometrical variations [8]. Also, can be utilized to form the members according to the internal stress distribution. These sorts of members can provide the required strength and use the minimum weight and material, as well as satisfy architectural or functional requirements. Non-prismatic members with constant, linear, and parabolic depth or width variations are commonly used in industrial structures, bridges, and high-rise buildings [9]. Non-prismatic beams are also used in simply supported or continuous bridges worldwide and buildings as shown in Figure 1-1and Figure 1-2 [4].

Figure 1.1 Typical non-prismatic member in building and bridge [4].

Figure 1.2 RC buildings with hunched beams recently constructed in Mexico City[4] .

1.2.3 Structural Behavior Reinforcement Concrete Beam of Non-prismatic Section

The general behavior of non-prismatic members is different from that of prismatic members to these cases [10 , 11] following.

1. In a tapered beam, the main internal tension or compression is inclined, providing a vertical component that may be capable of resisting shear.
2. The varying in cross section towards the supports is unlikely.
3. The discontinuity of the centroid axis in tapered beam causes a strong coupling between bending moment, shear and axial forces.

The cracking of these beams begins with small flexural cracks. With increased load then flexural cracks transform into flexural shear cracks, with more shear cracks developing. Flexural-shear cracks increase in length and size until they reach the e soffit of the flange. By increasing the load, shear stress failure occurs for beams with large hunch, while instability failure occurs for beams with a small hunch.

The change in angle of non-prismatic inclination affects the behavior at failure, thus bringing about two distinct types;

a) Beam of small depth in Support, failure of this type of beams occurs due to the instability of the failure as a result a large crack has occurred above the line

connecting the loading point with support which leads to the creation of a weak arch in the top and the beam failure.

Figure 1.3 Flexural Failure in Beam

b) Beam with large depth in support, failure of this type of beam occurs due to shear compression as a result a large crack occurred below the line connecting the loading point with support which leads to the creation of a stronger arch in the top. A greater shear load is transferred from the arch to support and this results in more resistance to rotation about the load point, until it occur crushed in concrete [12].

1.3 Ultra-High-Performance Concrete UHPC

1.3.1 Evaluation of Concrete Technology.

In recent years, the process of concrete development become an important role in civil engineering to produce several new types of concrete mixtures. Because the engineers are now using higher compressive strength that limit their designs, produce a new concrete type that differ from ordinary concrete. Several experiments have been conducted to reduce the water content to a minimum and to add new

plasticizers to increase the workability of the mixture without adding extra water. Other experiments had been performed to increase compressive strength by substituting a percentage of the cement used with pozzolanic materials such as silica fume. In addition to the use of these additives materials, the methods of curing the concrete after casting have been changed by developing new methods of treatment, including heat treatment used in Ultra-High-Performance Concrete mixture (UHPC) and pressure treatment by pre-setting the concrete mix.

1.3.2 Components of Ultra High-Performance Concrete Mix UHPC

1. Contains a high-volume ratio of the cement material.
2. Contains a high-volume ratio of fine sand with a maximum diameter of the granule sand does not exceed 600 μm.
3. It contains pozzolanic materials such as silica fume and it used as a replacement ratio of cement weight.
4. Contains steel fibers with high tensile strength and a good aspect ratio (length of fiber/diameter of fiber).
5. Contains a very low water content of cement material.
6. Contain a proportion of the plasticizer to compensate for the very small amount of water ratio.

1.3.3 Applications of UHPC

Nowadays, the UHPC mixture has become widely used in buildings and concrete bridges, especially in applications that require precast elements. This mixture was used in Canada, Europe, Asia and various countries of the world. due to the superior characteristics of this mixture.

- The Sherbrook Pedestrian Bridge in Canada was the first bridge in the world which was designed with UHPC, completed in 1997, The bridge is of post-

tension open space truss design and 60m in length. Using UHPC in the bridge allowed the top deck to be only 30 mm in thickness [13 , 14].

Figure 1.4 Sherbrook Pedestrian Bridge, in Canada.

- The Footbridge of Peace in Seoul, South Korea was the first bridge in the world where UHPFC was used as a full replacement for normal concrete. The bridge, which was completed in 2002, is 120m long and has arch height of about 15m with 30 to 100mm deck depth Figure 1.5 [15].

Figure 1.5 Seoul Footbridge in South Korea.

1.4 Methods of Concrete Damage Plasticity Simulation

The numerical simulation of crack propagation and the analysis of crack growth in reinforced concrete members is still an unsolved problem. The development of reliable analytical models can reduce the number of required test specimens for the solution of a given problem, recognizing that tests are time-consuming and costly and often do not simulate exactly the loading and support conditions of the actual structure [16]. Full-scale simulations of structural systems which cannot be produced and tested in a laboratory environment can result in a better understanding of the failure and cracking behavior of these systems. Many computer software packages are available for these simulations. The commercially available ABAQUS software has dedicated concrete material models that are quite effective in realistic simulations. Recent advancements in computational simulations have paved the possibility for carrying out the design and analysis of concrete structures in a more realistic manner. Non-linearity in concrete due to its complex composition has been given thought in this constitutive modeling to faithfully capture the response of concrete. The concrete damaged plasticity CDP model is a modified form of the Drucker-Prager criterion [17]. The model takes into account the isotropic compressive and tensile plasticity of concrete to represent its inelastic behavior in association with its isotropic damaged elasticity. This model is a continuum, plasticity-based, damage model for concrete, that provides a general capability for modeling concrete and other quasi-brittle materials in all types of structures (beams, trusses, shells, and solids) and uses concepts of isotropic damaged elasticity in combination with isotropic tensile and compressive plasticity to represent the inelastic behavior of concrete [18]. Fracture is one of the main failure modes for engineering materials.

However, most of the time design codes apply large safety factors to avoid its appearance. Additionally, to the devastating consequence of a brittle failure, their

evolution is difficult to study in practice. Therefore, predicting the initiation and the propagation path of a fracture is of great importance for practicing engineers and scientists. Several techniques are based on Griffith's linear elastic brittle fracture, which is modeled using the energy release rate. Essentially, once the energy release rate hits a critical value, the crack can grow or propagate further [19]. The theory of failure has become important now a days as it has entered into design analysis and experimental research. Modeling fracture has been studied in several ways to simulate the initiation and propagation of cracks, like the finite element method (FEM) and other different methods. These methods have their advantages and drawbacks in handling certain parts of the simulation. In the conventional finite element method, the "physical model" is divided into small pieces called "elements" and connected by specific points called "nodes". This process is called "mesh". These elements may include internal defects such as cracks, voids, interfaces, etc. Many difficulties have been in the meshing process. On one hand, the element boundary must coincide with the geometric edge of the defects, which will induce some distortion in the element; on the other hand, the mesh size shall depend on the geometric size of these small defects, resulting in "non-uniform mesh distribution" in which the meshes around the defects are very fine, while those far from defects are coarse. The smallest mesh size determines the critical stable time increment in the explicit analysis. So, the small elements around the defects will greatly increase the computational cost.

Moreover; defects, like cracks, will only propagate along the element edge, and not along a natural arbitrary path. When the structure members are exposed to external loads, they develop stresses that may cause failure if these stresses exceed the strength of the material. These stresses usually occur at cracks or near the surface of cracks, and the presence of these cracks reduces the strength. This requires accurate modeling and careful analysis of the structure to assess the true strength. In

addition to that, modeling holes, modeling faults and landslides present another form of problems where the usual FEM becomes an expensive choice to get optimal convergence of the solution. The FEM has proved to be very well suited to the study of fracture mechanics. However, modeling the propagation of a crack through a finite element mesh turns out to be difficult because of the modification of mesh topology.

1.5 Aim of Study

The main aim of this study is to present a numerical study that verify a change in the geometry of non-prismatic UHPC beams of multi longitudinal openings and then investigate the shear behavior of UHPC using ABAQUS program, including;

1. Optimate diameter and locations of longitudinal openings that affecting on shear strength of UHPC beams.
2. Study effect of scale factor of UHPC tapered-beams on its shear capacity.
3. Studying of effect of amount of steel reinforcement.
4. Studying of the effects of geometric beam change such as the sectional dimensions and boundary condition of beams.
5. Studying the shear span effect of non-prismatic beams.

1.6 Layout of the Thesis

This thesis is divided into five chapters which can be clarified as follows:

1. **Chapter One:** It is the introduction that includes the introduction and general description of related issues., application of UHPC, study objective and outline of thesis.
2. **Chapter Two**: Shows previous studies that related on the UHPC and shear behavior of UHPC tapered beam and using Finite element by ABAQUS.
3. **Chapter Three:** It is the numerical formulation of developed models.

4. **Chapter Four:** Shows models of tapered beam, besides; the comparative analysis, and record the results of numerical work in sence of cracks, deflections, load capacity and the results discussion.

5. **Chapter Five:** It is the conclusions and recommendations that summarized the overall outcome of the study as well as suggested recommendations for the future work.

CHAPTER TWO: LITERATURE REVIEW

2.1 General

The available studies in the literature related to the current work are presented in this chapter. The studies are divided into three parts. The first part presented Beam of special section shape. The second part presented the available studies conducted on of tapered beam. The third part provides an overview of the experimental and analytical studies that dealt with the behavior of non-prismatic beams**.** Many engineering problems concerning with the analysis and design of structures were experimentally studied at the laboratory and theoretically. Appropriate solutions have been found for some of these problems. Studies are continued with the development in the base of engineering technology to avoid the other problems as well as improving performance. Experimental research supplies the basic information for finite element modelling to get reliable analytical models .

In this chapter, a historical overview of the most important studies that have been previously conducted in the field of the current study.

2.2 Historical Background and Development of UHPC

In 2005 Japan Society of Civil Engineers (JSCE) [20], high strength concrete HPC is no longer the strongest and most durable of the concrete materials making it one of the best recent discoveries in terms of Portland cementitious materials as a primary component of concrete as shown in Table 2.1. The new type of concrete did the same tasks as the conventional concrete mixture but due to changes in its composition it exhibits superior qualities to the conventional concrete.

Table 2.1 Comparison Between UHPC and HPC.

No.	Material Characteristic	UHPC / HPC
1	compressive Strength	2-3 times greater
2	Flexural Strength	2-6 times greater
3	Elastic Modulus	1.5 times greater
4	Microporosity	10-50 times lower
5	Permeability	50 times lower
6	Water Absorption	7 times lower
7	Chlorine ION Diffusion	25 times lower
8	Total Porosity	4-6 times lower
9	Abrasive Wear	Abrasive Wear
10	Corrosion Velocity	8 times lower

France and Canada between 1990 and 1995. Currently, although, this type of mixture is known as UHPC as a scientific name in design calculations and international codes as the Japanese code JSCE [19]. With the additional of other material companies like Lafarge Corporation and Sika Corporation, two of the most well-known construction materials companies, the development research for this type of concrete is still ongoing in two different companies (Bouygues Construction) and (Eiffage Group (EIG)). This resulted in the development of two products of ultra-high-performance concrete (UHPC), under the mediation of these two independent companies, the first company producing.

The researchers Richard and Cheyrezy [21], in the Bouygues company, published the first publication in 1994 where they developed UHPC200 which gives compressive strength up to 200 MPa, and the second publication in 1995 where they published the concrete type UHPC800, which has a compressive strength up to 800

MPa. There are thus two different varieties of UHPC, and each type has a unique mixing process, ratio of mixed components, treatment method, and outcome qualities. Table outlines the traits and elements of these two categories 2.2.

Table 2.2 Comparison Between UHPC200 and UHPC800 [20].

Composition	UHPC200				UHPC800	
	Non-Fibered		Fibered		Silica Fume	Steel aggregate
Portland Cement	1	1	1	1	1	1
Silica Fume	0.25	0.23	0.25	0.23	0.23	0.23
Sand 150-600 m	1.1	1.1	1.1	1.1	0.5	-
Superplasticizer	0.016	0.019	0.016	0.019	0.019	0.019
Steel fiber 12mm	-	-	0.175	0.175	-	-
Steel fiber L=3mm	-	-	-	-	0.63	0.63
Steel agg. 800 mm	-	-	-	-	-	1.49
Water	0.15	0.17	0.17	0.19	0.19	0.19
Compacting pressure	-	-	-	-	-	50MPa
Heat curing temp.	20	90	20	90	250-400	250-400

2.2.1 Ultra-High Performance Concrete Characteristics

The components of the concrete mixture are crucial in determining the characteristics. Therefore, the mixture of its components is to blame for the UHPC mix's exceptional qualities. The mixture's components may be summed up, and its water content is significantly lower than that of a typical concrete mix. The link between the granules of fine materials will be weakened by adding silica fume to its components in an effort to increase its compressive strength by avoiding the formation of free calcium hydroxide crystals in the cement matrix. The use of a low water-cement ratio, the addition of silica fume, which has a negative effect on this type of concrete, and the addition of steel fiber are the other causes of the low workability in this type of concrete. To solve this issue, it is necessary to add HRWRA to the mixture in order to increase workability.

1. **Cement:** The type of cement used and the quantity of cement used have the most effects on the qualities of the concrete. To increase the compressive strength of an ultra-high-performance concrete (UHPC) mixture, a lot of cement is often required.
2. **Silica Fume:** It is also referred to as microsilica, a very soft powder made of silicon and ferrosilicon. The diameter of its particles is 150 time smaller than the diameter of cement particles i.e., 150mm. Because of its high fineness and high silica concentration, this material is utilized to make high-performance concrete. Silica fume combines pozzolanically with lime (calcium hydroxide Ca (OH)) during the hydration of cement to produce the stable cementitious compound (calcium silicate hydrate CSH). The proportion of silica fume in (UHPC) is typically between (5-15) % of the cement content.
3. **Fine aggregate**: This form of concrete (UHPC) uses fine aggregate, which should pass through a sieve of 600 μm.
4. **Water**: Since there are many cement elements present in this type of concrete (UHPC) (cement +silica fume), the water ratio should be calculated as a percentage of all cementitious ingredients, as opposed to the cement alone, as it was in conventional concrete (w/c). Additionally, the ratio of plasticized materials should be added as a proportion to the cementitious materials, and some studies think that using plasticizers instead of cementitious materials can minimize the water content.
5. **Steel Fiber:** To enhance the ductile qualities and raise the tensile strength of UHPC, steel fiber is added.

In 2017 Aaleti et al [26] UHPC is an example of how concrete technology has advanced significantly, having high compressive strength and enhancing durability. UHPC materials offer a variety of interesting implementations. It enables the

construction of affordable, environmentally friendly structures with extraordinary slim line designs. It is the ideal building material because to its strength and ductility.

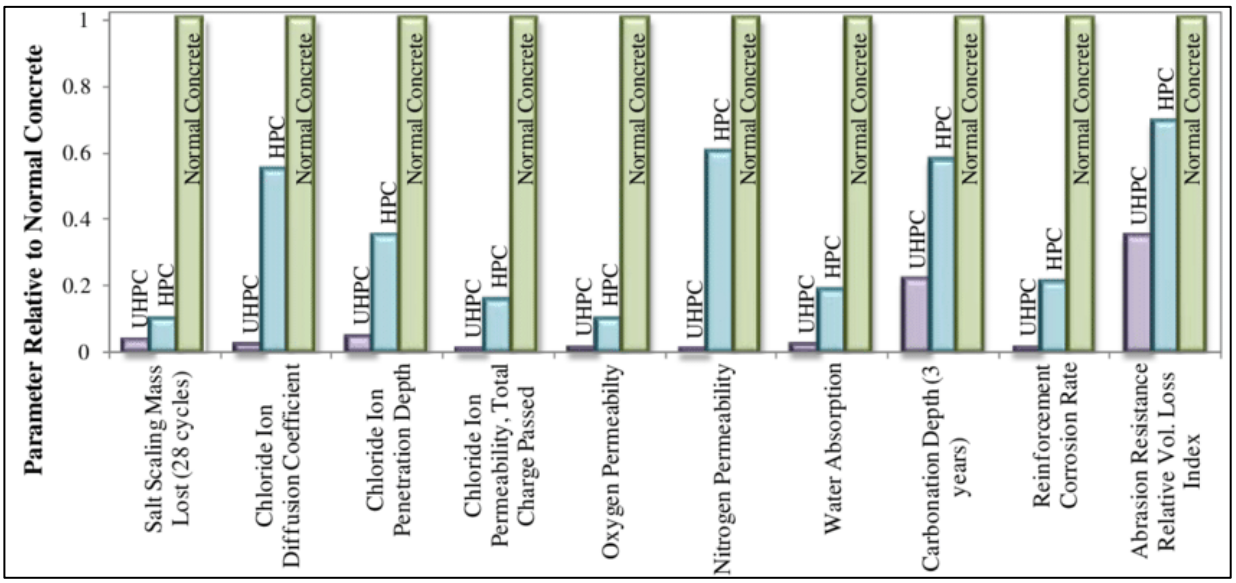

Figure 2.1Comparison of durability properties of UHPC and HPC with respect to normal concrete (lowest values identify the most favorable material) [25].

Additionally, its exceptional resistance to all forms of corrosion is a further advancement toward maintenance-free buildings. UHPC has incredibly unique qualities that are noticeably different from those of HPC and regular concrete. For the production, design, and construction of UHPC, eminent knowledge is required in order to fully utilize its excellent properties. There is an itemized exploration of global UHPC. Many structural or building elements have already been built using UHPC. For maintain the design life of older buildings, the construction members must be maintained and strengthened. In some cases, maintenance is also more cost-effective than demolishing the building and starting again.

2.2.2 Effect of Steel Fiber on UHPC Properties

In 2010 Lavanya [27], by experimenting with various ratios for various types of steel fibers. It was possible to determine the ideal ratio of steel fibers in the UHPC

mixture. The results showed that the ideal ratio was 3% for steel fibers with a length of 6 mm and 2% for steel fibers with a length of 13 mm and a diameter of 0.16 mm. The steel fibers utilized had specifications of 2000 MPa tensile strength and (38-81) aspect ratio. The ideal proportion of steel fibers in UHPC should fall between 2 and 3 percent by volume. According to additional research, using steel fiber with an aspect ratio of (45-72) will boost the flexural strength of UHPC.
The following variables affect how well the steel fibers bond together:

1. Matrix fracture and spalling
2. Debonding between the mix and the fiber.
3. Friction after the debonding stage.
4. The fiber itself friction.
5. plastic bending - Fiber yielding.

In 2003 ***Silvia et al****.[28]* Investigate the effects of the type of steel fibers used in the UHPC mixture, four different types of steel fiber were used: deformed steel (30/0.45), deformed steel (30/0.62), and deformed galvanized steel fibers (30/0.6). The ratio of water to cement (w/c ratio) was 0.24, and the following was the weights of the mixtures: 904 kilograms of cement, 226 kg of silica fume, 944 kg of 0.1 mm sand, 12.3 kg of carboxylate acrylic superplasticizer, and 181 kg of steel fibers. The findings demonstrated that compared to other types of steel fibers, the brass-plated steel fibers used in this mixture provide better compressive and tensile strengths.

In 2000 Gowriplan [29], Indicated that the steel fiber, depending on its quantity and orientation, plays a significant impact in the tensile strength of UHPC by bridging the fracture and preventing it from widening. It appeared that pulling out some of the steel fibers caused the drop in tensile strength. Additionally, it was

discovered that UHPC has a tensile strength of (8) MPa and a compressive strength range of (150–220) MPa.

In 2008 Si-Larbi [30], studied the flexural behavior of UHPC beam with steel fiber, and the aim of the study was to obtain the highest ductility member and the design was based on the European code, It examined the effect of was studied the effect of the existence of shear reinforcement with the longitudinal reinforcement. The result revealed that the using of shear reinforcement with Longitudinal reinforcement increases the load by 50% and the use of the UHPC reduced the dimensions of the section from (190*315) mm to (150*250) mm, Therefore, the dead load will decrease by 40%, and compressive strength increase from 40 MPa to 140 MPa.

2.2.3Modulus of Elasticity of UHPC

Many international codes and researchers have developed equations that relate compressive strength with the modulus of elasticity through scalar factors to make the process of quality control of the concrete construction better. The recommendations for the UHPC modulus of elasticity are compiled in Table 2-3.

Table 2.3 Relationship Between Compressive Strength and Modulus of Elasticity.

References	Equations related $f'c$ with Ec
ACI 318 [31]	$E= 4700\sqrt{f'c}$ in SI units for (normal strength and normal weight concrete) $E= wc^{1.5}\ (0.043)\sqrt{f'c}$ (we is the unit weight concrete (1500-2500) kg/m) • In case UHPC [59] $wc = 2480 \rightarrow E=5311\sqrt{f'c}$
Kakizaki et a1 [32]	$E=3650\sqrt{f'c}$ in SI units for f′c (83-138) Mpa
ACI 363R-92 [33]	$E=3320\sqrt{f'c}+6900$ for high strength concrete f′c 83 Mpa

Ma et al [32]	E=525000 $\sqrt{\frac{fc}{10}}$ for UHPC with no coarse aggregate
FHA [34]	E=46200 $\sqrt{f'c}$ for $f'c$ >193 MPa
AFGC [35]	Modulus of elasticity E=50 GPa
JSCE [36]	Modulus of elasticity E=50 GPa
Gowriplan [30]	Modulus of elasticity E=50 GPa
Samir [37]	E=4572 $\sqrt{f'c}$ for $f'c$ (79-119) MPa
Maha [38]	E =[(S1-S2) (ε2 - 0.00005)] S1 = Stress with 40% of ultimate load, MPa S2 =Stress with longitudinal strain (0.00005), MPa ε2 = longitude strain produced by stress S2
Mahesh [36]	*E=3.65* $\sqrt{f'c}$ (Mahesh found E of UHPC increased with time especially when using thermal treatment)

2.2.4 Shear Failure in UHPC Beams

An Ultra High Performance Concrete beam should be designed to meet the code requirements. Beam are designed for bending and shear to ensure ductile behavior under imposed loads during the service life of the structure. Shear failure is dangerous because it does not give a previous warning. Therefore, it is necessary to pay attention in this context. Shear capacity in the conventional concrete sections is mainly dependent on the shear concrete strength (V_c) and the steel reinforcement (stirrups) shear strength (V_s). However, shear strength in the specifications and researches equations depends on several factors that can be summarized:

1. Shear stresses occur in the area of compression of the concrete.
2. Failure in longitudinal reinforcement due to dowel action
3. amount of bonding between the aggregate
4. Tension stresses formed along the crack
5. Arch action

Kotsovos in 1987 [39], investigated experimentally various types of reinforced concrete beams for shear failure. Transverse reinforcement was distributed in five different ways. Study cases were "A: without transverse reinforcement, B: with transverse reinforcement within the shear span only, C: with transverse reinforcement throughout beam span, D: with transverse reinforcement within the flexure span in the region of the load points only, and E: with transverse reinforcement as for beam D, but with additional top longitudinal reinforcement throughout the shear span". Beams A, B, and C were studied with shear span /effective depth (a /d) =2.25 and 3. Beams D and E were only used to investigate (a/d) = 2.25. Beam C had top longitudinal reinforcement throughout their length. Transverse reinforcement consisted of closed hoops of 3 mm diameter mild steel and spacing of approximately 40 mm. The load-deflection relationships were discussed for all cases. It was found that transverse reinforcement within the shear span did not necessarily give sufficient ductility, it was better if the stirrups extended within the flexure span .

Bažant et al. in 1991[40], investigated the diagonal shear failure of reinforced concrete beams without stirrups. The beams are geometrically similar, and the size range is 1:16. The tests indicate a significant size effect and show a good agreement with Bazant's law for size effect. The scatter of the test results is much lower than that previously found by studying extensive test data from the literature. The previous test data were not obtained on geometrically similar beams as shown in Fig. 2-2. The tests also show that preventing bond slip of the longitudinal bars causes an increase in the brittleness number of the beam. It is concluded that the current design approach, which aims to provide safety against the diagonal crack initiation load, should be replaced or supplemented by a design approach based on the ultimate load, taking into account the size effect of fracture mechanic's type.

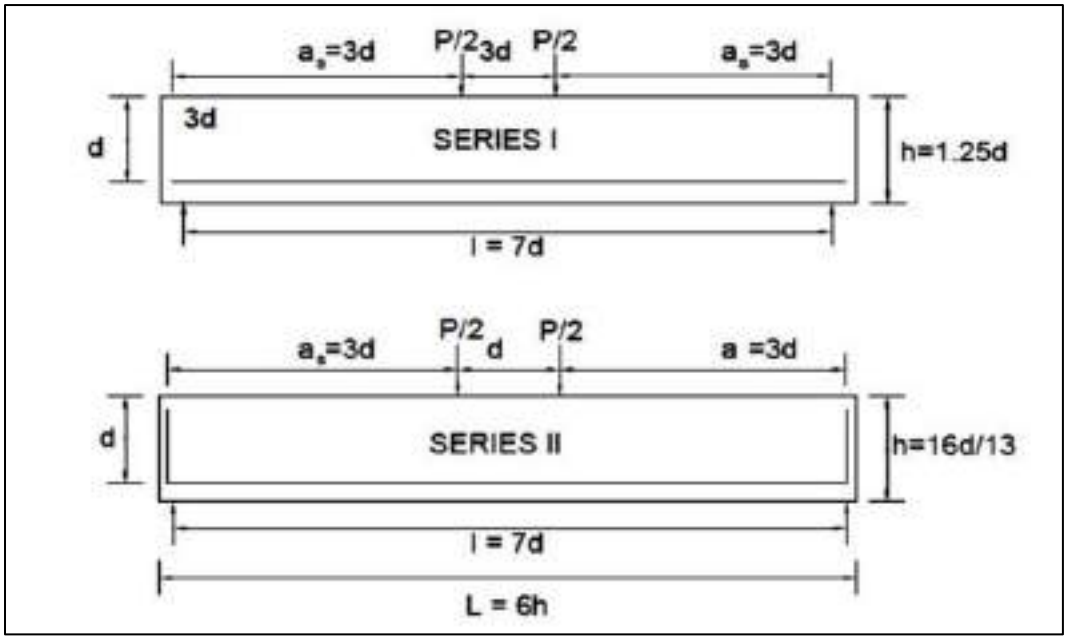

Figure 2.2Test Specimen Geometry (1 in. = 25.4 mm).

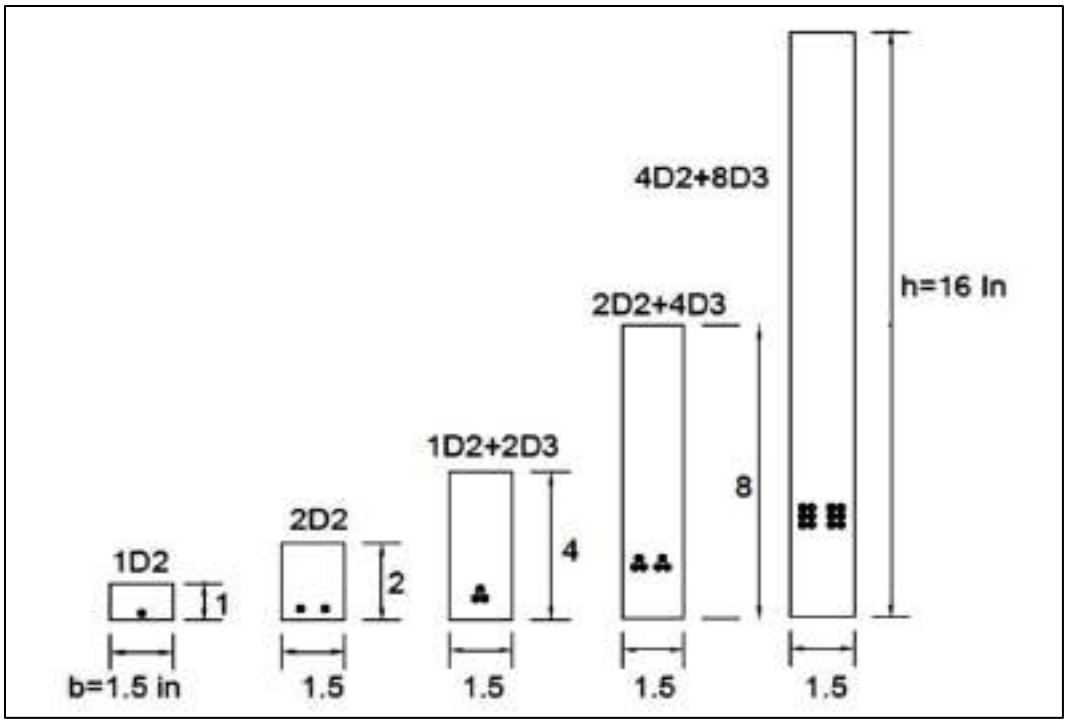

Figure 2.3 Test Specimen Geometry.

Słowik in 2014 [41], studied the shear failure mechanism and shear capacity in longitudinally reinforced concrete beams without transverse reinforcement. The beams were tested until failure under monotonic loading. The results showed that

the shear span-to-depth ratio and beam size were greatly influenced by the mode of failure. Two major diagonal cracks formed symmetrically at both opposite support zones of the beam when the load reached 50% of the maximum and the beams without developed the flexural cracks. The major diagonal cracks within the shear span propagated towards the applied load. The obtained ultimate shear forces for the short beams were by 26% higher compared to the longer beams of the same a/d.

Kristiawan et al. in 2017 [42], studied the shear failure of patched reinforced concrete beam without web reinforcements. The patch repair material used in this research was unsaturated polyester resin mortar with details as shown in Fig. 2-4.

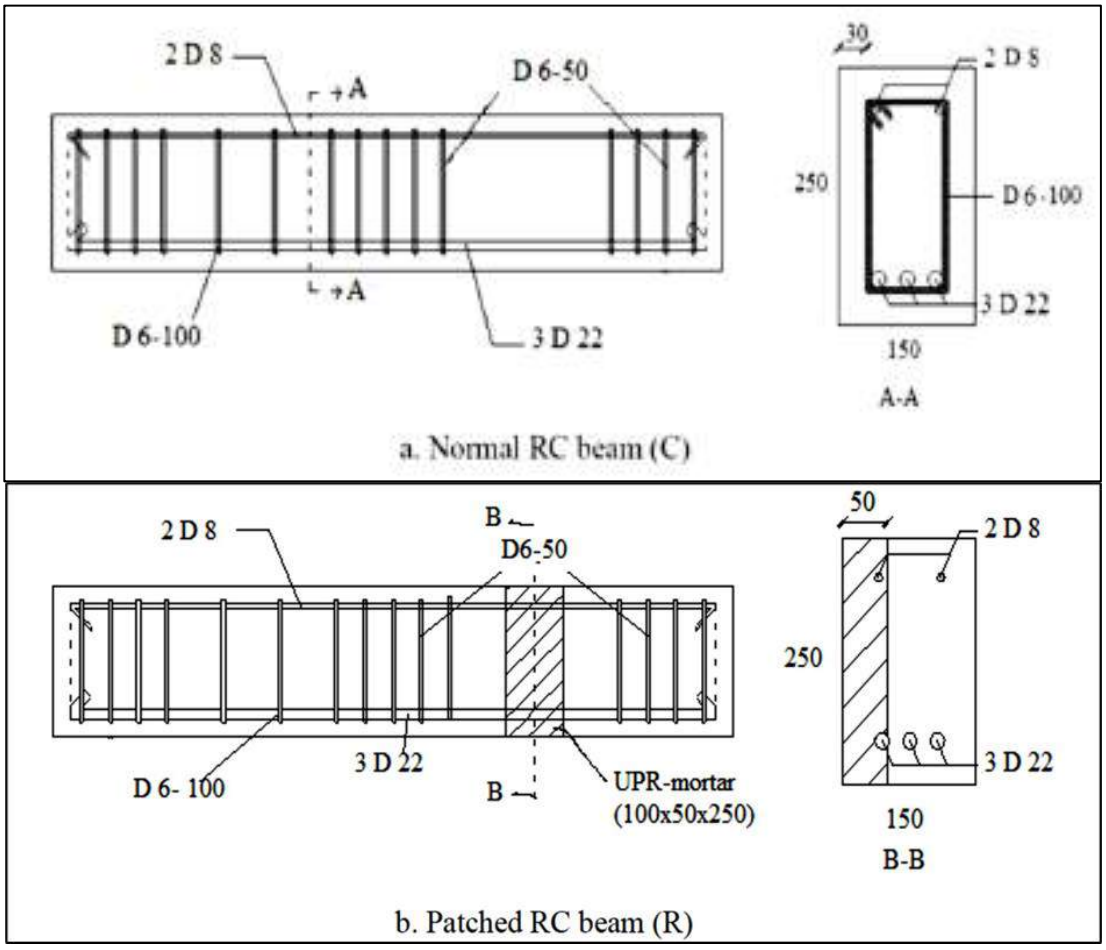

Figure 2.4 : (a) Reinforcements layout and cross section of C and R beam; (b) Reinforcements layout and cross section of C and R beam [42].

Two reinforced concrete beam specimens were similar in the dimension and the amount of reinforcements. One side of shear span was reinforced while the other side was left without web reinforcement to ensure the occurrence the diagonal crack that preceded the shear failure. The load and the deflection were recorded during the loading period until the beam failed in shear. The shear failure behavior of the patched reinforced concrete beam was compared to the normal reinforced concrete beam. The results showed that the beginning of the diagonal cracks leading to shear failure of the normal reinforced concrete beam was faster than patched reinforced concrete beam. It was also found that initial flexural cracks of the control and patched RC beam appear at similar load level. The initial diagonal crack of patched RC beam occurred at a lower level of loading compared to that of the control beam.

Słowik M. in 2018 [43], conducted the analysis of failure and crack propagation in concrete beams experimentally and by numerical simulations. Without transverse reinforcement in the beams. Numerical calculations were accomplished using the module APAKO of the commercial program ALGOR (ALGOR is a commercial program that includes a module called APAK0, which was used in the numerical calculations for the analysis of failure in concrete and reinforced concrete beams.). The analysis of failure and crack development in concrete and reinforced concrete beams with different reinforcement ratios was conducted through experimental investigation and numerical simulations. The presence of reinforcement was found to change the cracking process and impact the cracking resistance in reinforced concrete flexural members, even with low reinforcement ratios. The cracking moment, which determines the load capacity of plain and slightly reinforced concrete beams, was observed to be higher than the theoretical cracking moment calculated based on the theory of elasticity.

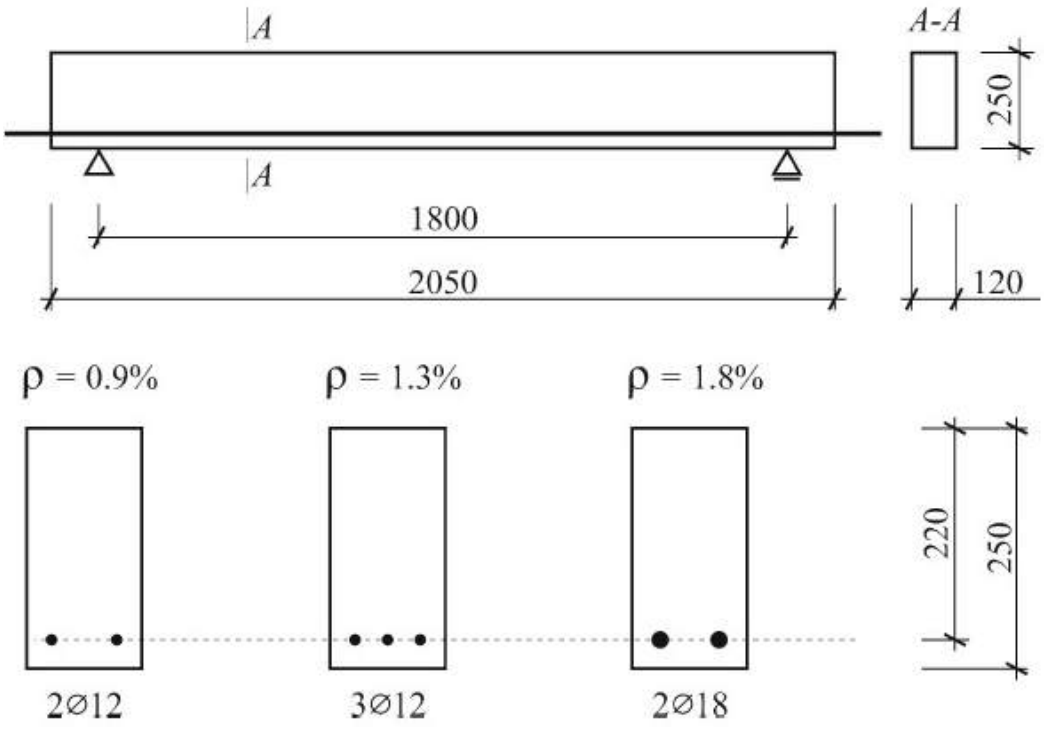

Figure 2.5 Beam's geometry and the location of reinforcement.

In 2005 JSCE [36], Concrete Committee of Japan Society of Civil Engineers, developed an equation to estimate the shear capacity of UHPC sections :

$$Vrpcd = \text{shear capacity of concrete} = 0.18\sqrt{f'c}\ \ (b\ d)\frac{1}{\gamma b} \qquad 2.1$$

- $f'c$ = Compressive Strength of UHPC MPa
- γb = safety factor taken as 1.3

$$V_{fd} = (Fvd/\tan Bu)\ .\ b.\ Z/\gamma b \qquad 2.2$$

- Fvd = Tensile Strength of UHPC
- Bu = Inclination of The Crack Usually Taken it 30̊
- Z = lever arm $= 0.9\ d$

Table 2.4 Other Proposal Equations Estimated the UHPC Shear Behavior [36].

References	Design Equations for The Shear Strength (MPa)
Modification of ACI Building equation by	$Vu = (0.7\sqrt{fc'}+7F)\frac{d}{a} + 17.2\ \rho w\frac{d}{a}$

Ashour et al (1992) [44]	*- ρw =flexural reinforcement ratio* *- a =shear span, mm* *- d =depth of tension steel in section, mm* *- f'c = compressive strength of concrete* *- F = Fiber Factor Given By*
Modification of ACI Building equation by Ashour et al (1992) [44]	$F = \frac{lf}{df} Vf\, Bf$ *- df =fiber diameter, mm* *- lf = fiber length, mm* *- Vf =volume fraction of steel fibers* *- Bf =bond factor =0.5 for round fibers*
Modification of Zsutty´s equation by Ashour et al (1992) [44]	*For a/d > 2.5* $vu = (2.11\sqrt[3]{fc'} + 7F))\ (\rho w\ \frac{d}{a})^{0.33}$ *For a/d <2.5* $vu = 2.11\sqrt[3]{fc'} + 7F)\ (\rho w\ \frac{d}{a})^{0.33}\ \frac{2.5d}{a} + vb\ (2.5 - \frac{a}{d})$ $vvb = 0.41\ \tau b\ F, MPa$ *- τb = average fiber-matrix interfacial bond* *- stress=4.15 MPa* *- F = fiber factor*

The shear behavior of tapered concrete buildings has received limited attention. It is obvious that a suitably inclined force in compression or tension may give some resistance to shear [45] Park and Paulay [46] propose that Equation (1.1) should be used to calculate the effective shear force in haunched beams without shear reinforcing (derived by considering the equilibrium of a tapered beam).

$$V_{eff} = V - (M/Z)(\tan\theta') \qquad 2.3$$

Where:

V_{eff} = the effective shear force on a section.

V= the shear force on the section from the applied loads.

M= the bending moment at a section, z is the lever arm between centers of tension and compression.

θ'= angle of beam slope from the horizontal, this value is positive in sections where the member depth increases in the direction of increasing moment.

When the principal tensile stress in the concrete exceeds its tensile capacity, cracks occur in the steel reinforced section and as the applied loads are increased, inclined cracks often spread from the member's tension face towards the neutral axis. It was imaginable that in sections that taper towards their supports, the interaction of these diagonal cracks with the course of the compression force that reaches the supports may be more crucial along with the factors that contribute to a reinforced concrete beam's ability to resist shear, as shown in Figure 2.6 [45].

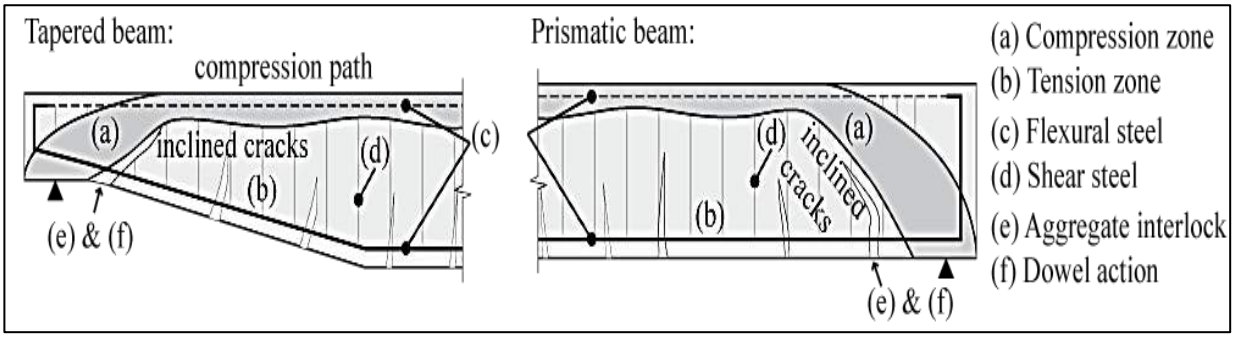

Figure 2.6 Contributing factors to shear resistance in tapered and prismatic section.[45]

2.3 Reinforcement Concrete Beam of Special Section Shape

In 2019 Hamoda et [22], the purpose of the study was to look at how geometric parameters affected reinforced concrete beams with disturbed depth using

experimental and numerical methods (shape and width). The installation of ten reinforced concrete beams with simple supports was part of the experimental testing program. The position of the re-entrant corner influences the yield load, ultimate load capacity, and cracking characteristics. According to experimental the findings, raising the beam nib height-to-recess length ratio from 0.19 to 0.23 and 0.38 increases the yield load and ultimate load; respectively, by 27% and 94% and 4% and 64%. Additionally, when nib length decreases, the mode of failure varies from pure flexural to compression-shear failure. The effectiveness of the developed numerical model in capturing the nonlinear behavior of the RC beam with unequal depths as depicted from load-defection response, cracking, failure modes, and strain development in reinforcement was demonstrated by the good agreement between experimental and FEA results. Therefore, the created three-dimensional FEA model was be employed as a tool for future research.

In 2021 M. J. Sada et. [23], the experimental investigation on hybrid trapezoidal reinforced concrete section was studied. The investigation of ten simply supported reinforced concrete beams subjected to four-point load was presented in the study. Two groups were investigated, each with five beams and an equal cross-sectional area. The first group is used to test flexural behavior, while the second group is used to test shear behavior.

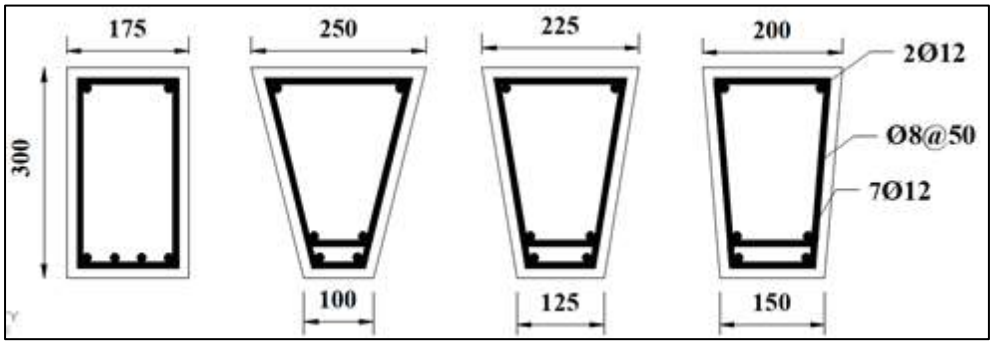

Figure 2.7 Geometrical Details of Developed Specimens.

The variables used in the experiment are compressive strength (25 and 50 MPa) and the use of a trapezoidal section with different side angles (75°, 80°, 85°). The experiment results showed that the trapezoidal section had high deflection results, with rates of increase in the flexural failure mode ranging from 20% to 57% and in the shear failure mode ranged from 22% to 60%, and the results concluded that the trapezoidal section has a significant effect on improving section capacity. When compared to the rectangular section, as well as an increase in the failure load in proportion to 6.77% when bending failure and in proportion 3 when shear failure. The effect of the area distribution within the section (shape sides orientation), was clear on the load of the first cracks, with the highest value of the crack load related to an angle of 80◦.

In 2011 H. Mahzuz, A. [24], investigated the performance of a triangular singly reinforced concrete beam The study's main goal was to develop relevant mathematical formulas for design. and an important comparison with rectangular section formula was made. The shear force and the bending moment are both compared. The entire study was carried out with a single-reinforced beam and the working stress design method (WSD). In terms of greater moment and shear taking ability, the results showed that triangular RCC sections outperformed rectangular ones. Because it uses less steel and has a smaller concrete volume, the triangular section ensures less dead load and economic safety.

In 2017, Khalil et al.[25] Extensive study has been done on the way of the behavior and shear strength of reinforced concrete beams. This study's primary goal was to validate and enhance the existing analytical and design approaches for shear analysis of typical reinforced concrete beams. Eight direct models of RC beams were tested as part of the experiment. When compared to the other specimens (B2, B3, B4, B6, B7& B8), the beams "B1 & B5" have the minimum gross moment of inertia,

which results in a reduced deflection value until the first crack develops, at which point the section behavior is dependent on the cracked moment of inertia. In comparison to the other specimens (B2, B3, B4, B6, B7, and B8), the beam "B1 & B5" cracked moment of inertia is the smallest, which caused the greeter deflection value after the first crack occurs until failure. The shear behavior of the beams depends upon the typical cross section area (the typical width) in resisting shear force.

2.4 The Longitudinal Opening (Hollow Core Beams)

In general, the presence of longitudinal web openings in concrete beams is an important topic that researchers which are interested here after as:

In 2013 AL-Maliki et al.[47], the behavior of five non prismatic RC beams with different hollow shapes and materials was investigated. All beams are (150x260x1170) mm in size, with a hollow core of (50 x 50) mm square steel or (50mm) diameter circular PVC. The beams are tested with simply supported ends under two points loads. The results show that the presence of a hollow core in the beam section decreased stiffness while increasing deflections and strains. When compared to circular PVC pipe, square steel pipe has increased load capacity and decreased deflections.

In 2020 G. Balaji et al. [48], The flexural behavior of reinforced concrete hollow beams under a gradually applied two point load is investigated in this study. The ultimate stage deflection is experimentally investigated and compared to RC hollow beams. Furthermore, this study focusing on material optimization by introducing hollow portions made of PVC pipe and GI pipe at tension zones in RC control beams. This experimental investigation includes the casting and testing of five reinforced concrete beams with different sizes. The flexural strength of hollow

beams with single openings is higher than hollow beams with double openings. Hollow beams have greater ductility than control beams. Both hollow beams and control beams failed due to flexure failure, as shown in Figure 2.8.

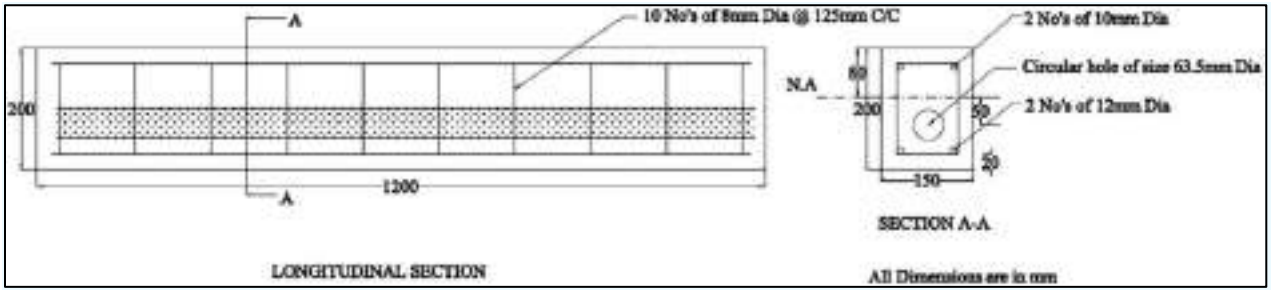

Figure 2.8 Reinforcement Detail of Hollow Beam with Single Opening.

In 2019 M. B. Abdulrahman et al. [49], investigated the structural behavior of Strength of reinforced reactive powder concrete hollow ten beams with dimensions (150mm width200mm height1000 mm length). Eight of which are hollow beams and two solid beams, were cast and tested to failure to research the structural behavior and strength of reinforced cementitious concrete beams with a hollow section subjected to two-point concentrated loading. The major parameters used in this study are the openings ratio (10% and 15%), hollow location (top or bottom), and hollow shape (circle or square). The results show that the strength capacity of a hollow beam is much higher when the hollow is at the bottom than when it is at the top, and the square hollow will lead to much more. This is because of stress concentration and crack initiation at the square corner. It was demonstrated that the strength capacity of the hollowed beam is significantly greater when the hollow is in the bottom position than when it is in the top position. The presence of hollow in beams causes the failure mechanism of solid beams to change from flexural failure to a combined flexural-shear failure for the hollowed beams.

In 2017 Murugesan et al. [50], investigated the influence of the longitudinal circular hole on the flexural strength of reinforced concrete beams, by testing

thirteen (1.700, 150, 250) mm beams. All hollow RC beams tested had one hole with a longitudinal diameter of (25, 40, or 50) mm. The longitudinal holes were created in the molds using a frictionless PVC pipe and a fixed reinforcements cage. Depicts the research parameters. The results revealed that the first crack load was affected by the distance between the center of the hole and the cross-horizontal section's centroidal axis. The larger diameter holes reduced the moment of inertia more than the others, resulting in a lower cracking moment strength.

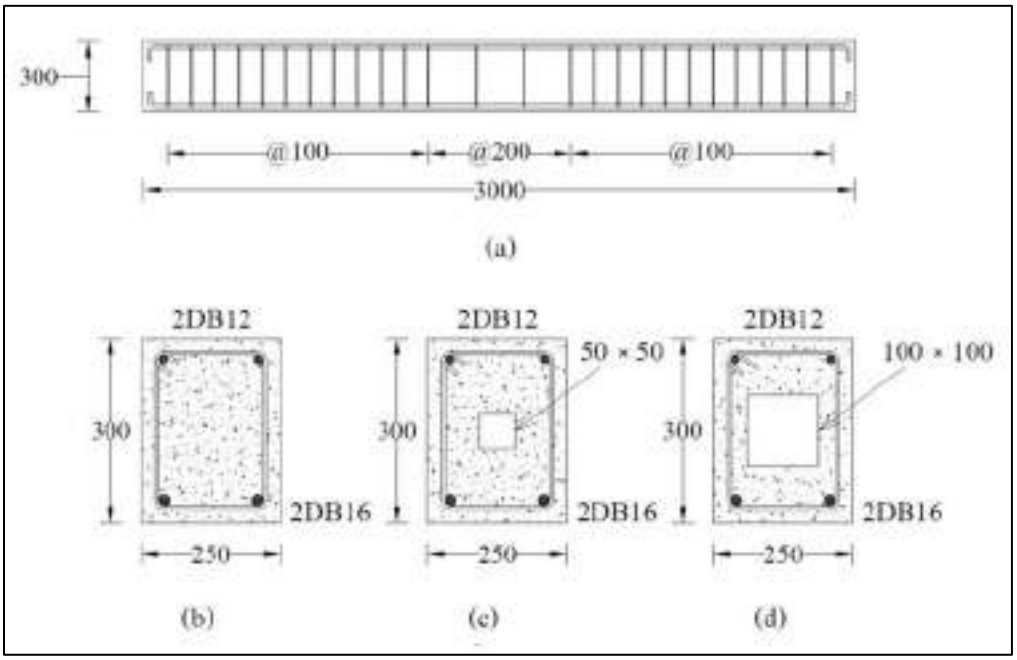

Figure 2.9 Typical beams in each group (a) longitudinal section, (b) solid section, (c) hollow section HS50, (d) hollow section HS100 [49].

In 2020 A. A. Abbass et al. [51], studied the fourteen reinforced concrete solid and hollow beams and tested using a four-point bending test to evaluate the flexural behavior of hollow concrete beams. The experimental program concentrated on two main variables: the percentage of size reduction and the inclusion of steel fiber. Furthermore, the longitudinal reinforcement ratio and the presence of lateral stirrups were within the parameters investigated. To evaluate the test parameters, four solid beams and ten hollow beams with central square holes and side lengths of 60, 80,

and 100mm were fabricated. Below is an explanation of the cracking patterns in the study.

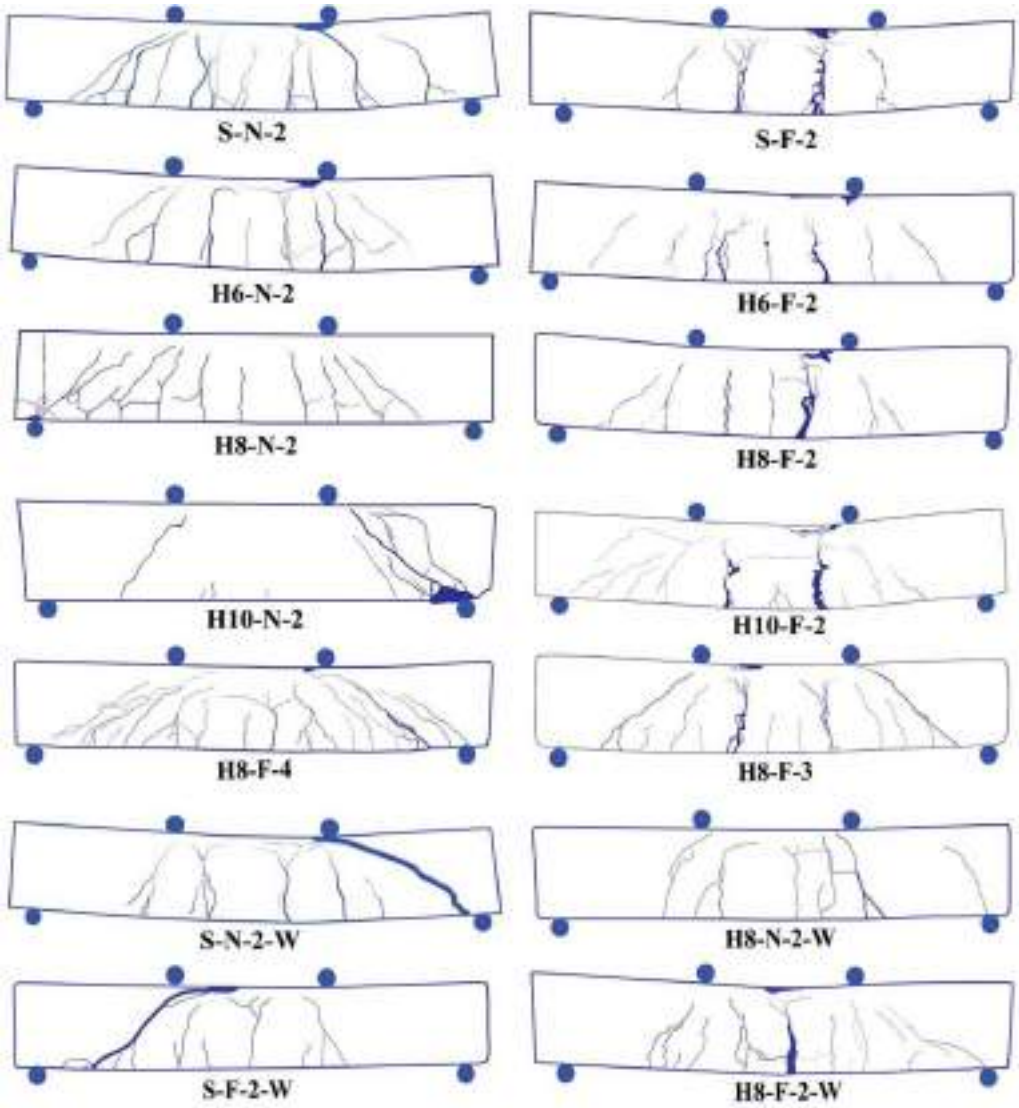

Figure 2.10 Cracking Patterns of all Tested RC Beams [50].

In 2014 Ahmad et al.[52] Investigated the behavior of six (solid and with opening) beams with details was (length 1m, height 0.18m, width 0.12m) that simply supported. The load that was tested was (partial uniformly distributed). Four beams had longitudinal openings of varying section (80mm x 40mm) and (40mm x40mm). Their parameters were the size of the opening, the effect of the stirrups, and the orientation of the stirrups. The existence of hollows reduces load carrying capacity and increases deflections, stirrups decrease whole deformations at all phases of

loading, especially after initial cracking, and ductility is increased when the hollow ratio is reduced or stirrups are increased by about 50%.

2.5 Modeling Concrete Beam using Non-linear Finite Element Analysis by ABAQUS

For several structures, concrete is the major constituent element. Concrete behavior is nonlinear, and complex. Increasing use of computer-based modeling and simulation methods has also increased the need to find an exact solution to the problems. This causes difficulties in the simulation and modeling of concrete structures. The general- purpose finite-element program ABAQUS was a good solution [53]. Concrete damage plasticity model is a modified model of the Drucker Prager criterion and it takes into account concrete's isotropic compressive and tensile plasticity to reflect concrete's inelastic behavior in combination with its isotropic damaged elasticity. This model takes into account tensile cracking and compression crushing of concrete.

Chaudhari and Chakrabarti in 2012 [53], studied a concrete cube 3D model using the smeared crack model and the concrete damage plasticity approach. The validation of the model under monotonic loading was discussed at the desired behavior. The concrete in both cases showed a perfectly nonlinear nature. The stress-strain curve obtained by using smeared crack modeling at mesh size 25mm gave maximum stress of about 29.39MPa at 0.00190 strain. The stress obtained for concrete damage plasticity model at mesh size 25mm was 32.33 MPa at a strain of 0.00195.

Sinaei et al. in 2012 [54], used ABAQUS software to model reinforced concrete beam behavior. The finite-element model with the concrete damage plasticity approach was used to analyze the non-linear behavior of reinforced

concrete element. In order to obtain accurate results from the FE model, all the elements in the model were purposely assigned the same mesh size to ensure that each two different materials share the same node. The type of mesh selected in the model was structured. The mesh element for concrete was 3D solid which is called C3D8R and for the rebar it was 2D truss which is called T3D2. The finite element model was validated using to converged that previous literature experimental tests. The load-tensile strain plot collected for the tensile steel reinforcement at mid span from the experiment was compared with the results from the finite element analysis.

Słowik and Nowicki in 2012 [55], presented a study on concrete beams reinforced longitudinally without transverse reinforcement. The study was experimentally and theoretically by FEM using ABAQUS software. The experimental program was designed to investigate the influence of the shear span-to-depth ratio on diagonal crack propagation and load carrying capacity of tested beams. In the performed numerical simulation the same longitudinally reinforced concrete beams as in the test were considered. During the numerical analysis, special attention was paid on the tensile stress distribution and on changes of diagonal crack propagation in dependence of the shear span-to-depth ratio. The load carrying capacity of reinforced concrete beams without stirrups was found to depend on shear span-to-depth ratio because the failure mechanism changes in accordance to this parameter. The results of numerical simulations showed the differences in maximum stress distribution according to a/d.

Rao et al. in 2017 [56], performed laboratory experiments and finite element modeling for both plain and reinforced concrete beams under flexural loading. The finite element modeling was conducted using ABAQUS software. Laboratory tests were carried out on a beam dimension 500mm x 100mm x 100mm. The stress-strain and load-deflection results from the experimental and analytical studies were

compared. It was found that plain concrete had been poor in tension, failed at lower loads and could bear low deflections. The addition rebars of the strength and deformability increased quite remarkably.

Rašeta et al. in 2017 [18], analyzed three different nonlinear material models for concrete. ANSYS, ABAQUS and ADINA programs were used to implement the study on simply supported concrete beam subjected to monotonic increasing load. The first model of concrete and reinforcement behavior applied was implemented in the Ansys program. For the modeling of concrete member part, 3-dimensional finite element SOLID 65 was applied, and for the modeling of the reinforcement finite elements BEAM188 was used. The second model of concrete behavior used was implemented in the program ABAQUS with Concrete Damaged Plasticity model for 2-dimensional finite elements, CPS4. The third model of concrete behavior that was used to implement in the ADINA program was 2-dimensional finite elements, 2D Solid. The reinforcement was modeled using the basic rod. The results of the analysis of the stress-strain state and the vertical displacement of the beam mid-span were presented. Based on the results of the analysis it was found that the differences in stresses and strains between the 3-dimensional models and models with the assumption of plane stress were not higher than about 8%. Also, differences in the results for the stress and strain of the reinforcement between the "hand" design and applied models in programs ANSYS, ABAQUS and ADINA did not exceed about 11%. Analysis of maximum vertical displacements of the middle bottom RC beam edge showed that the differences between the calculated values did not exceed about 2%. It concluded that in the cases, where it was possible, the simplified models could be used compared to the three-dimensional, because the models with 3D solid finite elements were much more computationally expensive, compared to the models with 2D finite elements that gives satisfactory results with engineering accuracy.

Rama et al. in 2017 [57], presented a study on the fracture characteristic for different grades of concrete using Concrete Damage Plasticity (CDP) model. Indian Standard and EUROCODE were used for the basic input parameters of concrete. Numerical evaluation was done using Finite Element Analysis Software ABAQUS/CAE. Mesh sensitivity analysis was also carried to study the influence of type and size of elements on the overall accuracy of the solution. The mesh element types were varied among quadrilateral or triangular elements. The mesh element sizes adopted for mesh were 2mm, 5mm, 10mm, and 25mm. Different input parameters like dilatation angle, eccentricity was varied and their effect on fracture properties was addressed. This study was done by modelling beam with a/d = 0.1, where a/d represents initial crack to depth ratio. The study of the effect of the variation of mesh element type, mesh element size, grade of concrete, the model used for calculation of compressive behavior, final tensile damage value, dilation angle, eccentricity, and notch-to-depth ratio, on fracture parameters was done. The proposed Concrete Damaged Plasticity (CDP) model was able to predict fracture properties of concrete which were at equal with the experimentally obtained values. The results indicated that the fracture properties of concrete for various grades could be accurately predicted without laboratory tests using CDP model. It was also found that the peak load decreased when increasing the shear span-to-depth ratio.

George et al. in 2017 [17], carried out finite element analysis to study the non-linear behavior of concrete by constitutive modeling of concrete damaged plasticity (CDP) model. Two-dimensional deformable shell structures have been considered to simulate unreinforced concrete beam subjected to three-point bending test. The beam was modeled as a simply supported beam with two different elements: triangular (CPS3) and quadrilateral elements (CPS4R). Mesh refinement had been studied to predict the desired results accurately. Different sizes of beam and the

spans to depth ratio of the specimens, were considered to be 2.5, 4 and 8. Load vs. displacement curves were estimated. It was observed that the peak load for the quadrilateral mesh was higher the triangular mesh. At a finer mesh, beam with triangular and quadrilateral elements were subjected to similar peak load. The load carrying capacity of the beam decreases with the increase in span to depth ratio. Concrete Damage Plasticity model was found to be mesh dependent.

Dere and Koroglu in 2017 [16], studied nonlinear finite element modeling of reinforced concrete and plain concrete. The reinforcing bars were embedded in structural members made of concrete. Compressive and tensile uniaxial stress-strain relationship as well as damage parameter curves for concrete material to be effectively used in ABAQUS were suggested. The performance of the suggested constitutive and damage models was verified with a simple nonlinear model (cube element) to display the resulting force-displacement response under monotonic and cyclic loading. Through study of 3D nonlinear FE models, practical simulations of reinforced concrete structural systems became possible. From the curves obtained, for nonlinear analysis of reinforced concrete structural systems CDP model was found to be promising.

Mostofineja et al. in 2019 [58], investigated the structural performance of reinforced concrete beams strengthened in shear through near surface mounted (NSM) technique experimentally and theoretically by simulating their behavior using finite element analysis by ABAQUS software. The effect of concrete compressive strength and varying ratios of steel transverse reinforcement was studied using parametric analyses. In the experimental section, four reinforced concrete beams were cast with and without stirrups to study the effect of NSM technique as a shear strengthening method as shown in Fig. (2-10). For this purpose, specimens with the dimensions (2000x300x200 mm) were prepared and tested in

four points loading up to failure. The experimental load– displacement curves of the mid-span as well as failure mechanisms of the beams were compared with the FEM. The experimental results indicated that NSM technique in hances the shear capacity up to 69% and 41% in the beams with and without stirrups, respectively. Both experimental and numerical results showed that as the transverse steel reinforcement ratios increase, the effective strain of CFRP strips decreases.

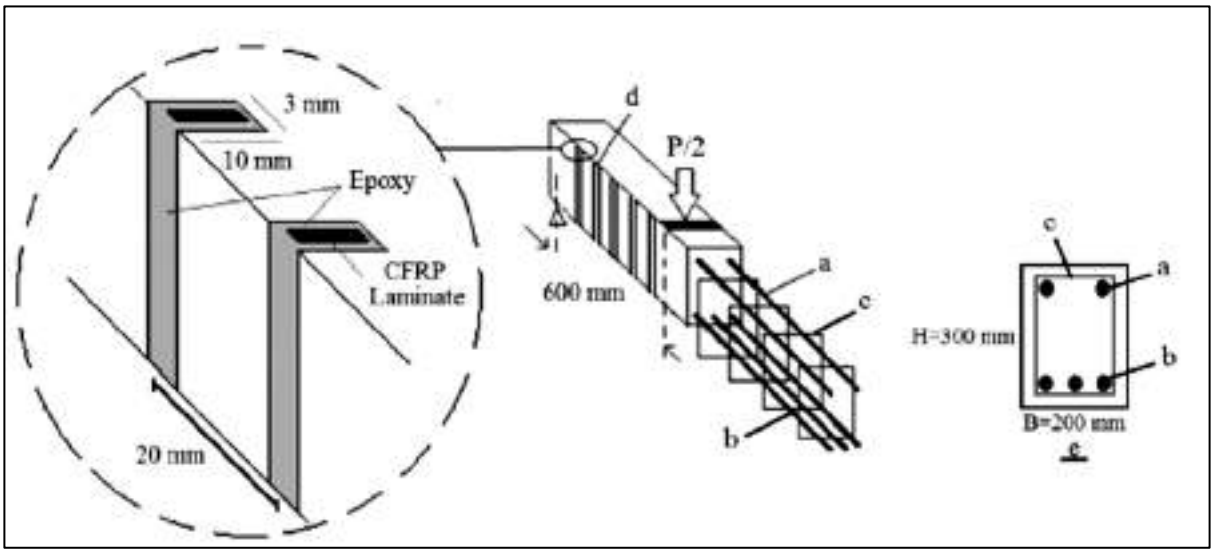

Figure 2.11 Details of NSM strengthened specimen: (a) compressive bars; (b)tensile bars; (c) stirrups; (d) a set of two grooves; and (e) section of the beams.

By decreasing the stirrup spacing to 65 mm, the shear failure of the strengthened RC beam changes to a flexural one. For the NSM strengthened specimens, ductility decreases for both beams with and without stirrups in comparison to control beams without strengthening. Ductility of the strengthened beam with stirrups decreased more. The numerical analysis showed that as the compressive strength of the concrete increases, the load capacity and the maximum deflection of specimens increase.

Tejaswini and Raju in 2015 [59], utilized FEM to model plain, under, balanced and over reinforced concrete beams using ABAQUS software. The results

were compared with experimental tests. A reinforced concrete beam's failure mechanism under three-point loads was modeled quite well using FEA.

Hansen-Dörr et al. in 2018 [60], studied a phase-field model to simulate fracture processes in heterogeneous materials. The local material structure was modelled in a diffuse manner, e.g., by a local reduction of the fracture toughness. In order to obtain a physically meaningful crack propagation, the interaction between the length scales of the diffuse microstructure and the regularized crack was studied. The method was verified in several numerical benchmark problems and applied to simulate fracture processes in heterogeneous materials.

In 2019 Rombach and Faron [61], studied a numerical simulation of crack propagation and the analysis of crack growth in reinforced concrete beams without stirrups. The study of crack patterns in FEM was done with elastic and plastic behavior by using ABAQUS. The XFEM was used to predict the fracture behavior of concrete members. The analysis included a study of failure due to bending and shear. For validation, the results of the different finite element models were compared with the crack patterns of real beam tests. The results clearly demonstrated that both the FE-analysis with the CDP material model and the crack propagation analysis using XFEM showed a good agreement with the tested one.

In 2010 Miehe et al. [19], proposed a new variational framework for rate independent diffusive fracture that bases on the introduction of a local history field. This study followed previous work in Fig. 2-11 on phase-field-type fracture. It contained a maximum reference energy obtained in the deformation. history, which may be considered as a measure for the maximum tensile strain obtained in history. The proposed algorithm was considered to be the canonically simple scheme for the treatment of diffusive fracture in elastic solids. The performance of the phase field

formulation of fracture was demonstrated by means of representative numerical examples.

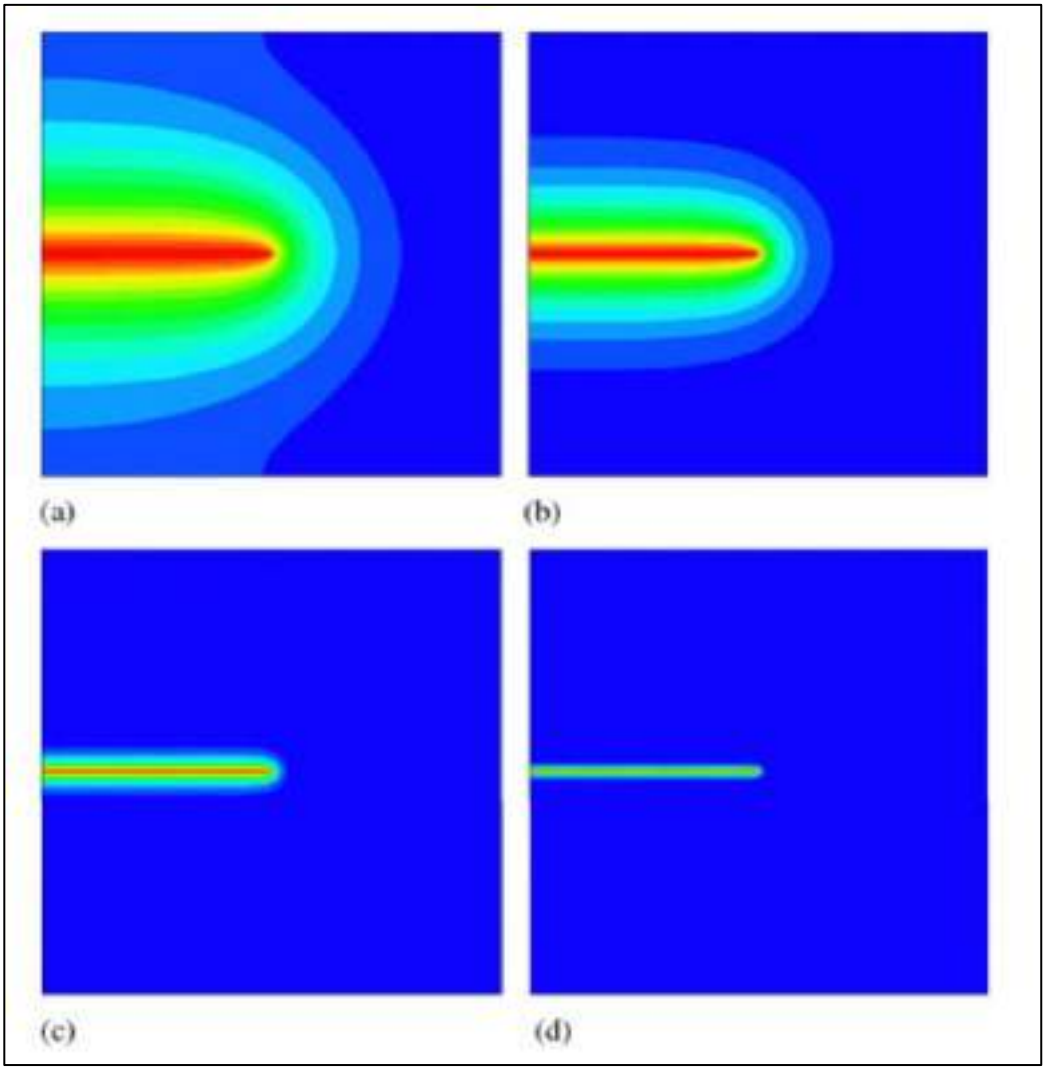

Figure 2.12 Regularized crack surfaces governed by the crack phase-field d for different length scales. (a) lc=0.20, (b) lc=0.10, (c) lc=0.02, and (d) lc=0.007.

In 2020 Kriaa et al. [62], used the finite element method to predict the brittle fracture path using the phase-field approach. A finite element model was developed using MATLAB. A comparative study was performed between the isotropic and the hybrid formulations. Numerical tests were computed to compare these formulations. Because of the lack of experimental validation, tensile tests on double notched specimens made of quenched steel were achieved in order to validate the phase-field

approach. A good agreement between the experimental and numerical results in terms of crack pattern was illustrated for the hybrid formulation. The crack path was found to depend on the axial distance between the two notches. The same phenomena were revealed numerically using the hybrid formulation. Therefore, the phase-field modeling of brittle fracture with the hybrid.

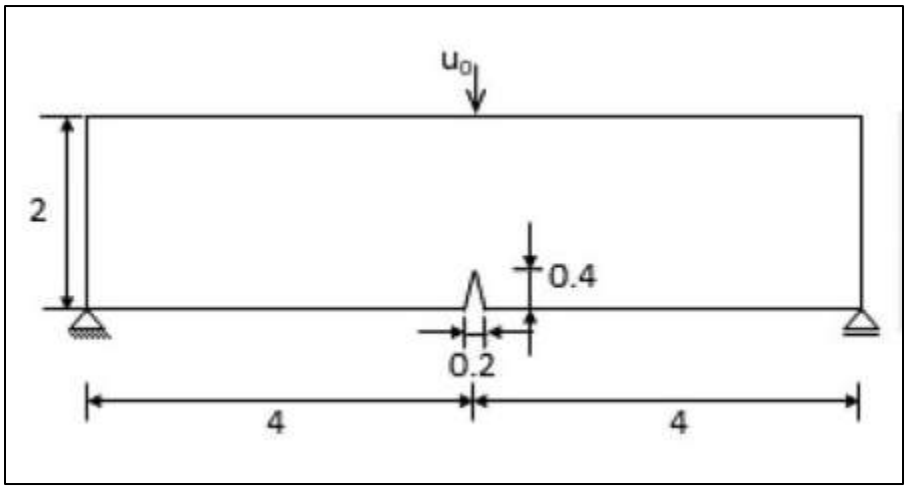

Figure 2.13 The three-point bending test: Geometry and boundary conditions.

2.6 Summary

1. There are limited theoretical or numerical studies deal with Ultra High-Performance Concrete.
2. There are limited numerical studies shear strength of tapered beam.
3. There is limited study to simulate Ultra-High-Performance Concrete, shear strength and tapered beam simultaneously.
4. So, this study came to study this type of member and provide a parametric study on it.

CHAPTER THREE: NUMERICAL FORMULATIN AND MODELING

3.1 General

A numerical analysis known as the finite element method (FEM) is used to produce approximations of solutions to a variety of engineering issues. With the growing usage of high-speed electronic digital computers, the emphasis shifted to numerical methods of engineering analysis.

The fact that the finite element method offered a solution to numerous complex engineering issues was a significant benefit. The fundamental step in solving any problem using finite element analysis is to separate the structure into discrete, non-overlapping elements known as finite elements.

The original structure was as an assembly of these components at a select few joints known as nodes. By the element and the applied-load vector are calculated the stiffness matrix. Behind, compiling the stiffness matrices of the elements and constructing a general stiffness. As well as other, a set of the obtained linear or non-linear algebraic equations is then solve to get nodal outcomes like the values of the moment or the shear force and displacement... etc. significant outcome such as stresses and strains. As per the principles of strength of materials, the basic assumption for all materials is that they are homogenous. Concrete, also for the need of simplification, has been assumed to be homogenous. All the design theories and conclusions on the behavior of concrete had been derived based on this assumption. However, in reality, concrete is a complex mixture of cement, water, silica fume, HARWA, steel fiber and, which makes it a heterogeneous material. In addition, it is

quasi brittle in nature. In the recent past, the study on the damage of concrete has been of interest to forecast its failure due to compression crushing and tensile crack [17]. To study the deformation and stress-strain behavior of concrete, the structure must be analyzed until failure. The deformation of the structure is linearly elastic until a specific limit, and beyond this point, plastic deformation (irreversible) occurs[57]. Currently the advancement in computing techniques and the computational capabilities of high-end computers have led to a better study of the behavior of concrete. However, the complex behavior of concrete sets some limitations in implementing FEM. The complexity is mainly due to the nonlinear stress-strain relation of the concrete. For nonlinear analysis, many commercial software is available, such as ANSYS, ABAQUS, and ADINA. ABAQUS/Standard will be employed in this thesis to study the shear behavior of ultra-high performance concrete tapered beam using a nonlinear finite element analysis and extended finite element analysis [64] .

3.2 ABAQUS Overview

ABAQUS, is one of the largest universal finite element analysis software. It is increasingly commonly used in research worked and engineering. It has high speed, high accuracy, low-cost analysis of the numerical calculation of finite element analysis software, and visualization results, especially when it used in the nonlinear analysis of reinforced concrete structure. [65]

3.3 Finite Element Analysis

3.3.1 Basic Concept

A mathematical formulation of physical problems which depended on assumptions of neglecting certain quantities may reduce the problem into a linear one. Linear solutions are easy and have a less computational cost when compared to

nonlinear solutions. On the other hand, in nonlinear analyses, the aforementioned assumptions are not valid. However, in some cases assumption of linearity may result in an unrealistic approximation of the response. The type of analysis, linear or nonlinear, depends on the goal of the analysis and errors in the system's response that may be tolerated. In some cases, nonlinear analyses are the only option left for the analyst as well as the designer.

3.3.2Nonlinearities Classification

Structures may exhibit nonlinear behavior due to material nonlinearities. Long columns, flexible arches, and some thin shell structures are examples of such special cases. On the other hand, material nonlinearities occur in all reinforced concrete structures and should be considered in any accurate rational analysis[66]. Also consider that the nonlinear stage of its plastic properties when the mechanical properties of the steel and concrete are analyzed. In ABAQUS, the nonlinear characteristics of the material are achieved by the definition of the steel and concrete constitutive model [65].

3.4 ABAQUS Modeling Procedure of Reinforced Concrete Members

The numerical simulation of a reinforced concrete and their constituent components acting as a composite made up of concrete and steel. The simulating procedures are divided into many stages in ABAQUS program addressed as shown in Figure 3.1

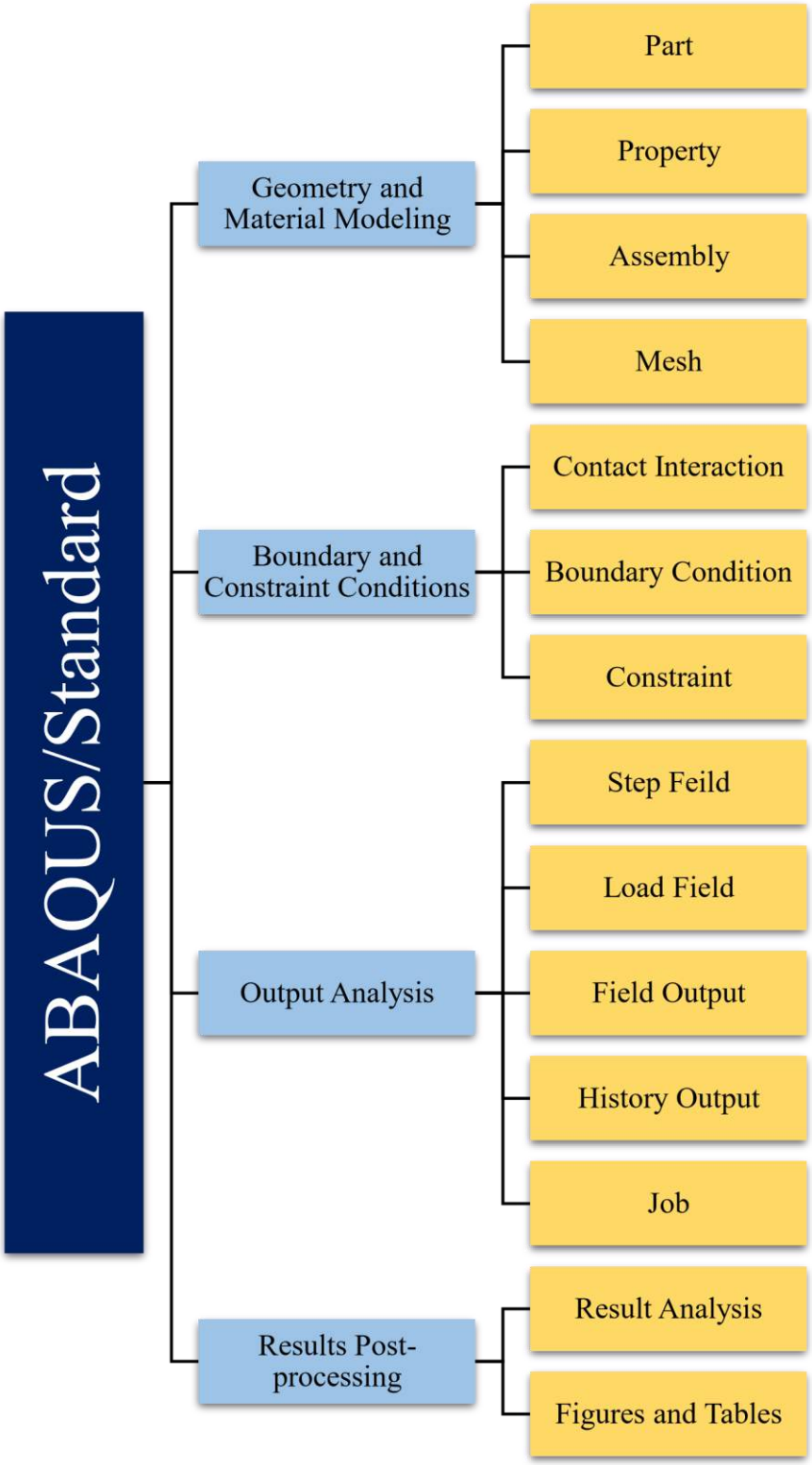

Figure 3.1ABAQUS Modeling Procedure [67].

The necessary stages will be explained in detail to make the finite element models of the reinforced concrete beam [67].

3.4.1 Parts Field

Sketch of each section was created separately with ABAQUS, which can then be extruded in any direction. The concrete beam was defined as a three-dimensional "Deformable" body. The second part was the longitudinal reinforcement.

3.4.2 Material Property

Material field property includes linear and nonlinear stress-strain curves of the material as an input to the components in the part field. The section also assigns the desired material to the part. Each material that is created (concrete or steel), has its own name. Each part (beam or rebar) is an independent geometry. In reinforced concrete beam, the need to define the properties is as follow:

3.4.2.1 Material Model for Concrete

Numerous researchers have come up with different methods and formulae in an attempt to simulate the concrete behavior, both in compression and tension. Concrete itself is a composite structure. It is consisting of a cementitious material that is interlocked together and bound with cement. Therefore, an adequate concrete model needs to be utilized to ensure that the required reliability is obtained. Following five basic parameters are available in the concrete damage plasticity model :

1. **Dilation angle (ψ) :** It is the parameter characterizing the interpreted as a concrete internal friction angle. When the value of the parameter is small the material develops a brittle behavior, in opposition, when the value takes high values, the behavior is close to a ductile one. According to the experimental

results of researchers on a two-point loaded tapered beam, it was observed that this parameter took values between 20° and 45°. Meanwhile, other researchers suggested values between 30° and 55°[67] .

2. **Eccentricity (ϵ)** : Plastic potential eccentricity, ϵ is a small value which expresses the positive rate of the plastic potential-hyperbola to its asymptote. As shown in Fig. (3-2). Eccentricity can be determined as a strength ratio of tensile to compressive strength [68]. Eccentricity = 0.1 is the recommended value in CDP model.

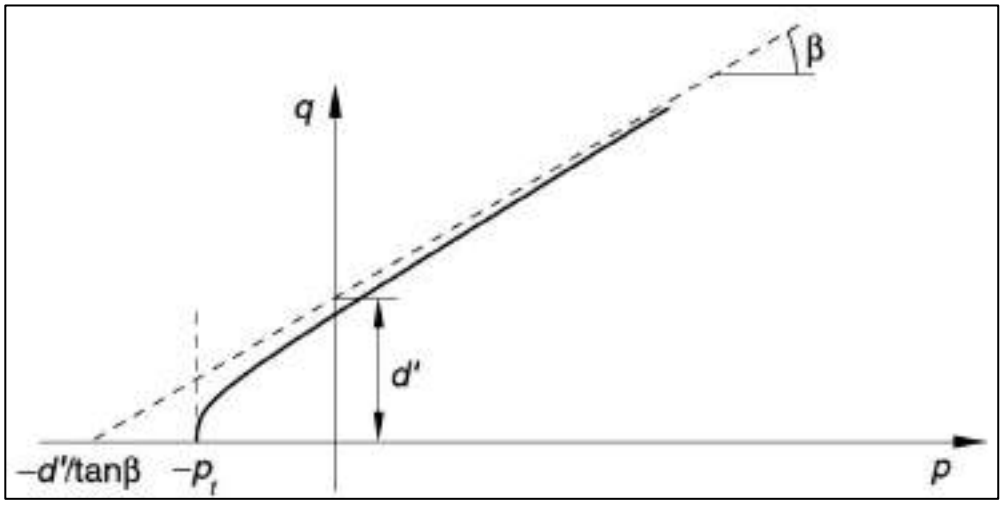

Figure 3.2 Hyperbolic surface of plastic potential in meridional (p-q) plane. $\boldsymbol{pt}$: initial hydrostatic tension strength, $\boldsymbol{\beta}$: friction angle, $\boldsymbol{d}$: hardening parameter.

3. **Strength ratio σb0/σc0 :** Another parameter describing the material state Fig. (3-4) [67]. The most reliable in this regard are the experimental results reported [56]. As approximation (fb0 / fc0) with the elliptic equation, uniform biaxial compression strength is equal to 1.16248 fcm, where fcm is compression strength.

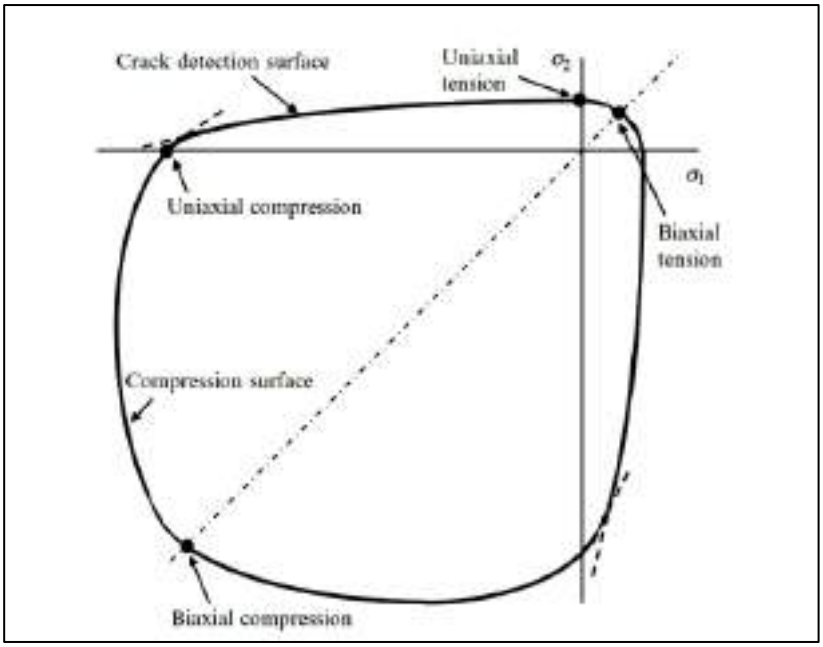

Figure 3.3 Strength of concrete under biaxial stress in CDP model .[68]

4. ***Kc***: Its parameter that governing the deviatoric failure surface of the cross section instead of a circle Fig (3-4). Physically, parameter Kc is interpreted as a ratio of the distances between the hydrostatic axis and respectively the compression meridian and the tension meridian in the deviatoric cross section. The default value is always above 0.5, while the failure surface of the cross section becomes a circle at 1.0 value (as hypothesis strength of Drucker–Prager). Kc= 2/3 is the recommended value in CDP model. This shape is similar to the strength criterion (a combination of three mutually tangent ellipses) formulated by William and Warnke (1975). It is a theoretical-experimental criterion based on triaxial stress test results. [68] Kc= 2/3 is the value used in this thesis.

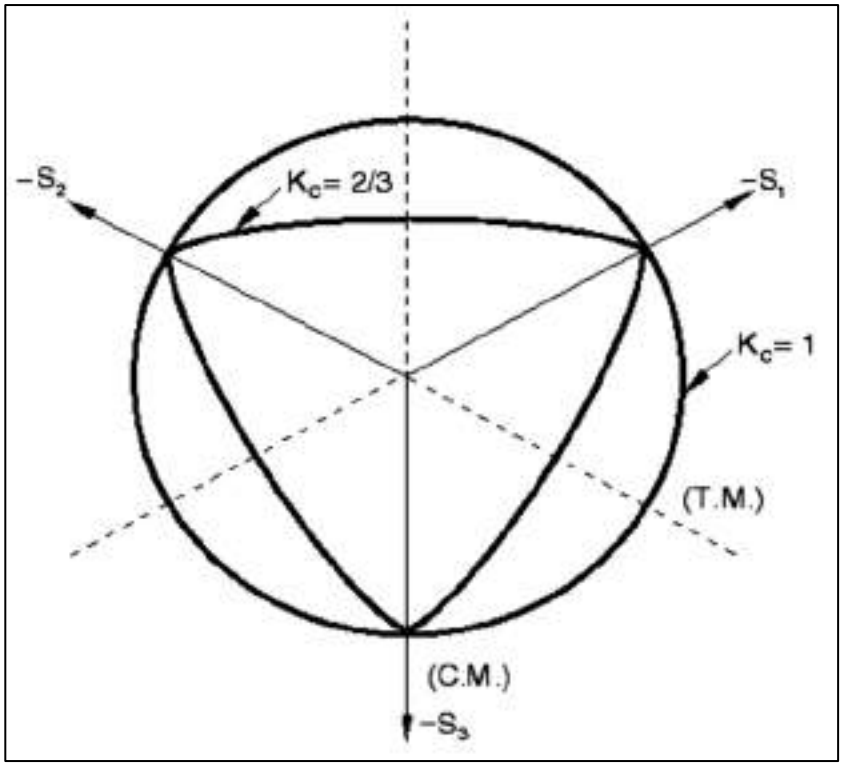

Figure 3.4 Deviatoric cross-section of failure surface in CDP model [68].

5. **Viscosity parameter (ŋ)** : It is also known as relaxation time. Advanced material models which develop stiffness degradation and strain softening, lead to convergence issue. One of the most popular techniques to overcome this kind of problems is the constitutive equations regularization, in which for small increments of time the tangent stiffness of the material become positive .

The viscosity parameter default value is zero in ABAQUS/Standard [68]. Therefore, the viscosity parameter was used 0.0001 in this study. The unquestionable advantages of the CDP model are the fact that it is based on parameters having an explicit physical interpretation. The exact role of the above parameters and the mathematical methods used to describe the development of the boundary surface in the three-dimensional space of stresses are explained in ABAQUS user's manual. The parameters of CDP model that are used in the current study are listed in Table (3-1).

3.4.2.1.1 Stress-strain Curve for Uniaxial Compression

According to plasticity theory, yield limit is the limit below which the material property remains elastic and further loading beyond this point causes plastic flow[57]. Compression and tension behavior in the form of plasticity and damage coefficient is required to create the FE model.

Table 3.1 Parameters of CDP model under compound stress.

Parameter	Default Value	Used in Present Study
Eccentricity	0.1	0.1
Dilatation angle	36	39
f_b0/f_c0	1.16	1.16
K_c	0.667	0.667
Viscosity parameter	0	0.0001

The elastic properties of the material are specified by the passion's ratio (v) which is taken as 0.2.

The stress-strain relationship of UHPC exhibits linear behavior up to 80% of compressive strength, then the nonlinear behavior in strain-softening beyond compressive strength occurs [69], as illustrated in Figure. (3-5). The required stress-strain relation in ABAQUS is represented by the first crack stress until the peak state, along with the strain-softening as a regression portion of the curve. The corresponding strain represents the inelastic strains that cause the cracks to initiate and propagate. Most previous research that numerically analyzed the UHPC beams relied on the representation of concrete by CEB-FIP code equations or some other equations for high-strength concrete. There are no equations available to simulate UHPC. Therefore, a model proposed to simulate that behavior as follows;

For $\sigma c < f'_{cf}$ and $\varepsilon_c \leq \varepsilon_{co}$ at f'_{cf}

The ascending portion of stress (ε_c) up to compressive strength (f'_{cf}) can be represented by the following equation, based on the Hognestad parabolic stress-strain relation.

$$\sigma_c = f'_{cf} [667\ \varepsilon_c - (333\ \varepsilon_c)^2] \quad 3.1$$

(ε_{co}) is the strain at compressive strength (f'_{cf}) and is calculated as follows;

$$\varepsilon_{co} = 2.564\times 10^{-4}\sqrt{f'_{cf}} \quad 3.2$$

The inelastic strain that is required in ABAQUS is found as follows;

$$\varepsilon^{in} = \frac{\sigma_c}{E_c} \quad 3.3$$

The elastic modulus of UHPC is estimated as follows;

$$E_c = 3900\sqrt{f'_{cf}} \quad 3.4$$

The continuity of linear behavior to 80% of compressive strength does not mean that the first crack occurs at that stress. When the first crack arises in UHPC, the stresses transmit to the fibers, which are worked to maintain the linear behavior. When the stress exceeds 80% of compressive strength, the behavior turns nonlinear. This behavior occurs due to increasing the applied stress over the bonding stress between the fiber and the matrix causing fibers to slip and cracks to widen. Therefore, the cracking stress can consider at 30 % of compressive strength. This value of stress is compatible with the suggestion of FHWA in computing the elastic modulus [68], which suggests using values that correspond to 10% and 30% of the ultimate compressive strength. Therefore, the cracking strain is;

$$\varepsilon_{cr} = \frac{0.3\ f'_{cf}}{E_c} \qquad 3.5$$

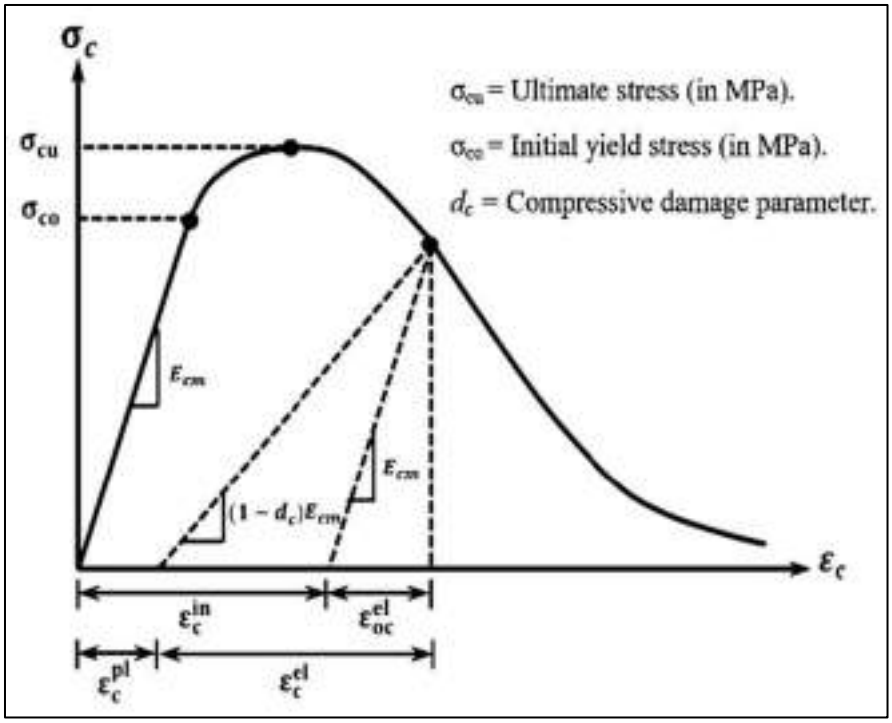

Figure 3.5 Definition of inelastic strains[70].

The most popular formulas are presented in Table (3-2).

Table 3.2 Stress-strain relation for nonlinear behavior of structure.[68]

Formula name/source	Formula form	Variables
Madrid parabola	$\sigma_c = E_c\ \varepsilon_c\ [1 - \frac{1}{2}(\frac{\varepsilon c}{\varepsilon c1})]$	$\sigma_c = f\ (E_c, \varepsilon_c)$
Desay & Krishnan formula	$\sigma_c = \frac{Ec\ \varepsilon c}{1+\left(\frac{\varepsilon c}{\varepsilon c1}\right)^2}$	$\sigma_c = f\ (E_c, \varepsilon_c)$
EN 19921-1	$\sigma_c = f_{cm}\left[\frac{k\eta - \eta^2}{1+(k-2)\eta}\right]$ $k = \frac{1.05Ecm\ \lvert\varepsilon c1\rvert}{fcm}, \eta = \frac{\varepsilon_c}{\varepsilon_{c1}}$	$\sigma_c = f\ (E_c, \varepsilon_c)$

Majewski formula	$\sigma_{c=\ c}\,\varepsilon_c\ if\ \sigma_c \le e_{\lim} f_{cm}$ $\sigma_c = f_{cm}\frac{(e_{\lim}-2)^2}{4(e_{\lim}-1)}\left(\frac{\varepsilon_c}{\varepsilon_{c1}}\right)^2 \pm$ $f_{cm}\frac{(e_{\lim}-2)^2}{2(e_{\lim}-1)} + f_{cm}\frac{e_{\lim}{}^2}{4(e_{\lim}-1)},$ $E_c = \frac{f_{cm}}{\varepsilon_c}(2 - e_{\lim}).$	$\sigma_c = f(E_c, \varepsilon_c)$

Where,

σ_c = Compressive stress of concrete (MPa) that validated for $0<|\varepsilon c|<\varepsilon cu1$.
$\boldsymbol{k}$ = Coefficient Factor.
$\boldsymbol{\varepsilon_c}$ = Compressive strain in the concrete.
$\boldsymbol{\varepsilon_{c1}}$ = Compressive strain in the concrete at the peak stress fcm.
f_{cm} = Mean value of concrete cylinder compressive strength (in MPa).

The characteristic compressive strain of concrete is taken as 0.002 at an ultimate strength 153.3 MPa as specified in Tu'ma et al. [71].

3.4.2.1.2 Tensile Strength of Concrete

Several studies tested the applicability of the CDP model to simulate the tensile behavior of fibrous concrete and UHPC. Othman and Marzouk [79] adopted the CEB-FIP model code (1990) to represent the compressive and tensile stress-strain behavior of UHPC. Chen and Graybeal [80] used a bilinear elastic-perfect plastic tensile behavior up to an ultimate strain of 0.0084. Zhang et al. [81] proposed a four-linear relationship to capture the effect of UHPC ductility after cracking. A new model adopted in this study consists of a linear portion to simulate the elastic tensile behavior up to cracking. The descending part consists of a tri-line. The first descending line is to 75% of the tensile strength (f_t) with a corresponding strain of four times cracking strain (ε_{cr}), considering that the UHPC loses 25% of its stiffness when a crack occurs and fibers contribute to bearing 75% (the remaining stiffness) due to transferring the tensile stresses to them. Next, the strain increases to 12 ε_{cr}

with tensile stress decreasing to 50%. That is due to debonding of the fibers from the matrix. Then the debonding fibers increase further upon propagation and enlargement of cracks until reaching an ultimate strain equal to 24 ε_{cr} with 10% remaining tensile stress, as depicted in Figure (3-6). The following equations represent that behavior;

For $\varepsilon_t \leq \varepsilon_{cr}$

$$\sigma_c = \varepsilon_t E_c \quad 3.6$$

Assuming the elastic modulus is the same for both tensile and compressive states, the cracking strain is;

$$\varepsilon_{cr} = \frac{f_t}{E_c} \quad 3.7$$

Where ε_t is the tensile strain of concrete at tensile stress, at, while f_t is the peak tensile strength. ε_{cr} is the cracking strain in tension.

For descending tri-linear tensile behavior;

For $\varepsilon_{cr} < \varepsilon_t \leq 4\,\varepsilon_{cr}$

$$\sigma_c = f_t\left[\frac{13}{12} - \frac{1}{12}\frac{\varepsilon_t}{\varepsilon_{cr}}\right] \quad 3.7$$

For $4\,\varepsilon_{cr} < \varepsilon_t \leq 12\,\varepsilon_{cr}$

$$\sigma_c = f_t\left[\frac{10.5}{12} - \frac{0.375}{12}\frac{\varepsilon_t}{\varepsilon_{cr}}\right] \quad 3.8$$

For $12\,\varepsilon_{cr} < \varepsilon_t \leq 24\,\varepsilon_{cr}$

$$\sigma_c = f_t\left[\frac{10.8}{12} - \frac{0.4}{12}\frac{\varepsilon_t}{\varepsilon_{cr}}\right] \quad 3.9$$

The elastic tensile strain, ε_t^{el}, and inelastic tensile strain, ε_t^{in} are computed as follows;

$$\varepsilon_t^{el} = \frac{\sigma_t}{E_c} \quad 3.10$$

$$\varepsilon_t^{in} = \varepsilon_t - \varepsilon^{el} \quad 3.11$$

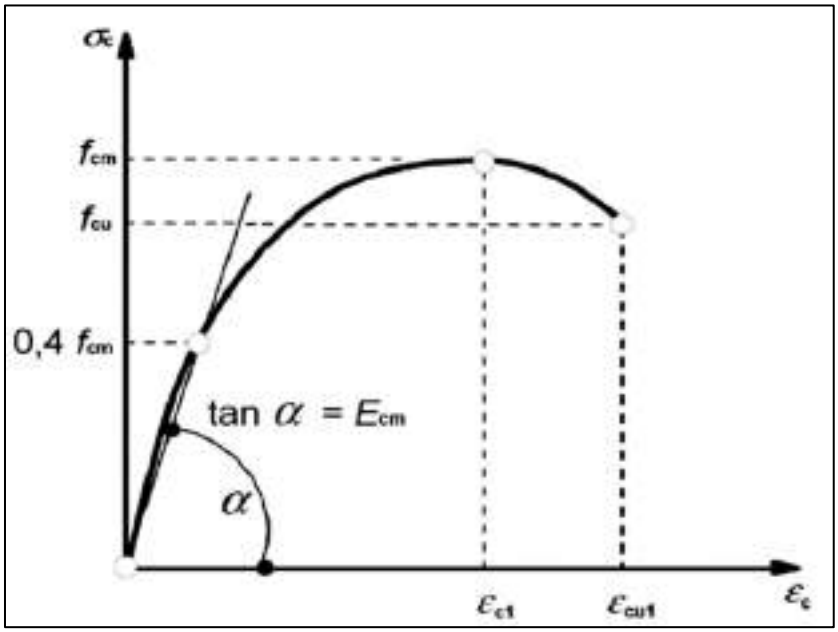

Figure 3.6 The relation of stress-strain for structural analysis of concrete material [68].

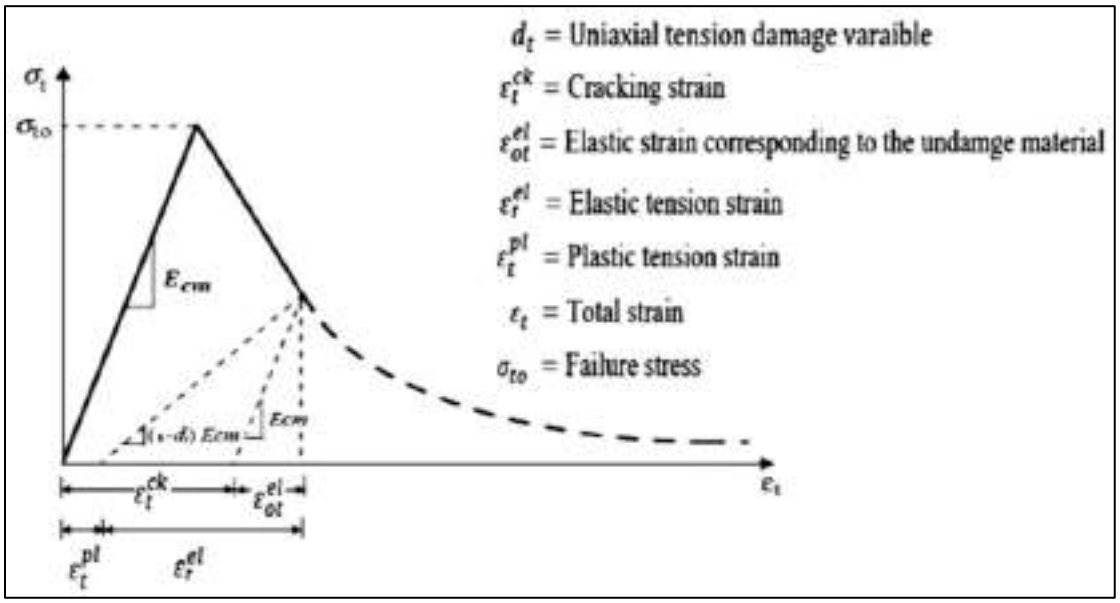

Figure 3.7 Stress-strain relationship of concrete in uniaxial tension[70].

3.4.2.1.3 Compression and Tension Damage Variables (d_c) and (d_t)

Stiffness degradation factors for compression (d_c) and tension (d_t) are other important parameters in ABAQUS for damage plasticity model to describe concrete

stresses evolution when the concrete material reaches the peak stress. They are assumed to be functions of the plastic strains. If the damage is not specified, the model behaves as a plasticity model;

consequently,

$$(\boldsymbol{\varepsilon}^{pl}_t = \boldsymbol{\varepsilon}^{ck}_t\,,\ \boldsymbol{\varepsilon}^{pl}_c = \boldsymbol{\varepsilon}^{in}_c). \qquad 3.12$$

The evolution law [d_c - $\boldsymbol{\varepsilon}^{in}_c$] was identified to consider the compression damage of concrete after it reaches the concrete peak stress, where d_c and $\boldsymbol{\varepsilon}^{in}_c$ are the compressive damage parameter and compressive inelastic strain, respectively. Similarly, the evolution law [d_t - $\boldsymbol{\varepsilon}^{in}_t$] was specified to capture the tensile damage of concrete when reaching the concrete tensile strength, in which dt and $\boldsymbol{\varepsilon}^{in}_t$ are the tensile damage parameter and cracking strain of concrete, respectively. $\boldsymbol{\varepsilon}^{in}_t$ is determined as the total strain minus the elastic strain according to the undamaged material .

Numerous methods are available to achieve the damage parameter. Nguyen and Kim [72] presented the following relations for defining prescribed parameters, d_c and d_t for compression and tension, respectively:

$$d_c = 1 - \frac{\sigma_c}{f_{cm}} \qquad 3.13$$

$$dt = 1 - \frac{\sigma_t}{f_t} \qquad 3.14$$

3.4.2.2 Material model for steel

The other basic component in this study is the bars for longitudinal reinforcement. The reinforcing bars have mainly the task to transfer normal forces . An elastic perfectly plastic model was used for the steel bar with an equal behavior in tension and compression. ABAQUS software required input data of Young Modulus (E_s) and Poisson 's ratio (v) to represent the elastic behavior, yield stress (f_y), and the inelastic strains for defining the plasticity behavior as shown in Fig.3.8

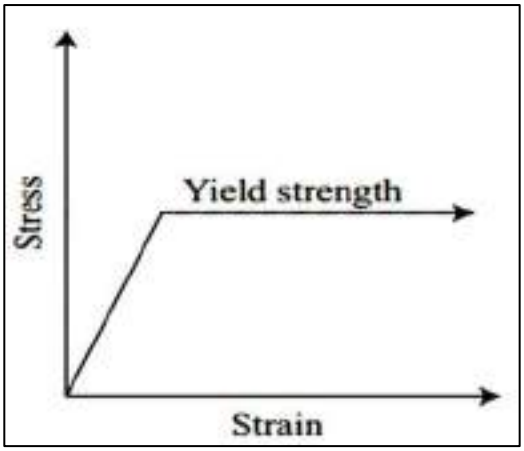

Figure 3.8 Behavior of steel.

3.4.3 Assembling

After creating the parts individually, they must be assembled to simulate the structural members as shown in Fig. (3-9).

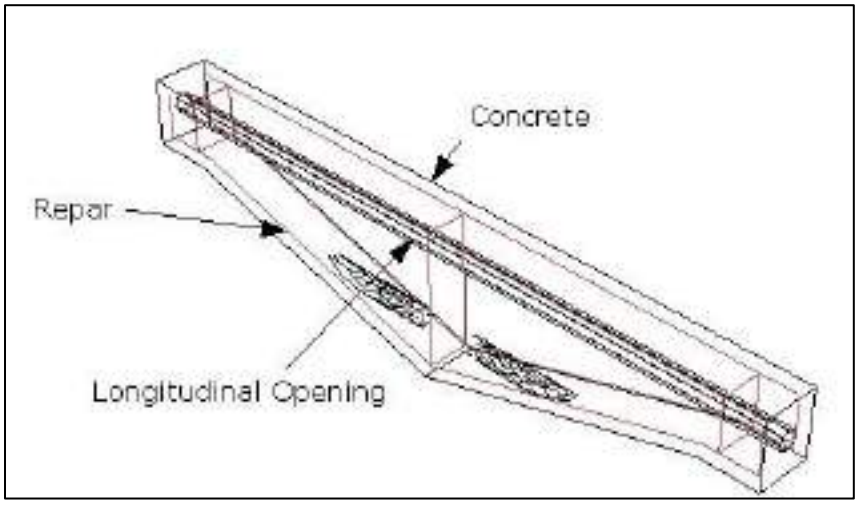

Figure 3.9 Assembling of beam parts.

3.4.4 Defining Step

Newton–Raphson equilibrium iterations provide convergence at the end of each load increment within tolerance limits for all degrees of freedom in the model. Residual load vector, which is the difference between the internal forces (the loads corresponding to the element stresses) and the externally applied loads are analyzed again by Newton–Raphson approach. Subsequently, the program carries out a linear

solution using residual loads and considering the initial stiffness of the structure, to check the convergence criteria. [73]

3.4.5 Interaction Between Elements

Once all parts are assembled at appropriate locations, a proper constraint is used to describe the interaction between components. In FEM, contact interaction is an important aspect. The fact is that the physical processes are important aspects and must be taken into account in boundary conditions and surface interactions in numerical simulation. An inappropriate definition may have an undesirable effect on the simulation overhead. ABAQUS/Standard provides more than one approach for contact definition including surface interaction, constraints, and contact condition procedure in the program.

3.4.6 Specify Boundary Conditions and Load

In this stage boundary and loading conditions are also specified. The reinforced concrete beam was simply supported as shown in Fig. (3-10). It was reinforced with singly longitudinal reinforcement without transverse reinforcement to explore the fracture behavior of shear failure. two-point loading were investigated in this study. The load was displacement controlled.

3.4.7 Meshing and Element Type

Meshing is the process of generating nodes and elements. A mesh is generated by defining nodes and connecting them to define the elements.

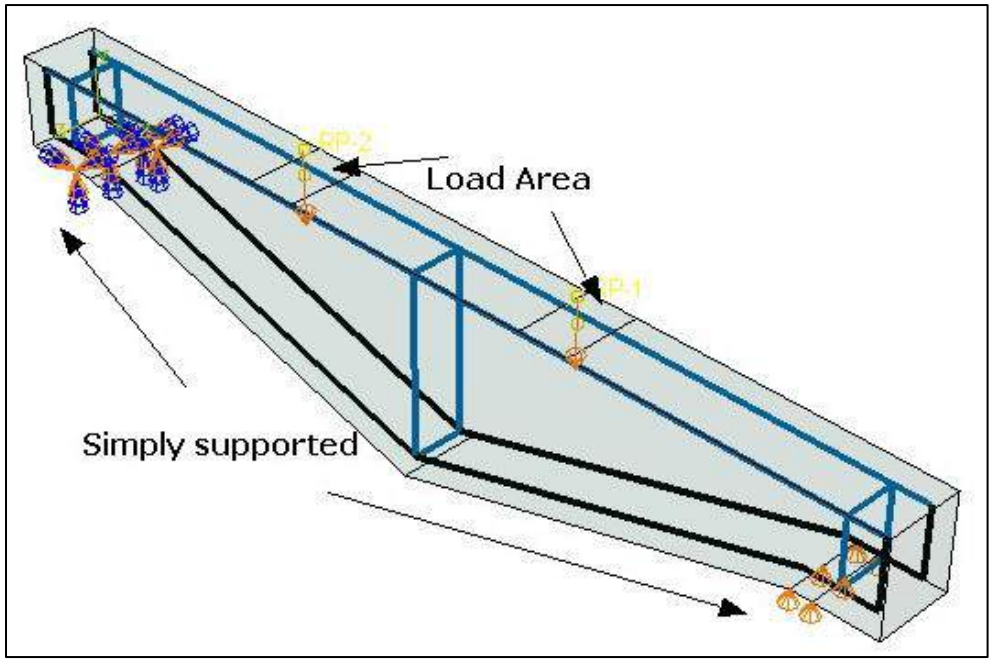

Figure 3.10 Boundary conditions of beam under two-point load.

To obtain accurate results from the FE model, all the elements in the model were purposely assigned the same mesh size to ensure that each of the two different materials shares the same node [70].

3.4.7.1 Solid Element

The concrete beam was modeled with C3D4, which is a three-dimensional 4-node mesh with a grain size of 3 cm element from the ABAQUS library as shown in Fig. (3-12). Linear approximation of displacement, reduced integration, eight nodes and three translational degrees of freedom were used. Stress at various points throughout the thickness of the element can be provided at each integration point. The first-order interpolation elements such as hexahedral exhibit potential stiff behavior with a slow convergence rate but prevent potentially mesh locking when a reduced integration analysis procedure is used, whereas second-order elements provide higher accuracy [74]. However, first-order elements were used to accurately provide the model for contact surfaces and prevent compact contact condition.

3.4.7.2 Beam Element

The reinforcement steel bar can be modeled as a wire in ABAQUS. The wire is 2-noded beam elements (A 2-node linear beam) having 3 degrees of freedom in each node (translations in X, Y and Z directions). The thickness of the wire is not geometrically modeled; however, a cross-sectional area is specified as input .

Beam elements are used A 2-node linear beam element to model slender, line-like structures that support loading only along the axis or the centerline of the element. No moment or forces perpendicular to the centerline are supported. A 2-node straight beam element that uses linear interpolation for position and displacement and has constant stress is available in ABAQUS/Standard [75]. For the reinforcing steel, a 2-noded beam elements (A 2-node linear beam) as shown in Fig. 3-11.

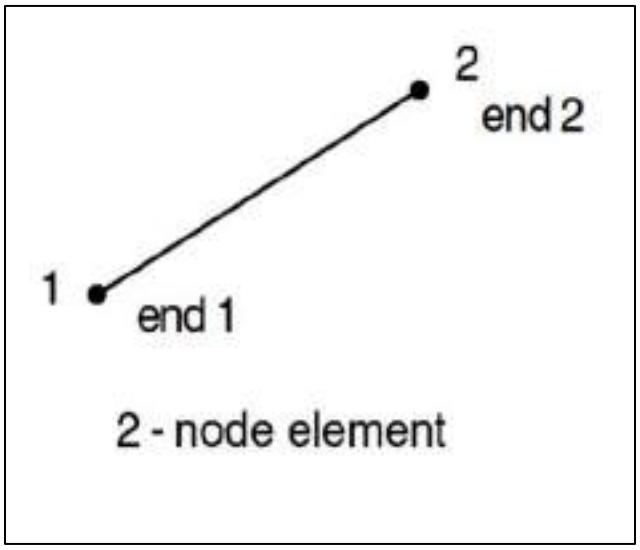

Figure 3.11 A 2-node linear beam description[74].

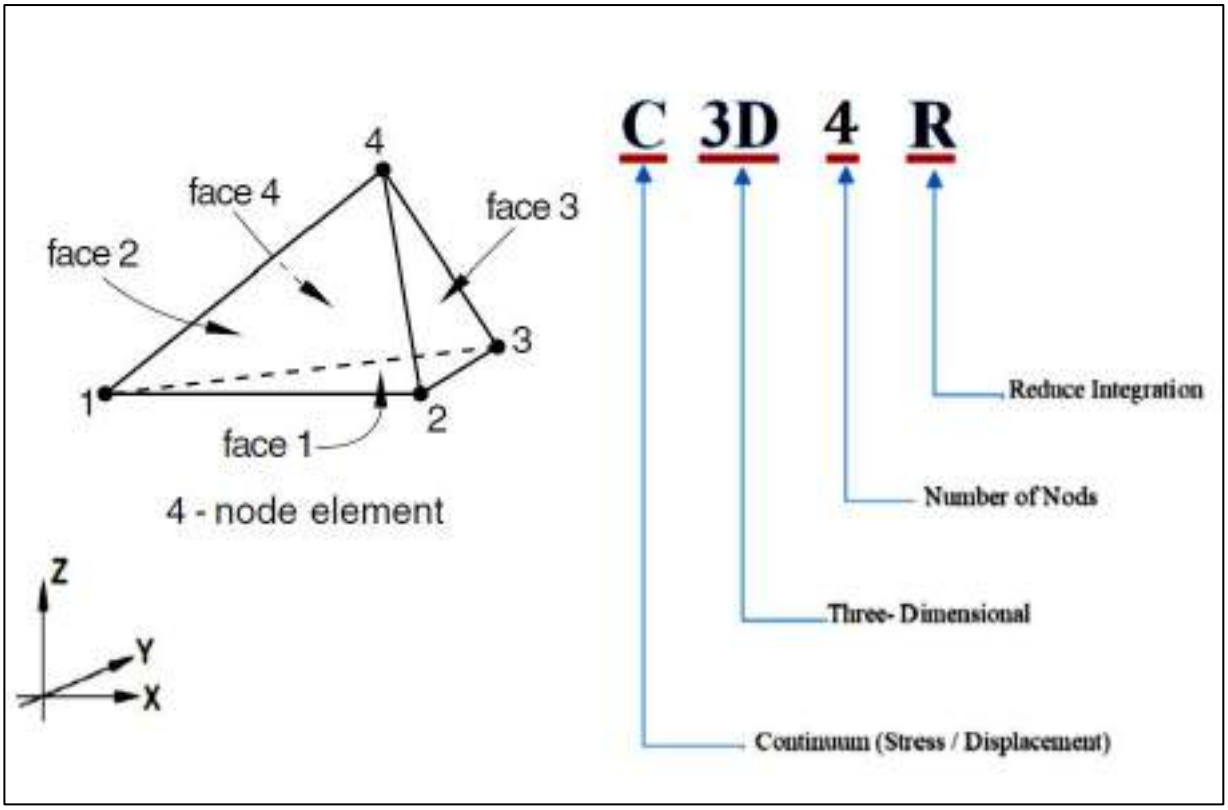

Figure 3.12 C3D4R element description[74].

3.4.8 Assigning Job

To solve any type of finite element problem, the relevant job analysis should be established. After creating job analysis, the data should be checked and submitted to get the results and visualized analytically .

3.4.9 Evaluating the Results

In this stage, the output results of the model can be evaluated such as the stress distribution, deflections, ultimate strength etc.

3.5 Numerical Formulation

3.5.1 The Fundamental Relationships

The derivation of the stiffness matrix as we learned earlier for the finite element is principle in any finite element analysis (FEA) that relates the

displacement vector (a) to the force vector (f), in order to derive this relationship, three condition must be met;

1. Stress-strain relations - constitutive relations.
2. Equations of equilibrium - equilibrium condition.
3. Compatibility of strains and displacements - kinematic condition.

The three–dimensional body in the FE analysis is represented by a number of elements, and a finite number of nodes that are identified on each element. Where the elements are to be joined. The equilibrium equation for a nonlinear structure in a static equilibrium is derived using the principle of virtual work [76], thus

$$W_{int.} = W_{ext.} \tag{3.15}$$

Where;

$W_{int.}$ = Internal work (strain energy) .
$W_{ext.}$ = External work (done by the applied force) .

The virtual internal work is :

$$\boldsymbol{W_{int.}} = \int_V \{\partial\, \varepsilon\}^T \{\sigma\} dV \tag{3.16}$$

Where :

$\{\partial\varepsilon\}$ = Elements of virtual strain vector.
$\{\sigma\}$ = Elements of real stress vector .
dV = Infinitesimal volume of the element .

By using the general stress-strain relationship, stresses $\{\sigma\}$, can be determined from the corresponding strains $\{\varepsilon\}$ as :

$$\{\sigma\} = [D]\{\varepsilon\} \tag{3.17}$$

Where :

$[D]$ = The constitutive matrix .

After substituting Eq. (3-17) into (3-16), the virtual internal work can be written as :

$$\boldsymbol{W_{int.}} = \int_V \{\partial\ \varepsilon\}^T\ \{D\}\{\varepsilon\}dV \qquad 3.18$$

The displacements $\{U\}$ within the element are related by interpolation function to nodal displacements $\{a\}$ by :

$$\{U\} = [N]\{a\} \qquad 3.19$$

Where :

$\{U\}$ = Body displacements vector (global displacements) .

$[N]$ = Shape function matrix .

$\{a\}$ = Unknown nodal displacements vector (local displacements) .

By differentiating Eq. (3-19), the strains for an element can be related to its nodal displacements by :

$$\{\boldsymbol{\varepsilon}\} = [B]\{a\} \qquad 3.20$$

Where :

B = Strain-nodal displacement relation matrix, based on the element shape functions.

Assuming that all effects are in the global Cartesian system, and then combining Eq. (3-20) with Eq. (3-18) yields:

$$\boldsymbol{W_{int.}} = \{\boldsymbol{\partial a}\}^T \int_V [B]^T\ [D][B]dV\,\{a\} \qquad 3.21$$

The external work, which is caused by the nodal forces applied to the element, can be accounted for by :

$$\boldsymbol{W_{ext.}} = \{\boldsymbol{\partial a}\}^T\{\boldsymbol{F}\} \qquad 3.22$$

Where :

$\{F\}$ = Nodal forces applied to the element .

Finally, Eqs. (3-15), (3-21) and (3-22) may be combined to give :

$$\{\boldsymbol{\partial\, a}\}^T \int_V [B]^T\ [D][B]dV\ \{\boldsymbol{a}\} = \{\boldsymbol{\partial a}\}^T\{\boldsymbol{F}\} \qquad 3.23$$

Noting that $\{\partial a\}^T$ vector is a set of arbitrary virtual displacements, the condition required to satisfy Eq. (3-23) can be reduced to :

$$[\boldsymbol{K^e}]\{\boldsymbol{a}\}=\{F\} \tag{3.124}$$

Where :

$$[\boldsymbol{K^e}] = \int_V [\boldsymbol{B}]^{\boldsymbol{T}} [\boldsymbol{D}][\boldsymbol{B}]\boldsymbol{dV} \tag{3.25}$$

Where;

$[K^e]$ = element stiffness matrix

dV = dx dy dz

Eq. (3-24) represents the equilibrium equation on a one-element basis. For all elements, the overall stiffness matrix of the structure $[K]$ is built up by adding the element stiffness matrices (adding one element at a time), after transforming the local to the (overall) global coordinates, this equation can be written as :

$$[\boldsymbol{K}]\ \{\boldsymbol{a}\}=\{\boldsymbol{F^a}\} \tag{3.26}$$

Where:

$[K] = \Sigma[K^e]$ = Overall structural stiffness matrix .

$\{\boldsymbol{F^a}\}= \{F\}$ = vector of applied loads (total external force vector).

n = Total number of elements .

3.5.2 The Procedures of Model in ABAQUS

The model analysis has four parts :

1. Material and geometry modeling.
2. Constraint and boundary conditions.
3. Analysis output.
4. Results of Post-processing.

The necessary software packages are ABAQUS. The source code in this study was in Appendixes A and B.

CHAPTER FOUR: RESULT AND DISCUSSIONS

4.1 General

A numerical investigation of the shear strength for the UHPC tapered beam have longitudinal openings was done. The study topics can be divided into the verification with experimental results which is carried out to check the validity and accuracy of the FE procedure. The experimental results were compared with the results obtained by FEM in terms of shear strength, load-deflection curves, crack patterns. The study also addressed the impact various parameters study that were expected to affect the behavior of these beams. These parameters are:

1. Existence of Steel Stirrups, to know its contributions on the overall shear capacity.
2. Longitudinal openings: study number, diameter and location of openings effect of shear capacity.
3. Shear Span Effect: study shear spans effective depth a/d ratio effect.
4. Reinforcement Ratio: study longitudinal and transvers reinforcement effect of shear strength.
5. Scale Factor: study multi semi-scale factor effect on the geometry of the model.
6. Crawn Length: study tapered length effect on the geometry of tapered beam.

4.2 Discretization of Finite Element

Three-dimensional finite element models using ABAQUS software are developed to simulate the tapered beam.

An important step in finite element modeling is mesh density selection. The convergence results are obtained by dividing the structure into a sufficient number

of elements. This is properly adopted when the mesh density has negligible influence on the results. The same properties of the tapered beam material were simulated with element size increasing. The load capacity for the same vertical displacement is the response parameter used for this comparison. 19155, 23685, 39118, 50366, and 65800 elements are used to carry out the accuracy of the convergence results. Table (4-4) shows the conclusions of comparison results and the two parameters' responses.

Table 4.1Convergence of results

No.	Total Time (Minute)	Number of Elements	Number of Nodes
1	19	19155	4316
2	20	23685	5363
3	39	39118	8537
4	55	50366	10817
5	76	65800	13929

4.3 Verification Study: Experimental – Numerical Comparative Analysis

In the current study, the structural behavior of non-prismatic beams with simply supported boundary condition is simulated depending on available experimental test [71]. According to that experimental work, nineteen reinforced concrete beams classified into six groups under two-point loading. The first group studied the inclination angle effect. Other groups has many variable such as steel fiber ratio, tensile bars, strengthen by NS-bar and CFRP sheet et al. The same flexural steel reinforcement quantity was provided (2φ25), (4 φ16), and (2 φ16 +2 φ12) along the length of beams 1900mm in different of specimens. The width was 150mm, depth at support H1 was 180 cm, the depth at mid-span varies as H2 = 175 H1 (315mm), H2 =2 H1 (360mm) and H2 = 225 H1 (450mm) which corresponds to the inclination angle of 9.7°, 12.8° and15.9°; respectively. All the openings were

done by using PVC pipes with a diameter φ 50 mm in both prismatic and non-prismatic sections. The whole details of the beam are listed in Figure 4.1 and Table 4.1. Only nine of non-prismatic beams were utilized in this study for the validation process. for the verification purpose in terms of Shear strength-deflection curve, ultimate shear strength and crack patterns. Table 4-2 clearly exhibits the verification analysis; the predicted rates are varied between 0.96 to 1.07. The experimental-numerical comparative views that relate to shear strength-deflection responses of developed beams illustrated in Figure 4-3. The developed numerical model is succeeded to indicate beams responses numerically with highly convergence with the corresponding experimental results and the responses of various specimens exhibit approximately the same flexural stiffness behavior.

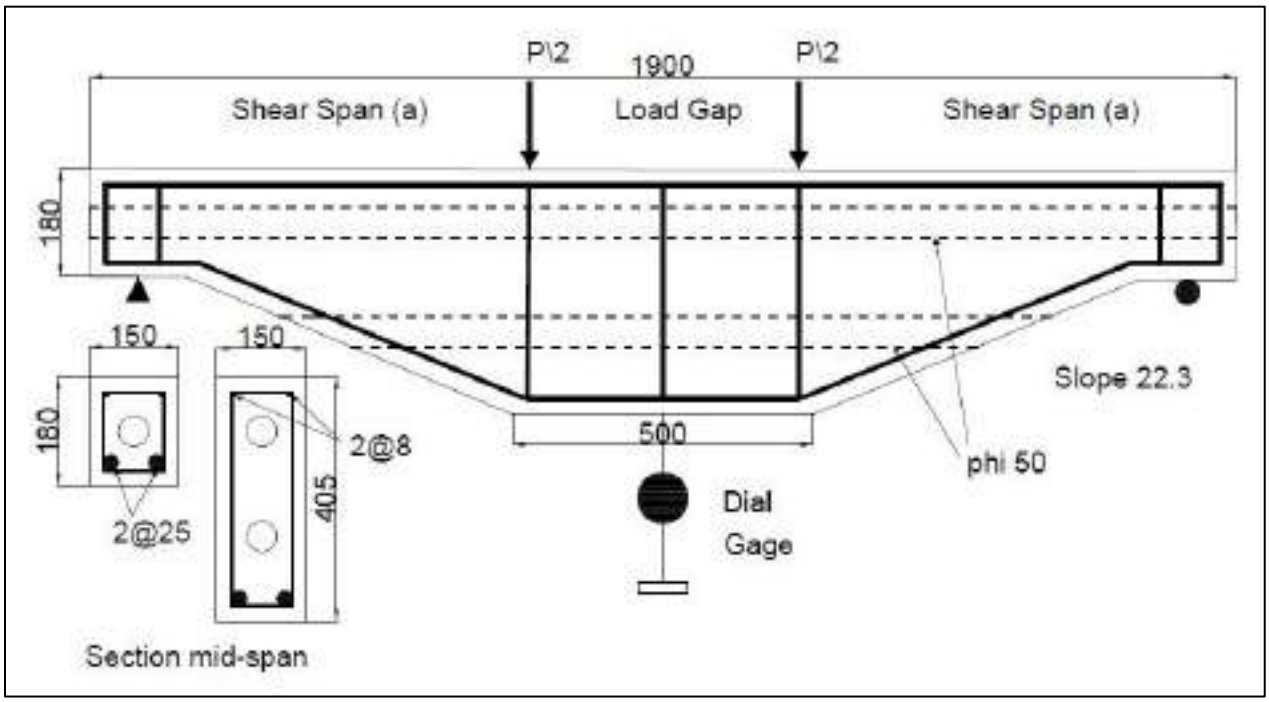

Figure 4.1 Geometry and details of tested beams.

Table 4.2 Specimen Detail of experimental test groups.

Beam ID	Tensile bar	a/d	No. of Openings	Inclination Angle
TB 2				9.7
TB 3	2φ25mm	2.73	Two	12.8
TB 10				15.9
TB 5			One in H1	
TB 6	2φ25mm	2.3	One in H2	15.9
TB 9			Two	
TB 7	2φ12mm+2φ16mm			
TB 8	4φ16mm	2.73	Two	15.9
TB 10	2φ25mm			
TB 1		2.94		
TB 9	2φ25mm	2.3	Two	15.9
TB 10		2.73		

Table 4.3 The ultimate load and deflection of the verification results.

Group	Code	$Vu_{(EXP)}$	$Vu_{(FEA)}$	$RP_{(EXP/FE)}$	$\Delta_{(EXP)}$	$\Delta_{(FEA)}$	$RP_{(EXP/FEA)}$
1st	TB 2	362	367	0.99	9.3	10.8	0.86
	TB 3	375	388	0.97	15	13.9	1.08
	TB 10	432	403	1.07	17.35	18.9	0.92
2nd	TB 5	462	454	1.02	15.5	16	0.97
	TB 6	486	499	0.97	17.59	16.9	1.04
	TB 9	460	451	1.00	15.45	17.6	0.88
3rd	TB 7	370	386	0.96	13.11	14.4	0.91
	TB 8	446	457	0.98	18.49	17.2	1.08
	TB 10	432	403	1.07	17.35	18.9	0.92
4th	TB 1	416	406	1.03	12.1	12.7	0.95
	TB 9	460	451	1.02	15.45	17.6	0.88
	TB 10	432	403	1.07	17.35	16	1.08
Mean				0.99			0.96
Standard Deviation				0.034			0.077

Besides, the companied failure modes that summarized the overall beams deformation under the action of applied loads till failure limit are illustrated in Figure

4-4 which shows the numerically predicated cracks patterns and total strain distribution that clearly confirmed cracks trends in the experimental study.

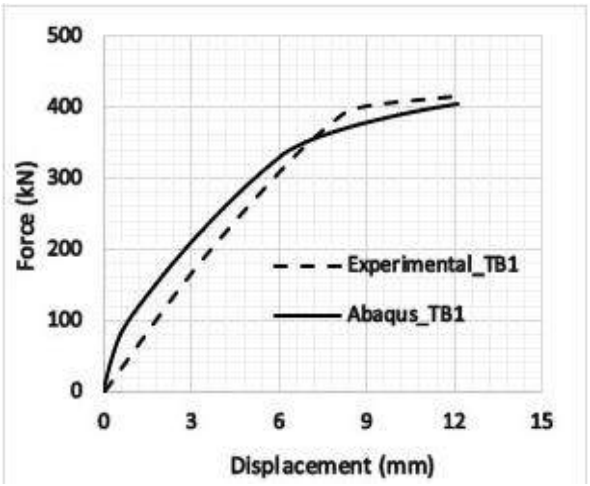

a. (TB1)

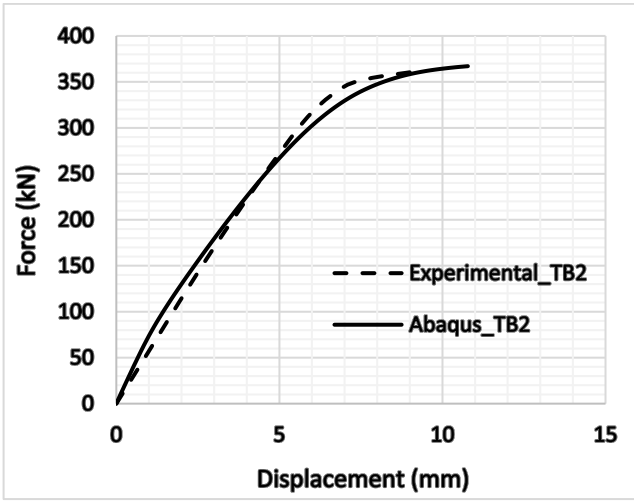

b. (TB2)

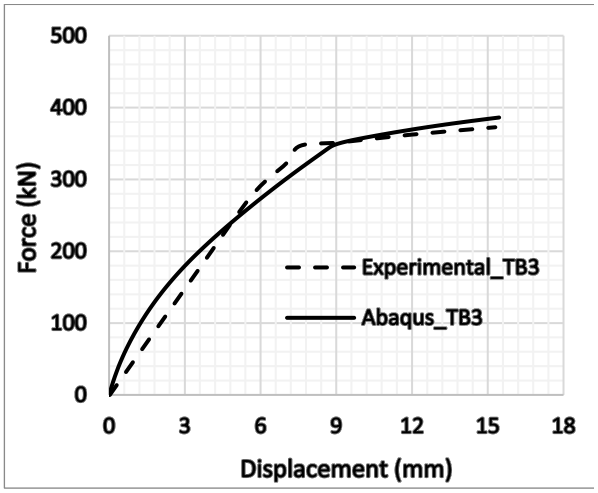

c. (TB3)

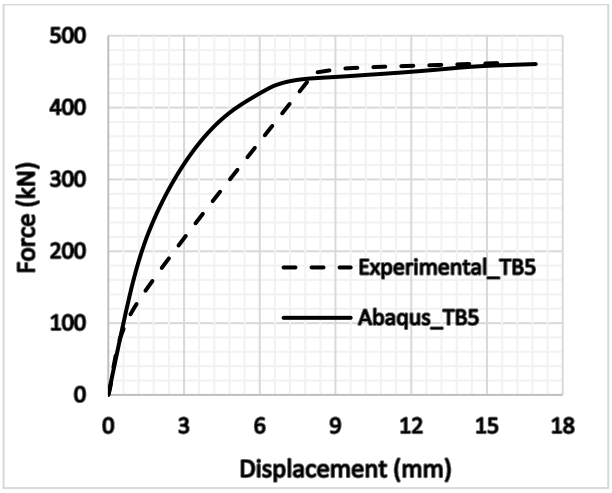

d. (TB5)

Figure 4.2 P-Δ curves; Experimental-Numerical Comparative Views.

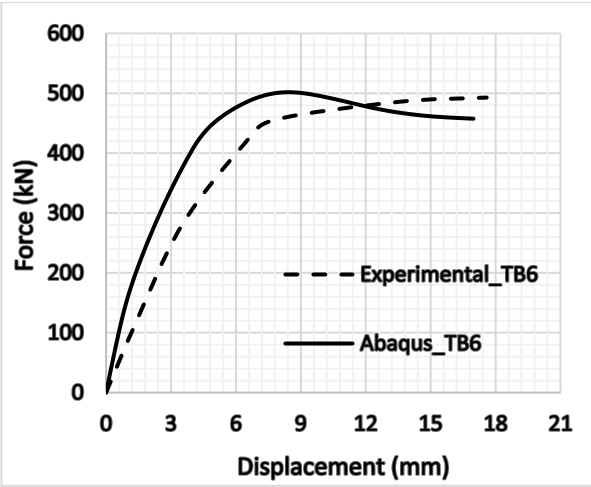

f. (TB6)

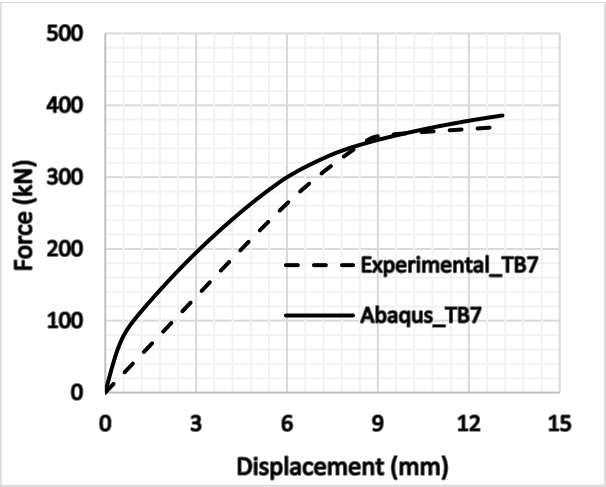

g. (TB7)

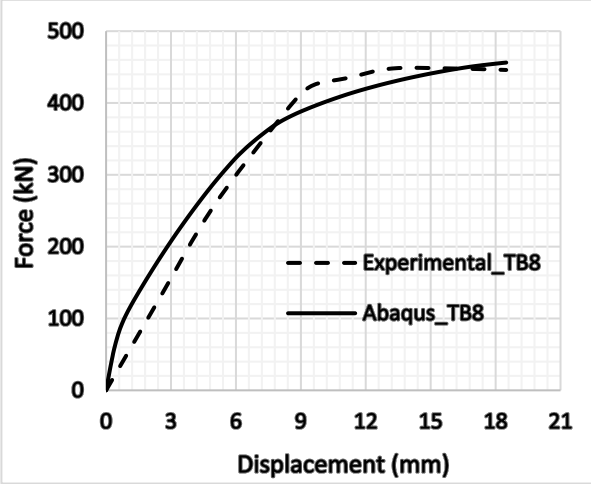

h. (TB9)

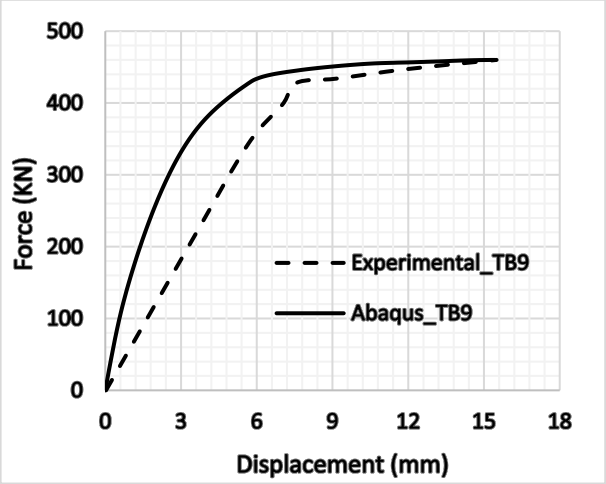

i. (TB10)

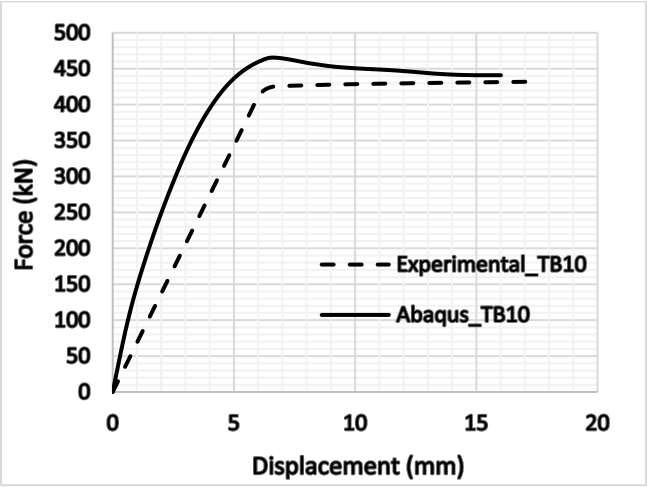

j. (TB10)

Figure 4.3 Continue.

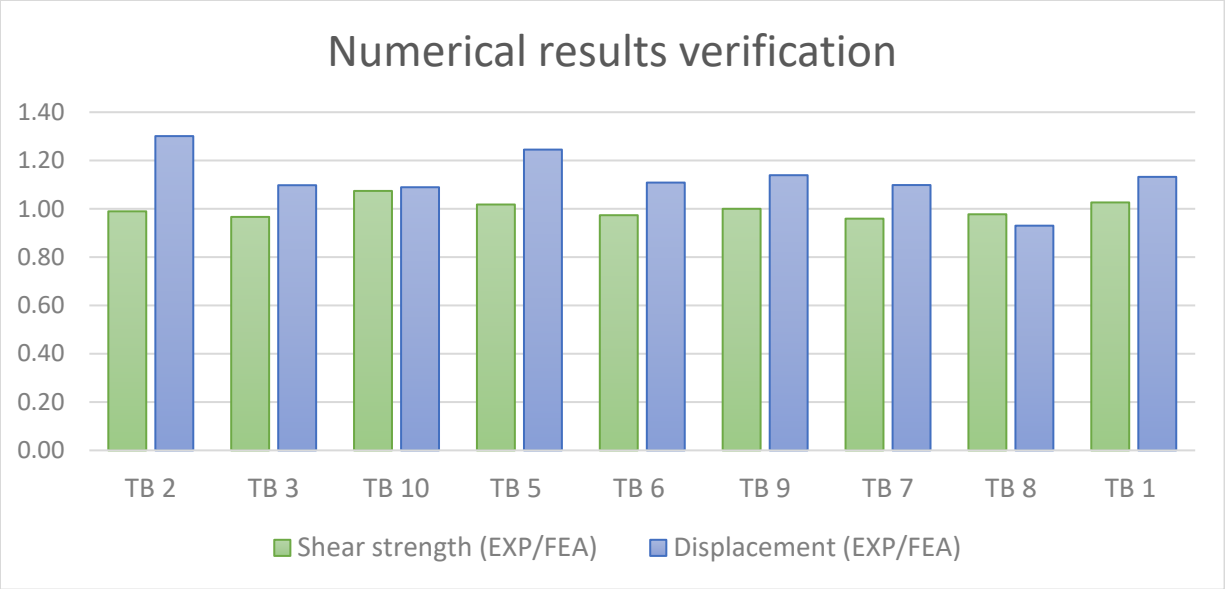

Figure 4.3 Numerical Results Verification; Ultimate Shear Strength Rating.

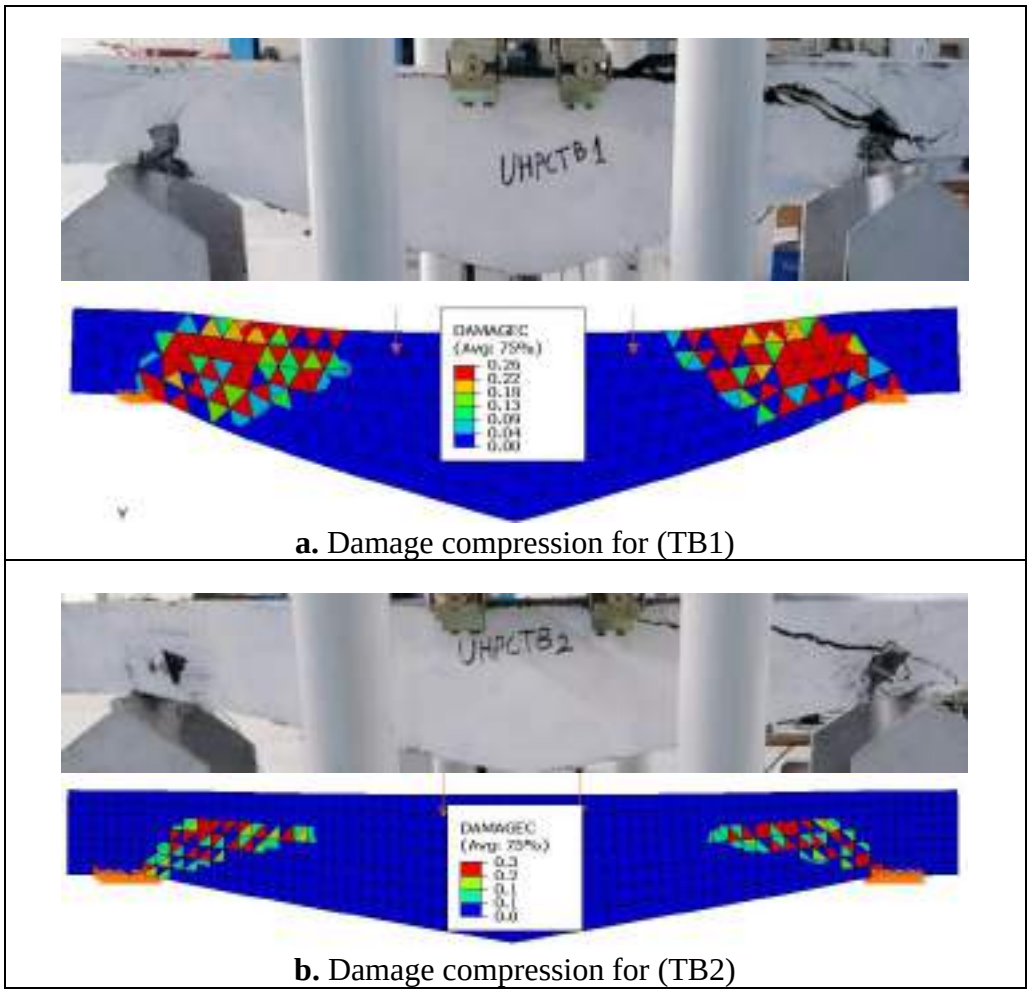

a. Damage compression for (TB1)

b. Damage compression for (TB2)

Figure 4.4 Experimental-Numerical Comparative Views.

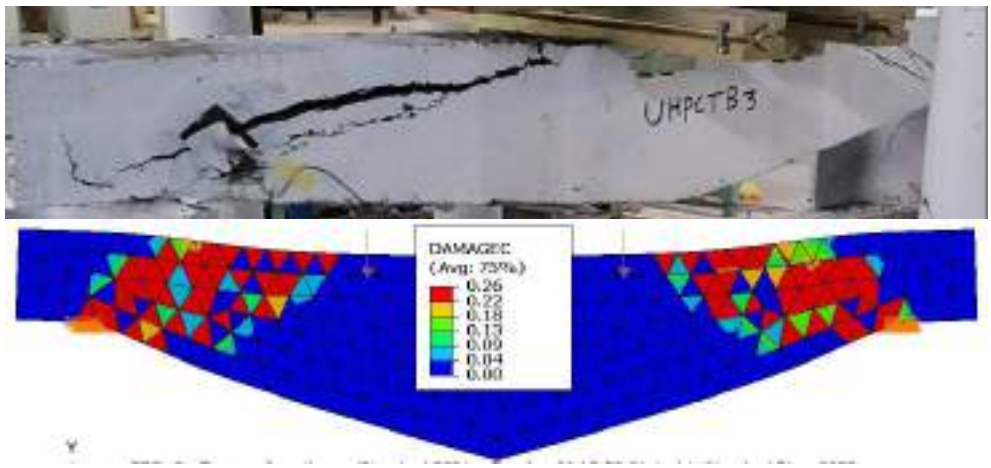

c. Damage compression for (TB3)

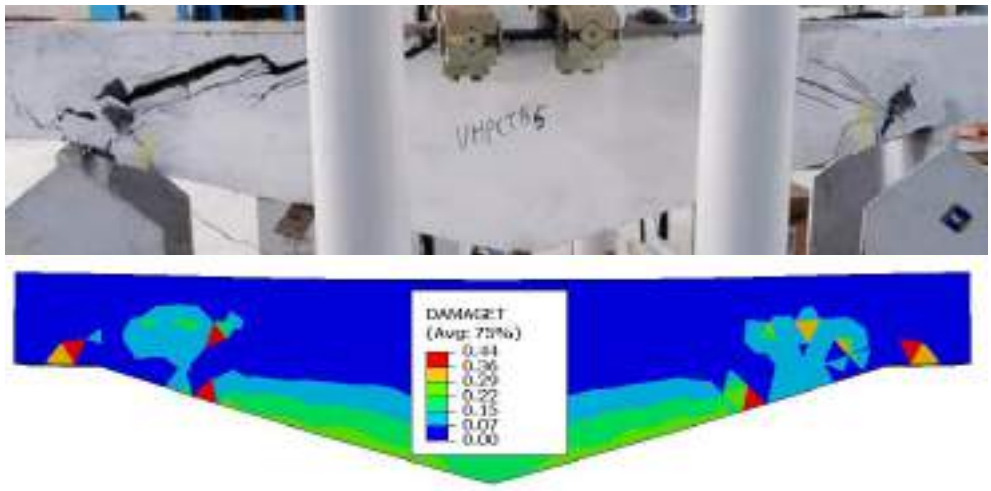

d. First crack for (TB5)

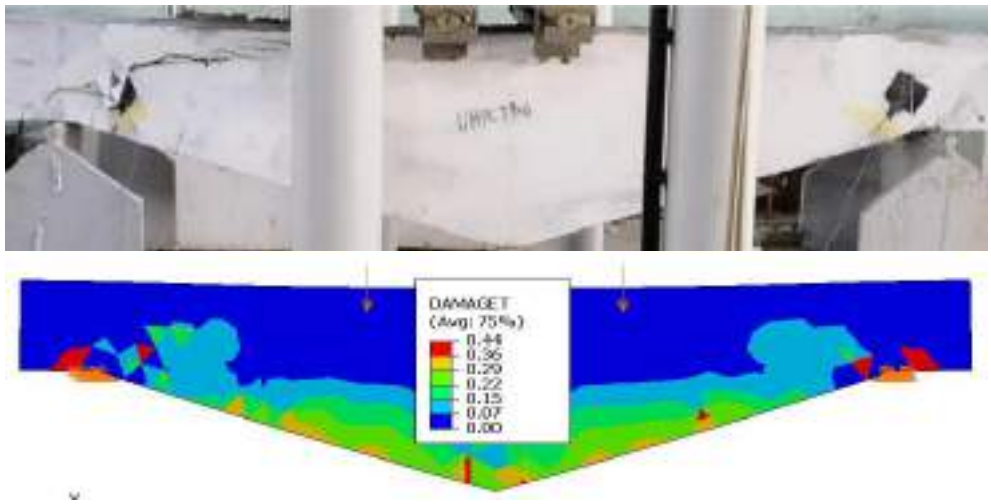

e. First crack for (TB6)

Figure 4.4 Countinue.

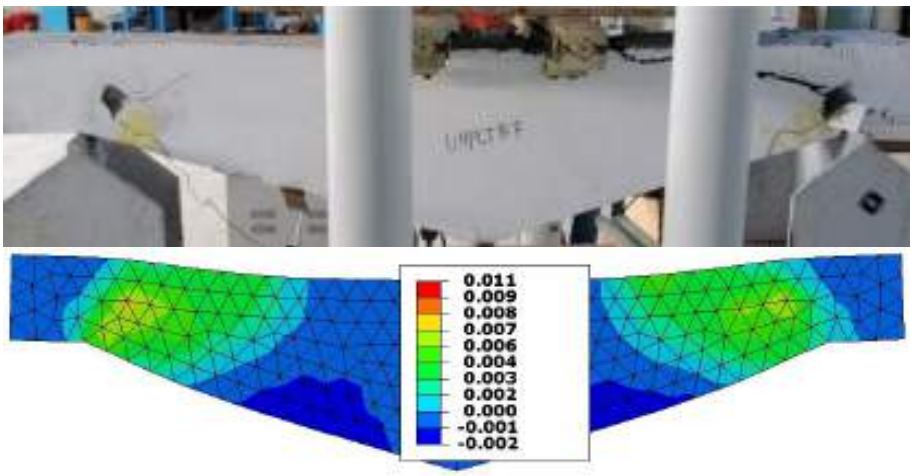

f. Strain distribution (TB7)

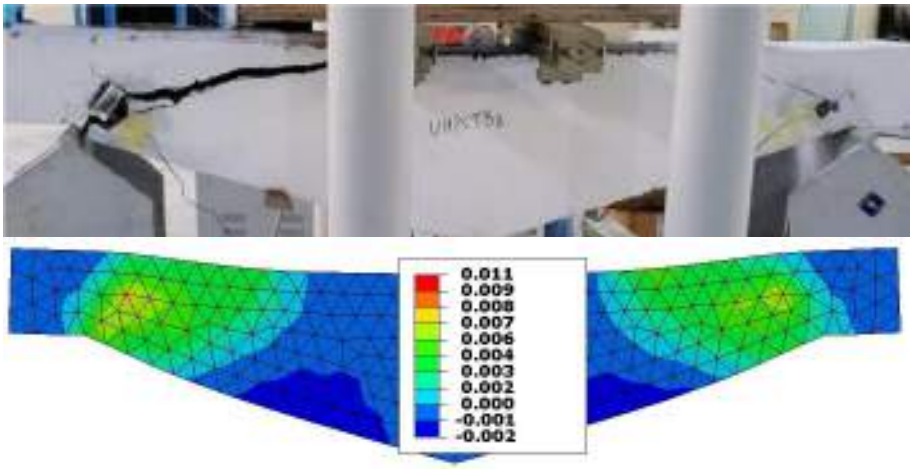

g. Strain distribution for (TB8)

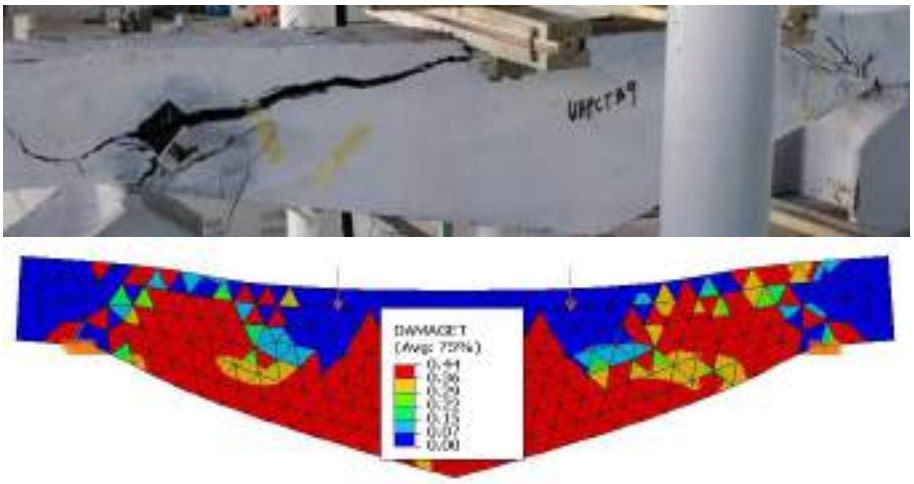

h. Damage tension for (TB9)

Figure 4.4 Countinue.

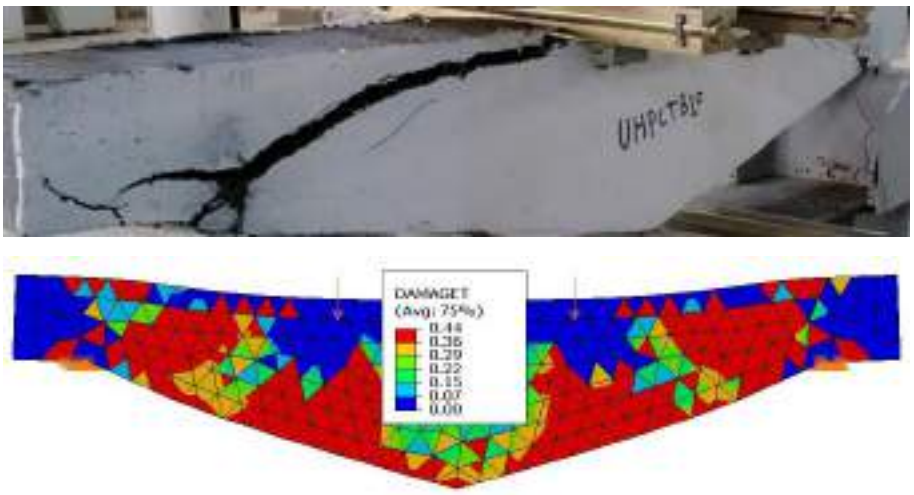

i. Damage tension for (TB10)

Figure 4.4 Countinue.

4.4 Ductility

Ductility is a measure of a material's ability to undergo significant plastic deformation before rupture or breaking, which may be expressed as percent elongation or percent area reduction from a tensile test. Ductility index ratio was selected as an index to assess the ductility of curved composite beam models. The ductility index (μΔ) is defined as the ratio of the maximum mid-span displacement over the first yield displacement of beams. The first yield displacement Δy corresponds to the load- deflection curve and maximum displacement Δu, Fig. 4-5 [77]. Therefore, the use of ductility ratio presents a better criterion in addition to the strength criterion for predicting the behavior of curved composite steel-concrete beams [77].

$$\mu\Delta=\frac{\Delta u}{\Delta y}$$

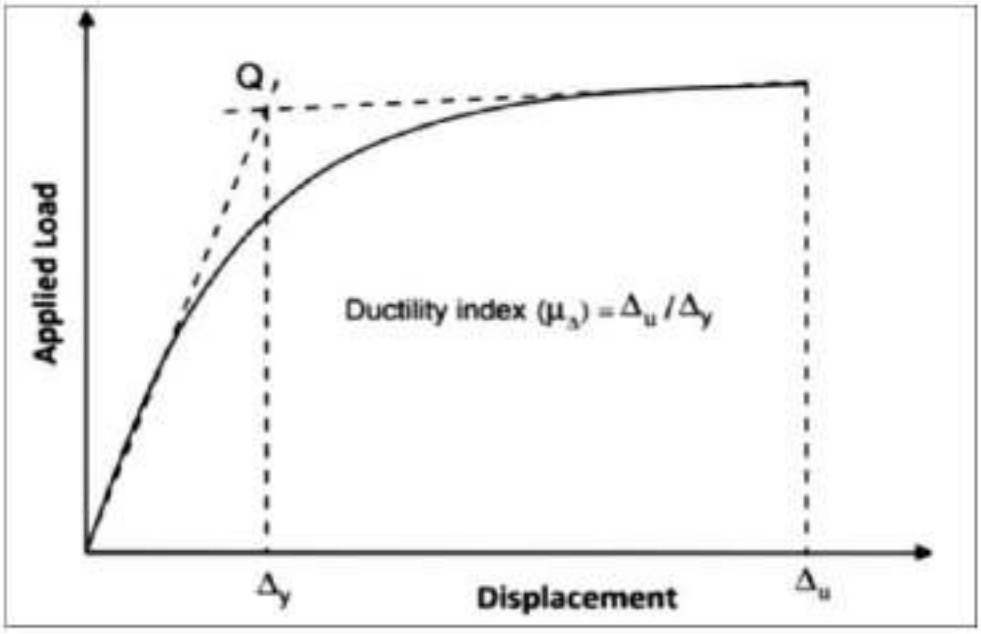

Figure 4.5 Show the ductility index calculation [78].

4.5 Parametric Study

In the present study the essential objective is to investigate the effect of several important parameters that are not well covered in past or expanded the previous studies on the inelastic behavior, crack patterns, ductility, stiffness, deflection and shear strength of opening tapered beam. The shear span to effective depth ratio, steel fiber ratio, inclination angle, location and number of openings, tensile bar's ratio and opening diameter are the considered parameters in this study. The FEM was carried out and developed using the general commercial ABAQUS software.

The parametric study results of the parameters obtained from the FE modeling including the yield load (Py), ultimate failure load (Pu) and the ultimate vertical mid-span deflection (Δu). The concrete compressive strength was 153.5 MPa. modulus of elasticity, compressive and tensile stress of concrete show the Table (4-4).

Table 4.4 Model's details for the tapered beams.

Beam ID	Dia. Open. (mm)	Loca. Open.	a/d	Scale Factor	Crown length	Tensile Reinforce.	Transverse Reinforce.	Boundary Condition
U-30	30	UP	2.7	-	1	$2\varphi25$	$\varphi8@845mm$	Simple Supported
U-50	50							
U-70	70							
D-30	30	DOWN	2.7	-	1	$2\varphi25$	$\varphi8@845mm$	Simple Supported
D-50	50							
D-70	70							
UD-30	30	BOTH	2.7	-	1	$2\varphi25$	$\varphi8@845mm$	Simple Supported
UD-50	50							
UD-70	70							
AD-1.5	50	BOTH	1.5	-	1	$2\varphi25$	$\varphi8@845mm$	Simple Supported
AD-1.75			1.75					
AD-2.0			2.0					
AD-2.3			2.3					
AD-2.7			2.7					
AD-3.0			3.0					
BC-S	50	BOTH	2.7	-	1	$2\varphi25$	$\varphi8@845mm$	SimpleSupported
BC-F								Fixed supported
SF1	50	BOTH	2.7	1.0	1	$2\varphi25$	$\varphi8@845mm$	Simple Supported
SF1.3				1.3				
SF1.6				1.6				
SF1.8				1.8				
SF2.1				2.1				
SF2.4				2.4				
TL200	50	BOTH	2.7	-	200mm	$2\varphi25$	$\varphi8@845mm$	Simple Supported
TL300					300mm			
TL400					400mm			
TL500					500mm			
LR-2.24	50	BOTH	2.7	-	1	$4\varphi16$	$\varphi8@845mm$	Simple Supported
LR-2.73						$2\varphi25$		
LR-3.01						$2\varphi25 + 2\varphi8$		
TR-845	50	BOTH	2.7	-	1	$2\varphi25$	$\varphi8@845mm$	Simple Supported
TR-200							$\varphi8@200mm$	
TR-120							$\varphi8@120mm$	

4.6 Scale Factor Effect

The change in the dimensions of the tapered beam from the length of the beam 1900mm, the width 150mm and the height at the supported 180mm and in the middle of the beam 405mm is gradually changed to five stages until it reaches dimensions close to semi-scale. Figure 4.7. the geometrical detail of tapered beam (SF-1.0) while Table 5. depicts the related results analysis. Results show an increase in shear strength and deflection compared to Model SF-1.0 by 348% and 135%; respectively, as shown in Fig. 4.8. This may be due to the representation of the volume of the concrete with dimensions that seem semi-scale where the concrete receiving his works as resistance the greater compression force. As illustrated in Figure 4.9, while Figure 4.10 show the related crack patterns and strain distribution.

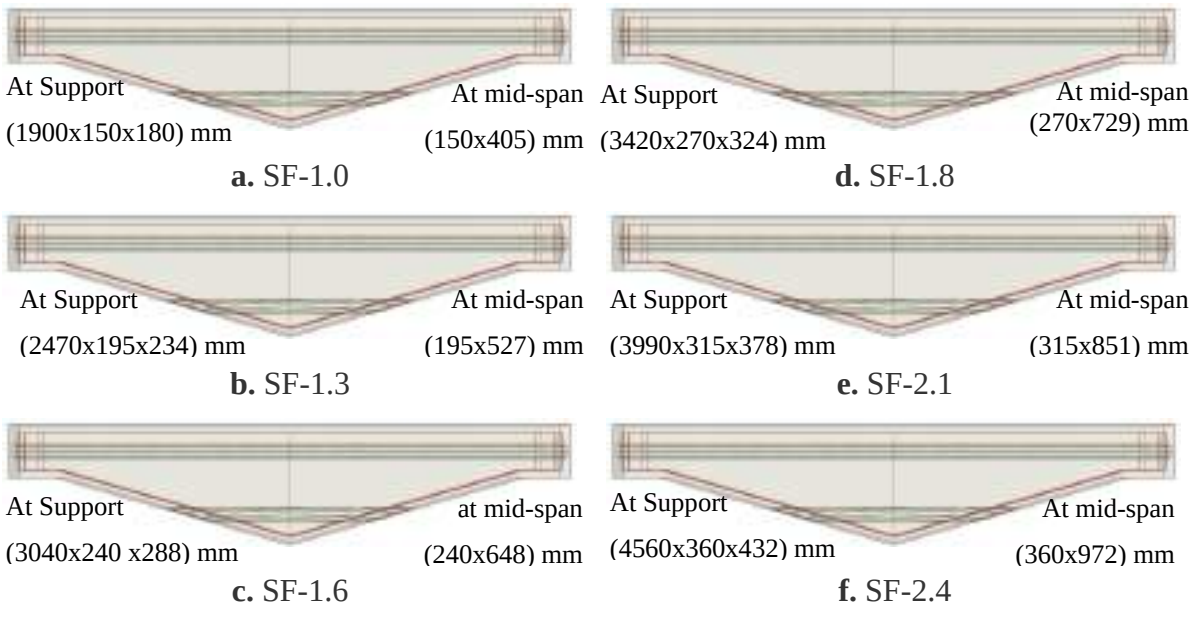

Note: Compresstion Rrinforcment: 2φ8, Tensile Reinforcement: 2φ25, Inclination angle: 15.9°, a/d Ratio:2.73, Diamrter of Opeinings:70mm, Grometry Daimention: (Length x width x depth).

Figure 4.6 Specimens' Modeling Details.

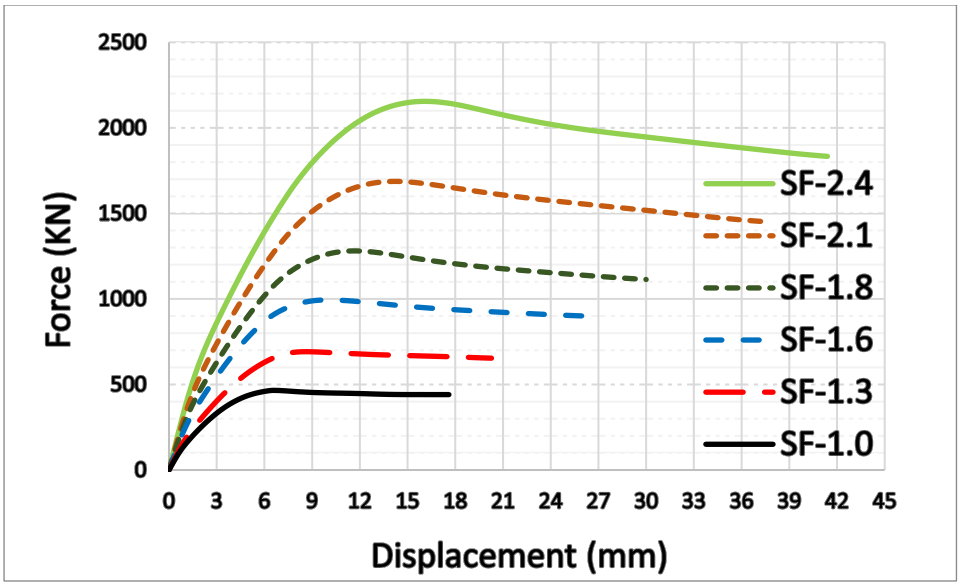

Figure 4.7 Load-Deflection Response: Scale Factor Effect.

Table 4.5 Results analysis: Scale Factor Effect.

Beam ID	Scale Factor	First Crack Load (kN)	Ultimate Shear Load (kN)	Ultimate Deflection mm	Splitting tensile (MPa)	Ductility Index	Failure Mode
SF-1.0 (STD)	**1.0**	172.0	465.4	17.6	9.4	6.07	Shear
SF-1.3	**1.3**	183.0	691.5	20.3	7.1	6.99	Shear
SF-1.6	**1.6**	284.5	994.1	26.4	7.9	7.14	Shear
SF-1.8	**1.8**	346.8	1280.7	30.0	7.9	7.32	Shear
SF-2.1	**2.1**	402.9	1687.1	37.5	7.6	7.50	Shear
SF-2.4	**2.4**	499.5	2085.3	41.4	7.6	7.96	Shear

Beam ID	Scale Factor	Yield Load (kN)	Deflection Yield (mm)	Diagonal Strain	Max Shear Stress (MPa)	Energy Absorption (kN.mm)	Initial Stiffness (kN/mm)
SF-1.0 (STD)	**1.0**	325	2.9	0.0048	492	913	112.1
SF-1.3	**1.3**	480	2.9	0.0036	491	1416	165.5
SF-1.6	**1.6**	625	3.7	0.0038	495	3027	168.9
SF-1.8	**1.8**	833	4.1	0.0036	496	4345	203.2
SF-2.1	**2.1**	1050	5	0.0039	570	7413	210.0
SF-2.4	**2.4**	1330	5.2	0.0034	760	10188	255.8

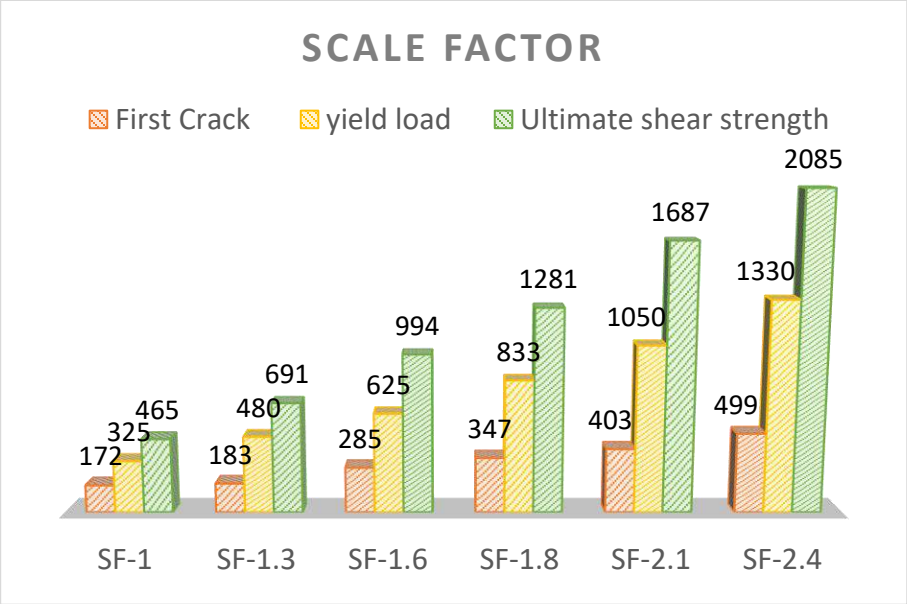

Figure 4.8 Results analysis: Scale Factor Effect.

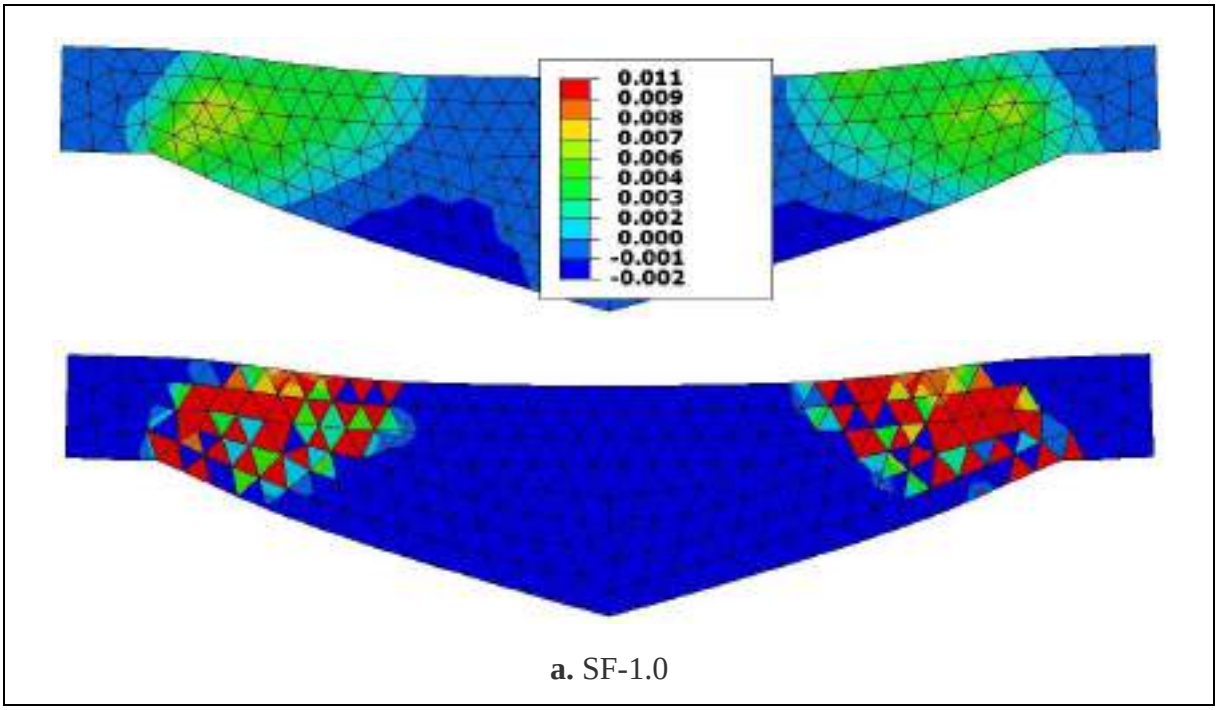

a. SF-1.0

Figure 4.9 Failure modes (crack patterns) and total Strain distribution of FE model by effect of Scale Factor.

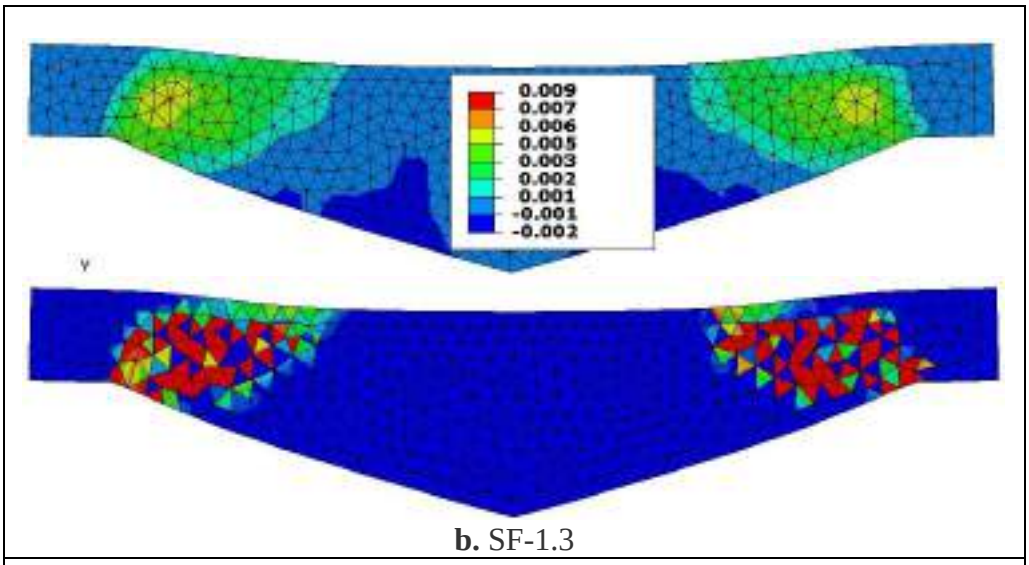

b. SF-1.3

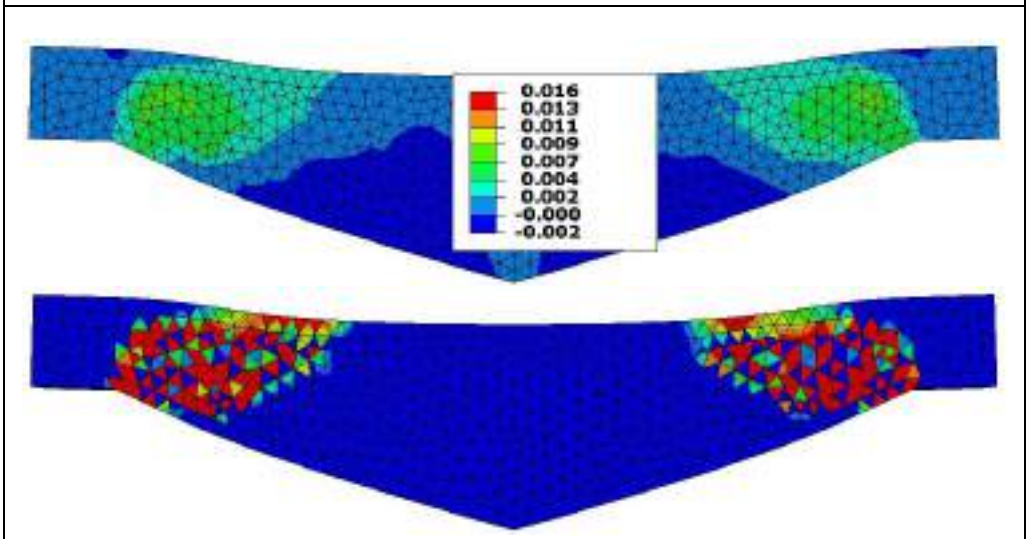

c. SF-1.6

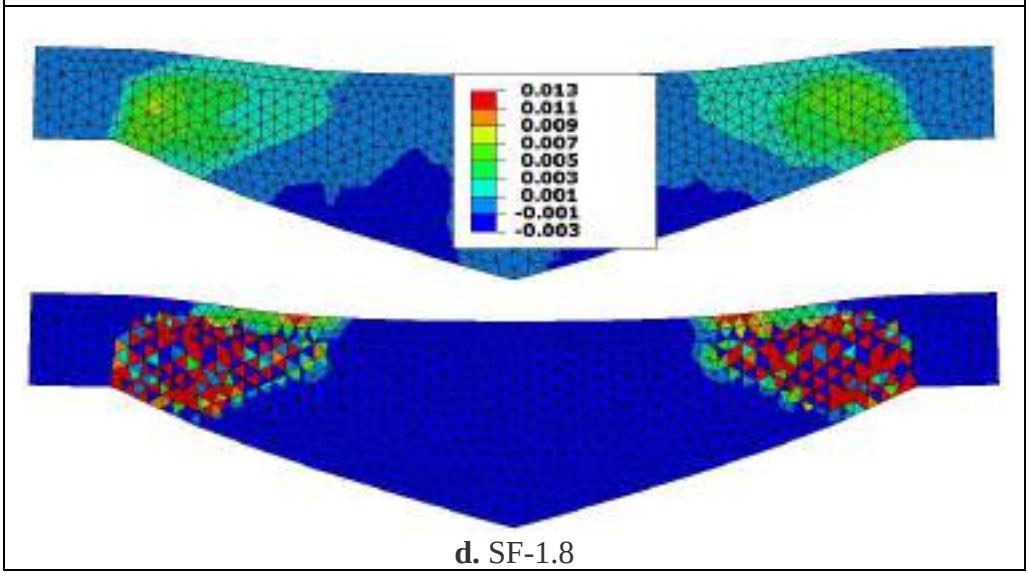

d. SF-1.8

Figure 4.10 Continue.

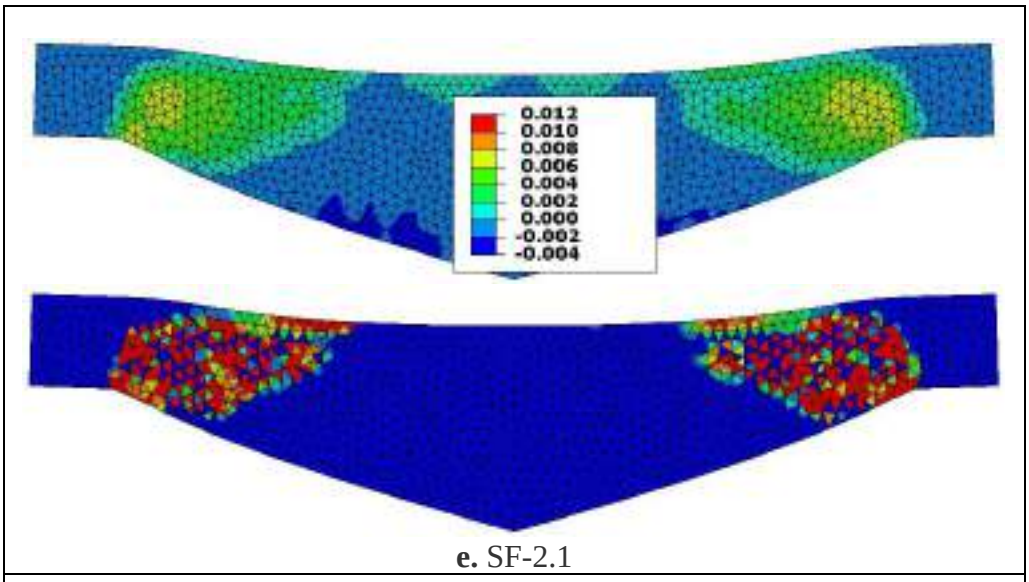

e. SF-2.1

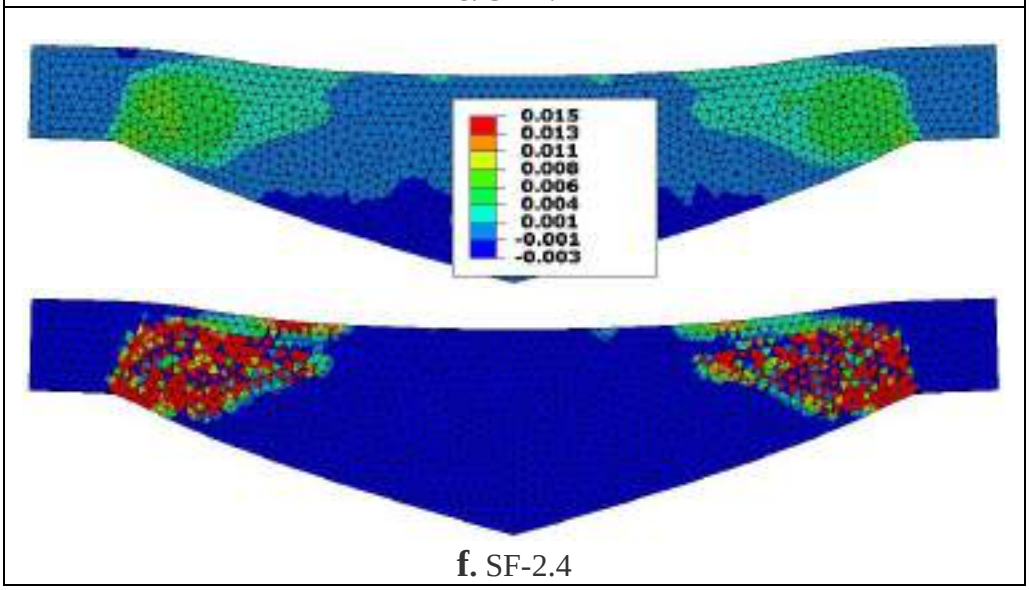

f. SF-2.4

Figure 4.10 Continue.

4.7 Crown Length Effect

The Tapered Length region within overall tapered modes is investigated numerically. The maintenance of section strength with uniformity region reduction means, higher strength rating (ultimate strength / beam overall weight) and mean reduction in the attainted dead load. Figure 4.11 shown the specimens modeling details. Wide range of extended regions distance as variable are considered, the adopted numerical modeling details are summarized in Table 4.5. The obtained

results show that, as uniformity region increased from 0 to 500 mm, the ultimate shear strength gets the increasing 13% improved from 465.4 kN to 526.7 kN. Table 4.4 exhibits results analysis that relates to a tapered length investigation. These observations could be clearly monitored by the introduced load -deflection curves that shown in Figure 4.12 and related ultimate strength-deflection, ductility indices in Figure 4.13, Figure 4.14 shows the observed failure modes in the scope of the crack patterns and total Strain distribution.

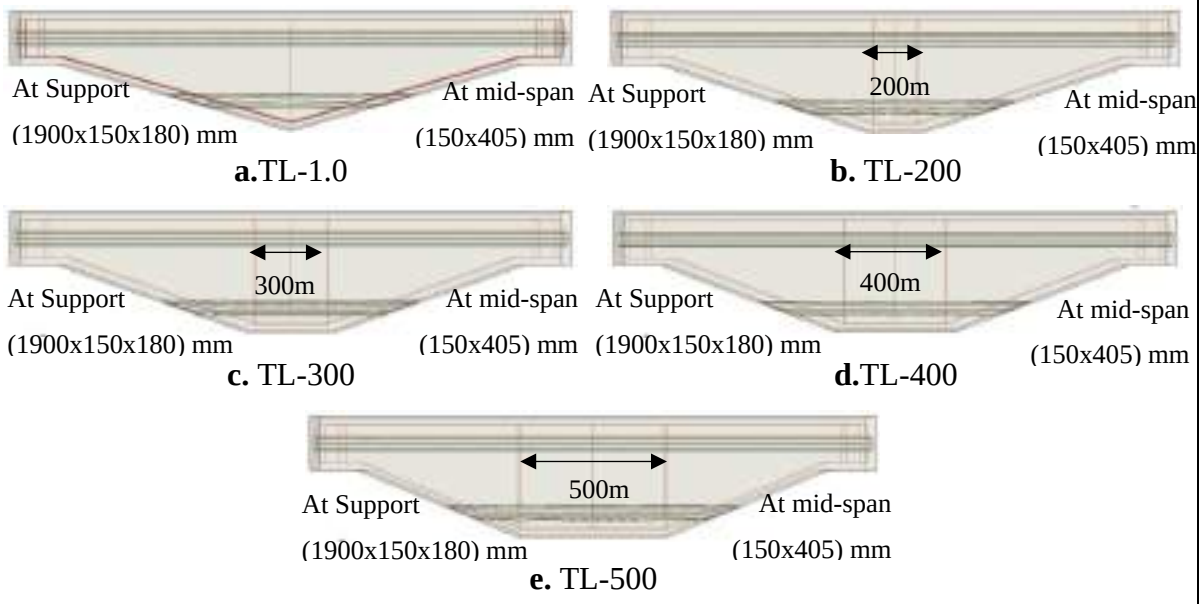

Note: Compresstion Rrinforcment: 2φ8, Tensile Reinforcement: 2φ25, a/d Ratio:2.73, Diamrter of Opeinings:70mm, Grometry Daimention: (Length x width x depth).

Figure 4.10 Specimens' Modeling Details.

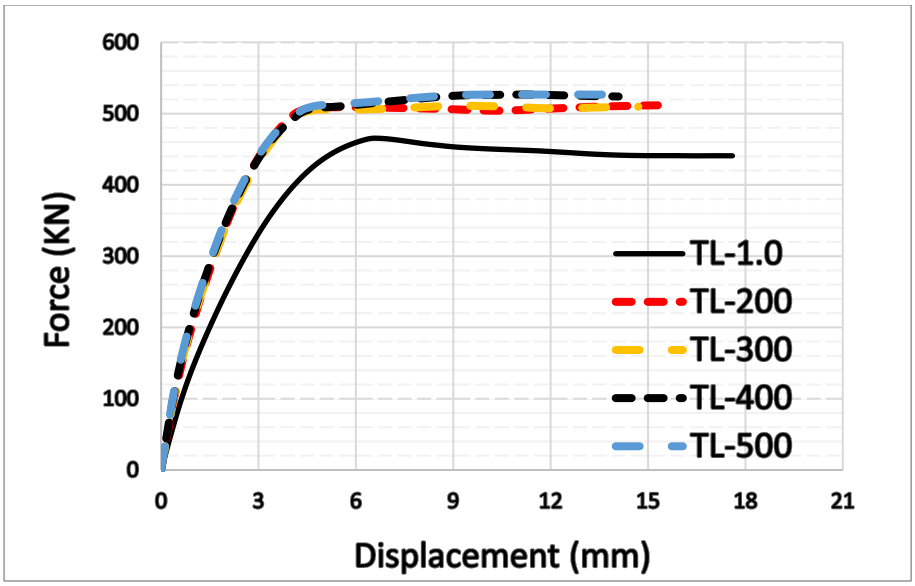

Figure 4.11 Load-Deflection Response: Crown Length Effect.

Table 4.6 Results analysis: Scale Factor Effect.

Beam ID	Tapered Length	First Crack Load (kN)	Ultimate Shear Load (kN)	Ultimate Deflection mm	Splitting tensile (MPa)	Ductility Index	Failure Mode
TL-1.0 (STD)	**1.0**	172.0	465.4	17.6	9.4	6.07	Shear
TL-200	**200**	173.6	511.7	15.30	12.1	5.28	Shear
TL-300	**300**	175.5	509.7	15.12	8.0	5.21	Shear
TL-400	**400**	190.1	524.0	15.10	8.6	5.21	Shear
TL-500	**500**	204.7	526.7	15.06	8.9	5.19	Shear

Beam ID	Tapered Length	Yield Load (kN)	Deflection Yield (mm)	Diagonal Strain	Max Shear Stress (MPa)	Energy Absorption (kN.mm)	Initial Stiffness (kN/mm)
TL-1.0 (STD)	1.0	325	2.9	0.0048	492	913	112.1
TL-200	200	345	2.9	0.0042	495	984	165.5
TL-300	300	350	2.9	0.0034	498	919	168.9
TL-400	400	360	2.9	0.0041	497	875	203.2
TL-500	500	360	2.9	0.0046	497	841	210.0

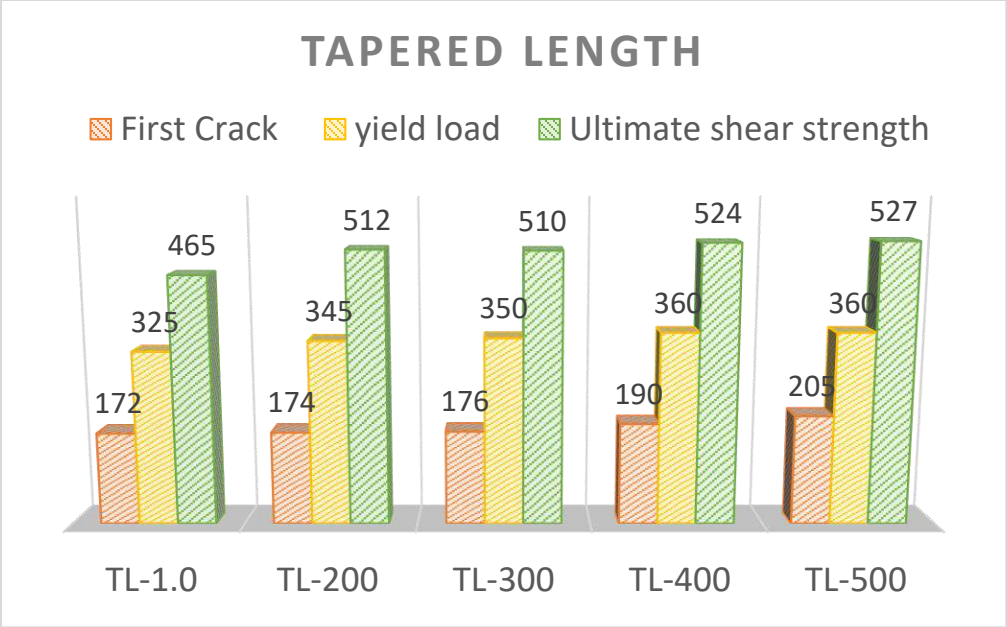

Figure 4.12 Results analysis: Tapered Length Effect.

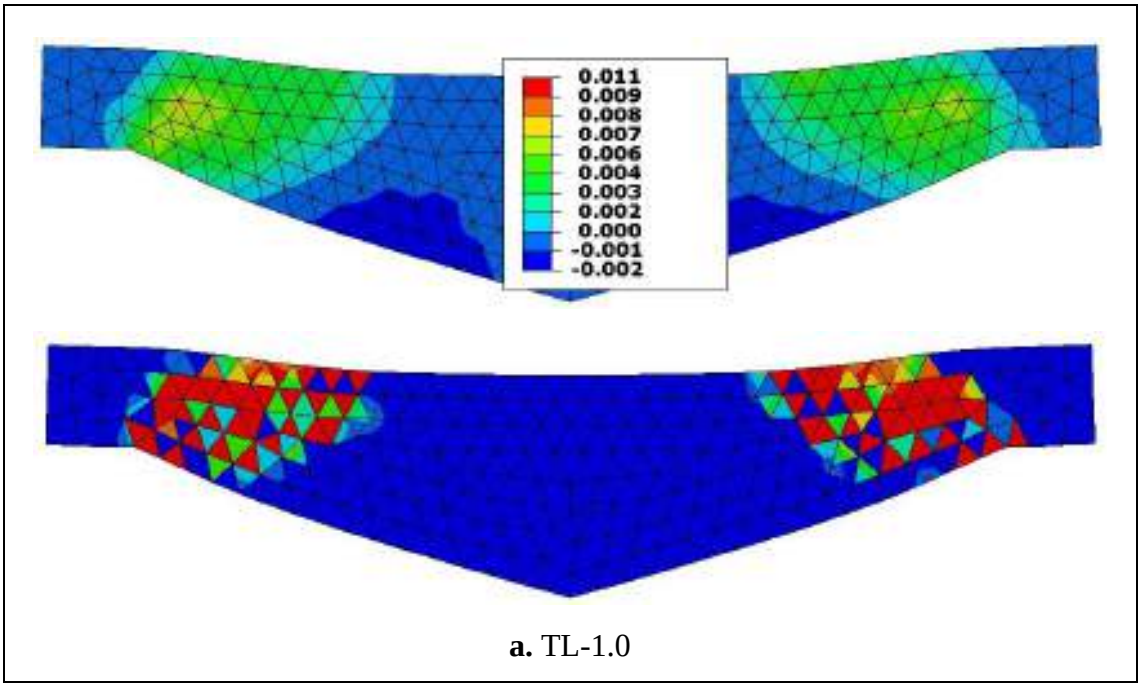

a. TL-1.0

Figure 4.13 Failure modes (crack patterns) and total Strain distribution of FE model by effect of Tapered Length.

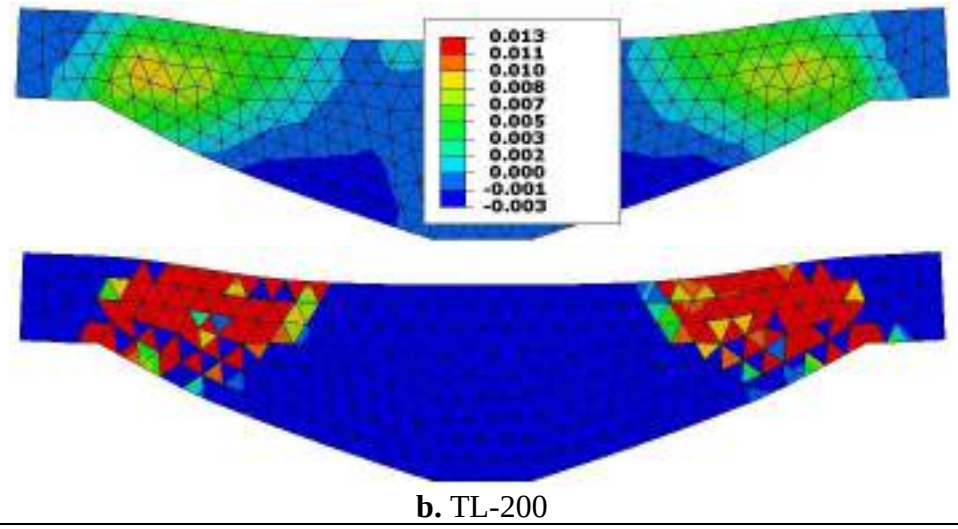

b. TL-200

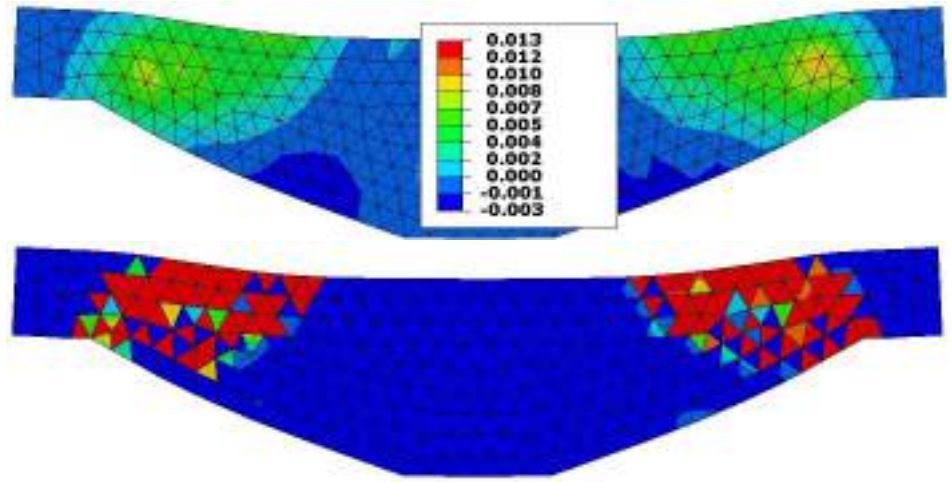

c. TL-300

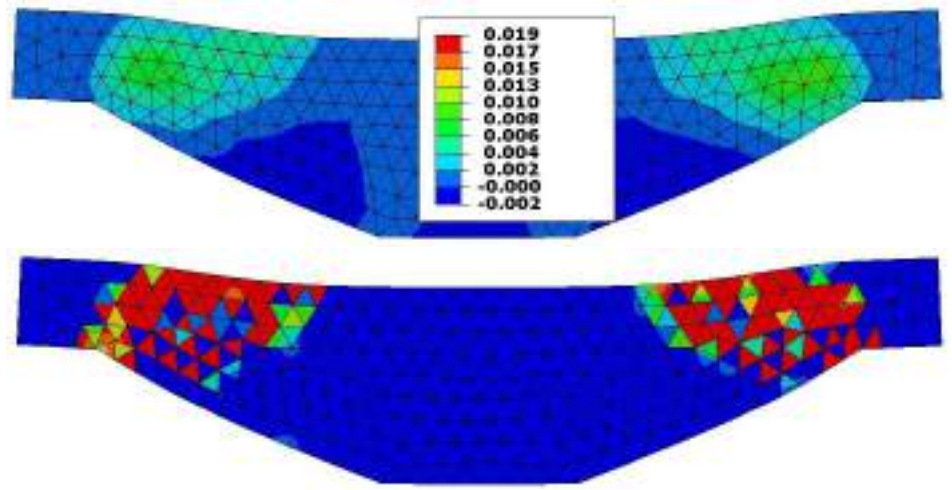

d. TL-400

Figure 4.14 Continue.

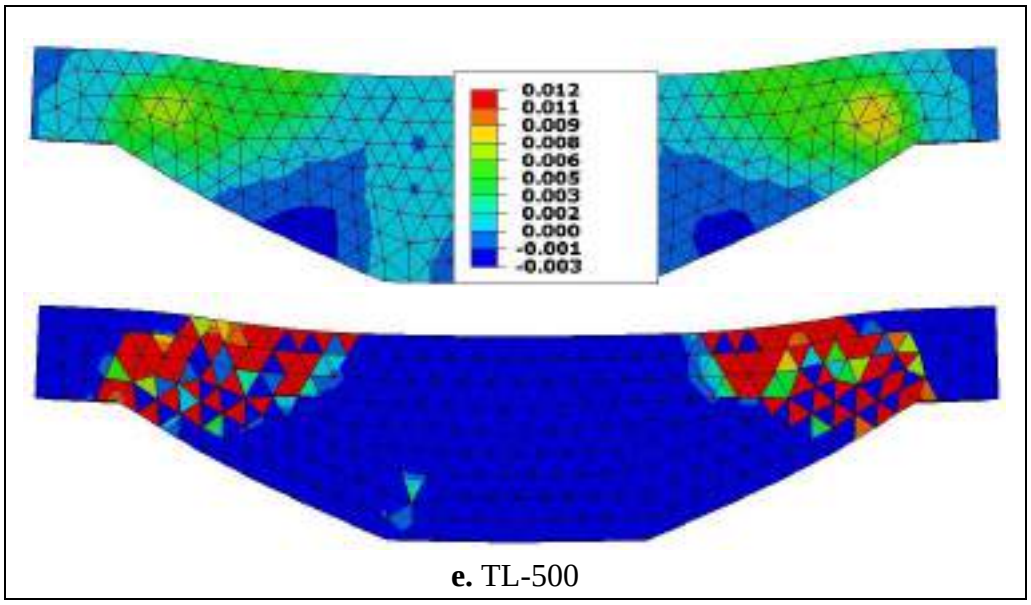

e. TL-500

Figure 4.14 Continue.

4.8 Shear Span to Effective Depth Ratio (a/d)

Six shear span to depth ratio (a/d) are considered (1.5, 1.75, 2, 2.3 2.7, 3) to inspect section shear resistance to know various stress distribution modes. The a/d more than 2 (specimens AD-2.3, AD-2.7 and AD-3.0 have the a/d ratio 2.3, 2.7 and 3 respectively) and the a/d less than 2 (specimens AD-1.5, AD-1.75 and AD-2.0 have the a/d ratio 1.5, 1.75 and 2 respectively). Table 4.2 lists the geometric description of adopted specimen sets while Table 4.6 exhibits the related results analysis which depicts that, the changing shear span that corresponds to turn stress distribution modes, as a/d have varying range 1.5, 1.75, 2.0, 2.3, 2.7, 3.0; respectively. Figure 4.15 and Figure 4.16 depicts the load-deflection response for specimens of various shear spans. The specimen AD-2.7 which it dominates by shear failure mode exhibits ductility response, If the load is approaching from the support, the deflection will decrease. While the specimen AD-2.3 exhibit acceptable ductile response, that characteristics of shear failure mode.

However, when the a/d ratio increases, the shear strength will be decreases this is may be due to the direct compression strut between the load and support, also due to the arch action when was the a/d ratio less than 2. As illustrated in Figure 4.17, while Figure 4.18 show the related crack patterns and strain distribution.

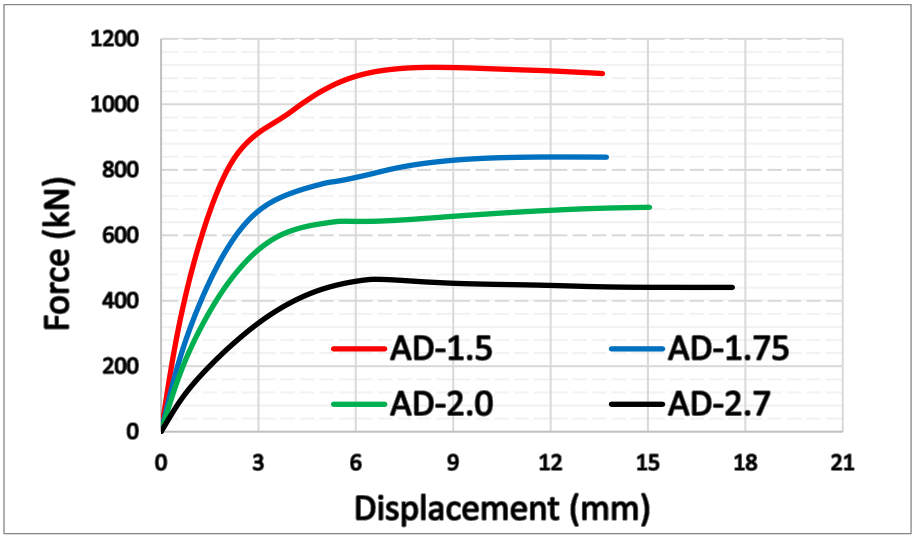

Figure 4.14 Load-Deflection Response: a/d ratio Effect.

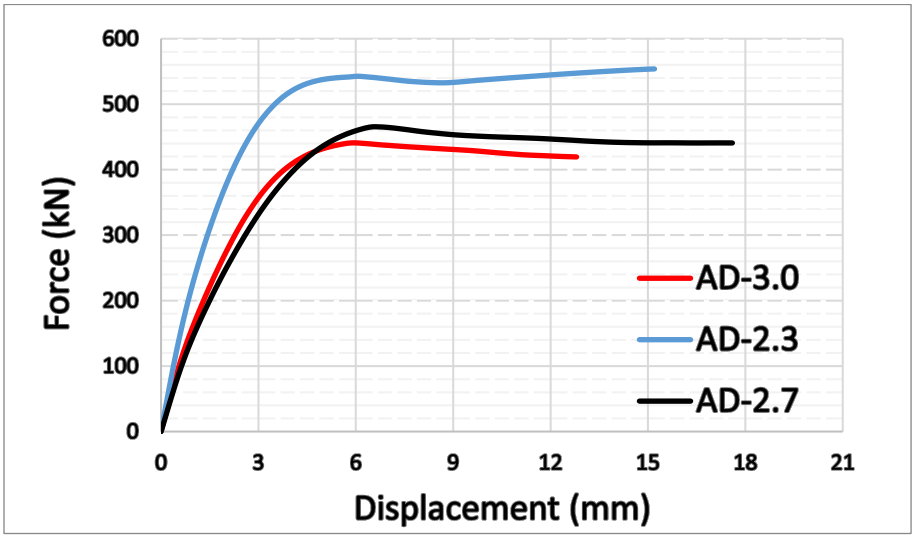

Figure 4.15 Load-Deflection Response: a/d ratio Effect.

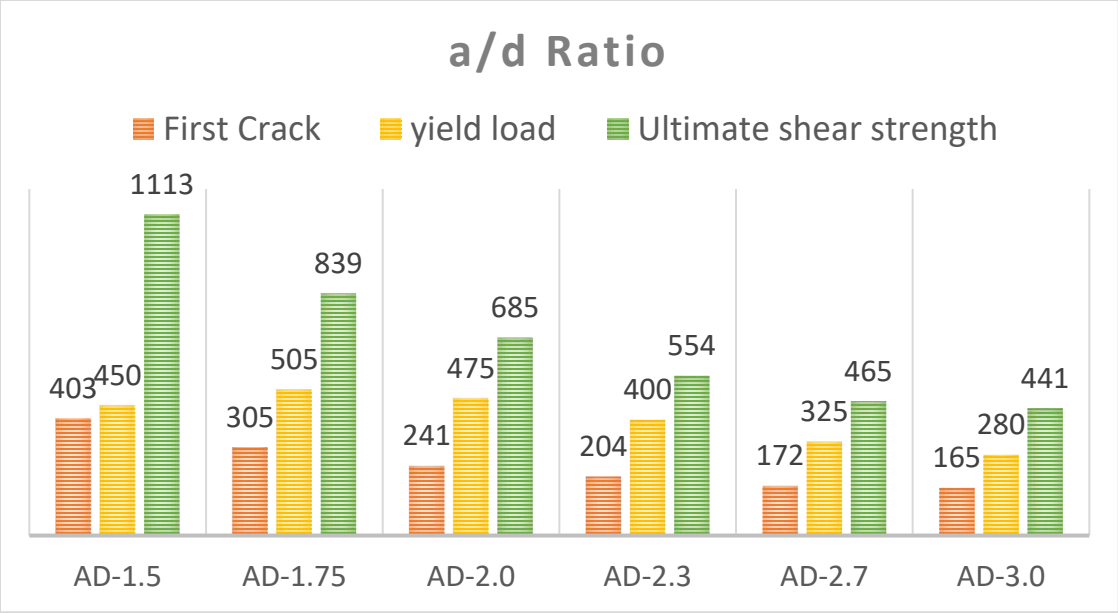

Figure 4.16 Results analysis: a/d ratio Effect.

Table 4.7 Results analysis: a/d ratio Effect.

Beam ID	a/d	First Crack Load (kN)	Ultimate Shear Load (kN)	Ultimate Deflection mm	Splitting tensile (Mpa)	Ductility Index	Failure Mode
AD-1.5	**1.5**	403.4	1113.0	13.6	12.6	8.00	**Shear**
AD-1.75	**1.75**	304.6	838.6	13.72	10.6	7.62	Shear
AD-2.0	**2**	240.8	685.5	15.048	8.0	7.52	Shear
AD-2.3	**2.3**	203.9	553.9	15.2	8.0	7.24	Shear
AD-2.7 (STD)	**2.7**	172.0	465.4	17.6	9.4	6.07	Shear
AD-3.0	**3**	164.5	440.9	12.8	6.9	5.82	Shear

Beam ID	a/d	Yield Load (kN)	Deflection Yield (mm)	diagonal Strain	Max Shear Stress (Mpa)	Energy Absorption (kN.mm)	Initial Stiffness (kN/mm)
AD-1.5	**1.5**	450	1.7	0.0039	645	1852	265
AD-1.75	**1.75**	505	1.8	0.0039	329	1358	281
AD-2.0	**2**	475	2	0.0049	648	1249	238
AD-2.3	**2.3**	400	2.1	0.0032	494	1056	190
AD-2.7 (STD)	**2.7**	325	2.9	0.0048	492	913	112
AD-3.0	**3**	280	2.2	0.0032	490	581	127

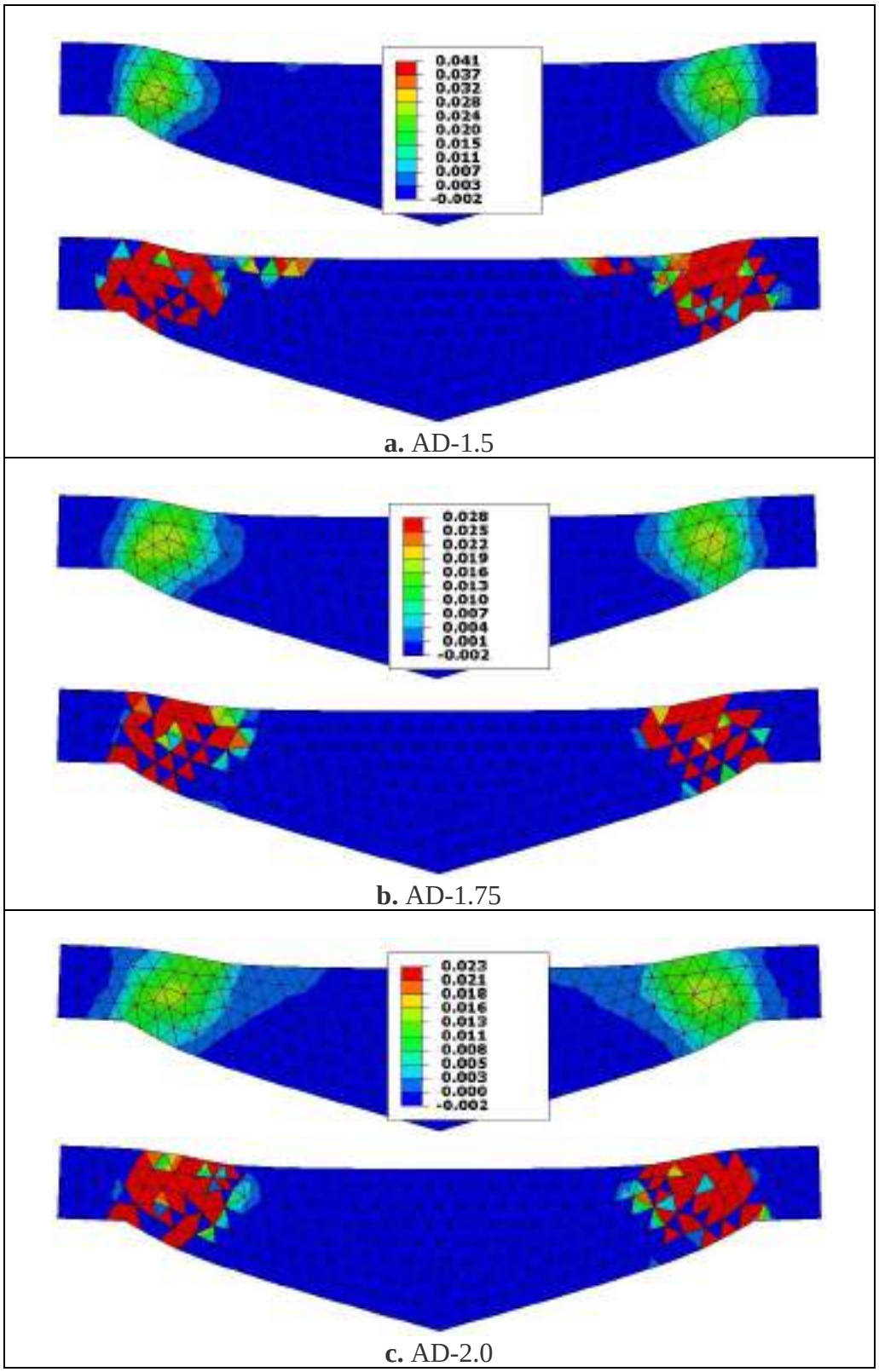

a. AD-1.5

b. AD-1.75

c. AD-2.0

Figure 4.17 Failure modes (crack patterns) and total Strain distribution of FE model by effect of a/d ratio.

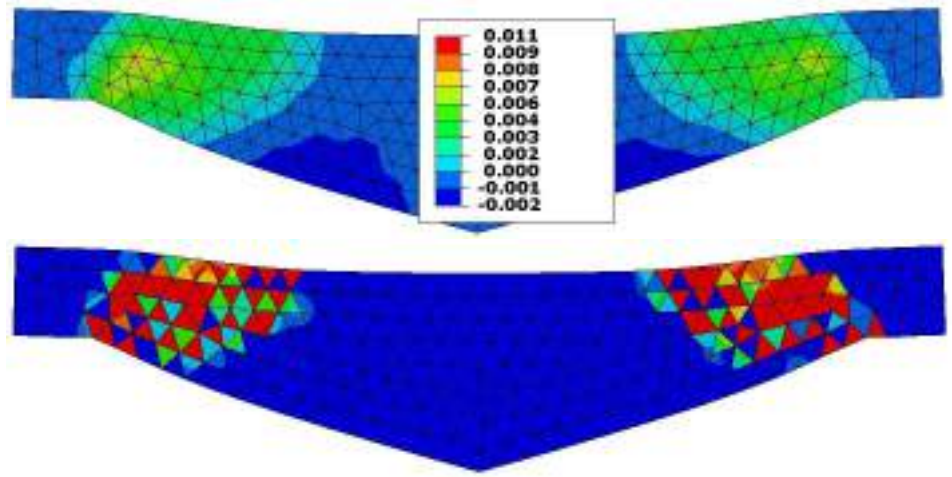

d. AD-2.3

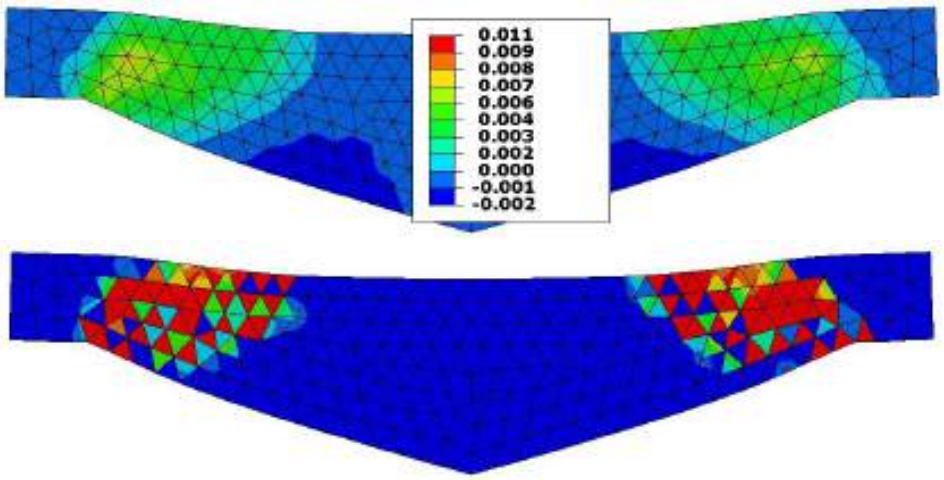

e. AD-2.7

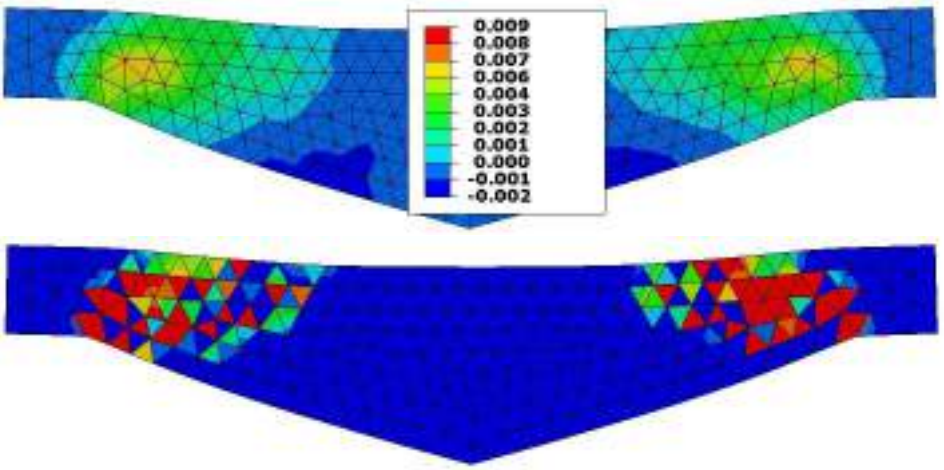

f. AD-3.0

Figure 4.18 Continue.

4.9 Longitudinal Openings

4.9.1 Openings Diameter

In this investigation, an attempt was made to study the shear strength of tapered beams having a longitudinal circular hole. The simulate of modeling have been determining the shear strength of tapered beams that have a single and double 30, or 50, or mm diameter of longitudinal hole. The diameter and location of the hole's center were changed. The tapered beam's cross section and reinforcement ratio in the tapered beam were kept constant. The same 153.3 MPa concrete compressive Strength was used in all of the beams. An increase in the size of the hole resulted in a decrease in the ultimate shear strength as shown in Table 7. All varied distributions of longitudinal openings with a diameter of 70mm were shown to have a lower ultimate load than all other hollow beams. The ultimate shear stress of the tapered beam rose as the diameter of the hole reduced. The longitudinal openings at the bottom of the non-prismatic beam and increasing its diameter causes the shear resistance to be stabilized and of higher value compared to having the same openings at the top as well as with the longitudinal openings at the top and bottom of the beam together. This may be due to the compression zone affecting the shear resistance remains complete because the longitudinal opening is in the tensile zone, which does not significantly affect its presence as shown in Fig. 4.20. The increase in the upper opening does not significantly affect shear resistance and therefore can be obtained saving in materials while remaining at the same level of resistance. Achieve higher optimization when there are two openings in both beam's area and 50mm diameter. As illustrated in Figure 4.21, while Figure 4.22 show the related crack patterns and strain distribution.

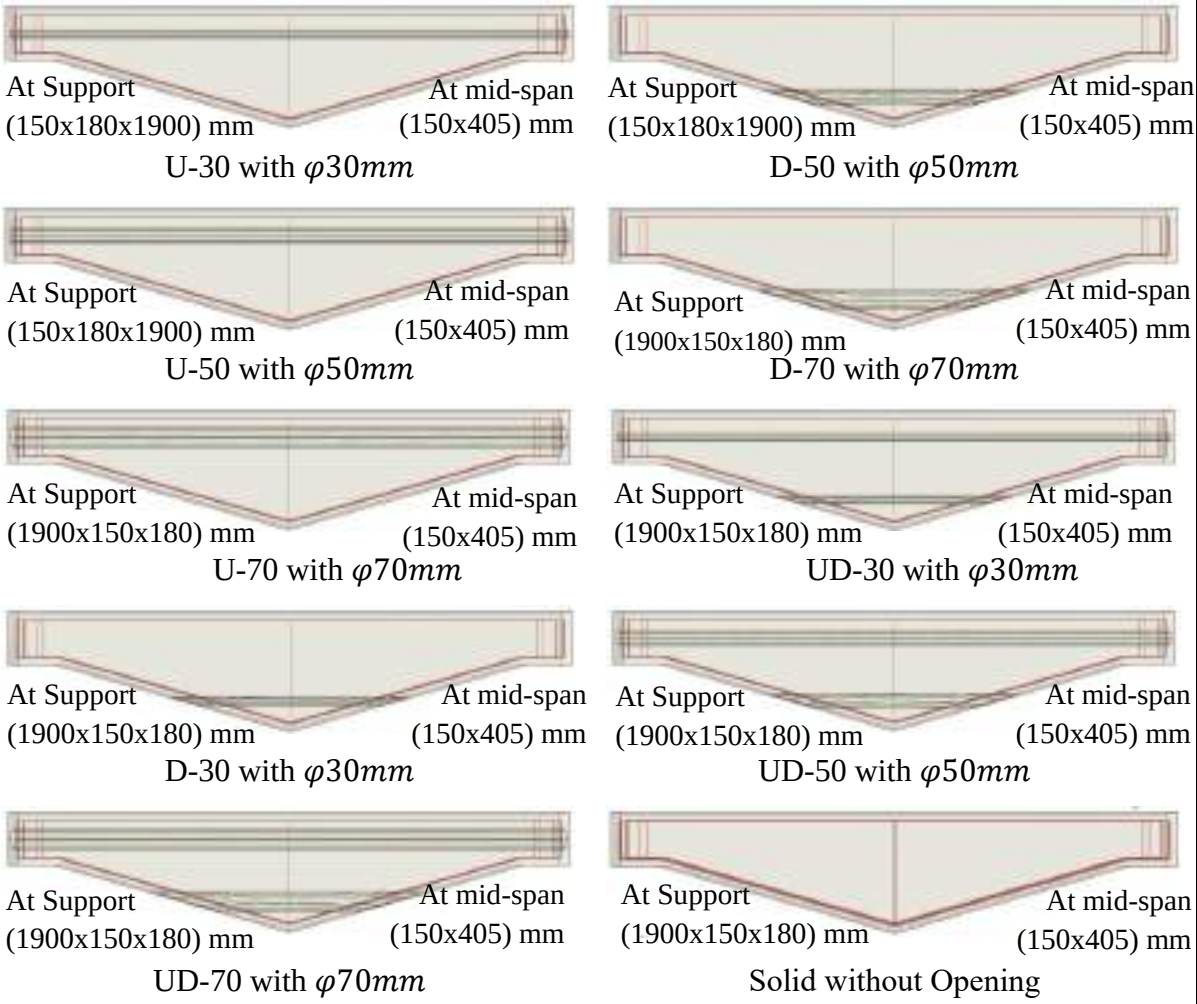

Note: Compresstion Rrinforcment: $2\varphi 8$, Tensile Reinforcement: $2\varphi 25$, Inclination angle: 15.9°, a/d Ratio:2.73, Grometry Daimention: (Length x width x depth), U: Up, D: Down, UD: Up and Down.

Figure 4.18 Specimens' Modeling Details.

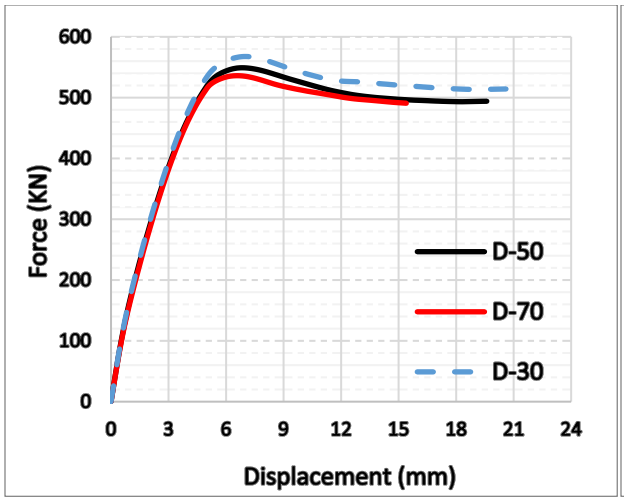

4.20a Openings in non-prismatic zone

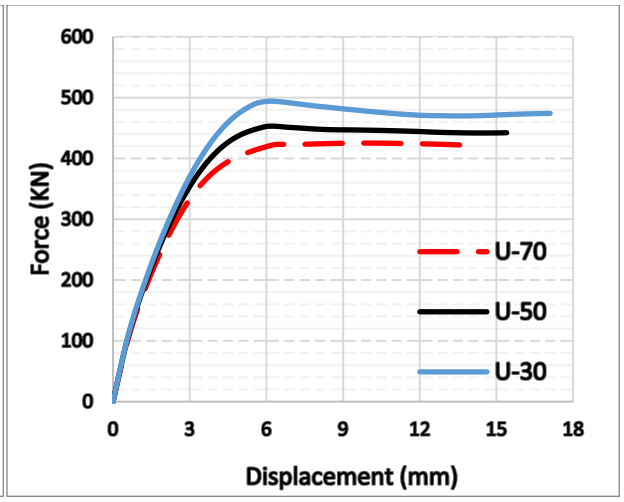

4.20b Openings in prismatic zone.

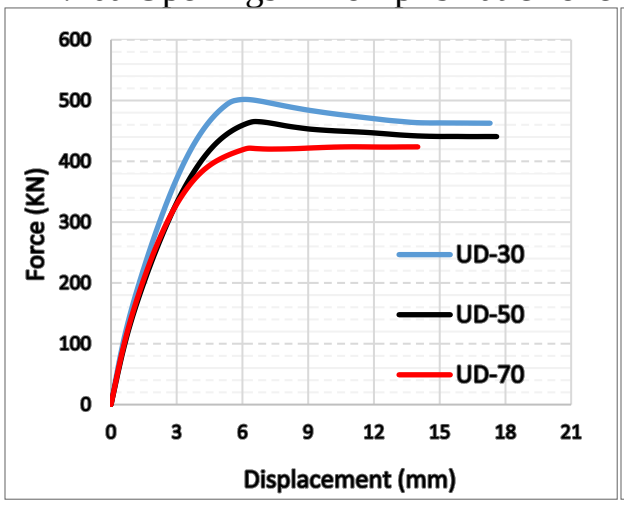

4.20c Openings in both zones.

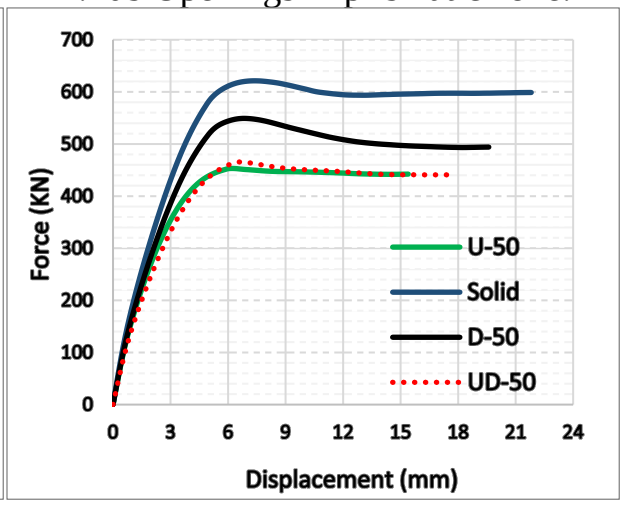

4.20d Openings in variable Cases.

Figure 4.19 Load-Deflection Response: Longitudinal Openings Effect.

4.9.2 Opening's Location

The existence of the opening along the beam longitudinal axis significantly lowers the compression and tensile strengths, which lowers the flexural and shear resistance. This study aims to determine the optimum position that give a better Shear force, besides its purpose for extension the services accessories through it and decreasing self weight. Three tapered beams; with one opening in compression (U-70), One opening in tension zone (D-70) and the last beam has two openings in both zones each were employed (UD-70). All diameter openings was 70mm in the

section. Results and explanations of the diameter openings and locations are shown in Table 5. The beam with the one opening in the D-70 tapered zone provided stronger shear resistance than the others, increased shear strength by 26% relative to the two circular openings. Also, the beam that has two openings (UD-70) has shown convergent results with one opening beam in the pressure zone that was 424 kN and 425 kN of shear strength for both models (UD-70, U-70) respectively, that meaning use two circular openings in beams reduces dead weight while maintaining the same resistance and deflections. Fig. 4.20e shows the load-deflection. As illustrated in Figure 4.20, while Figure 4.21 show the related crack patterns and strain distribution.

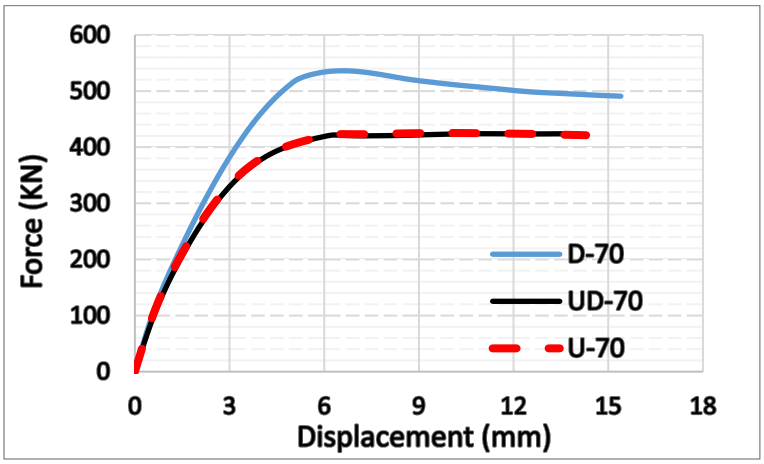

4.20e Openings in Various zone.

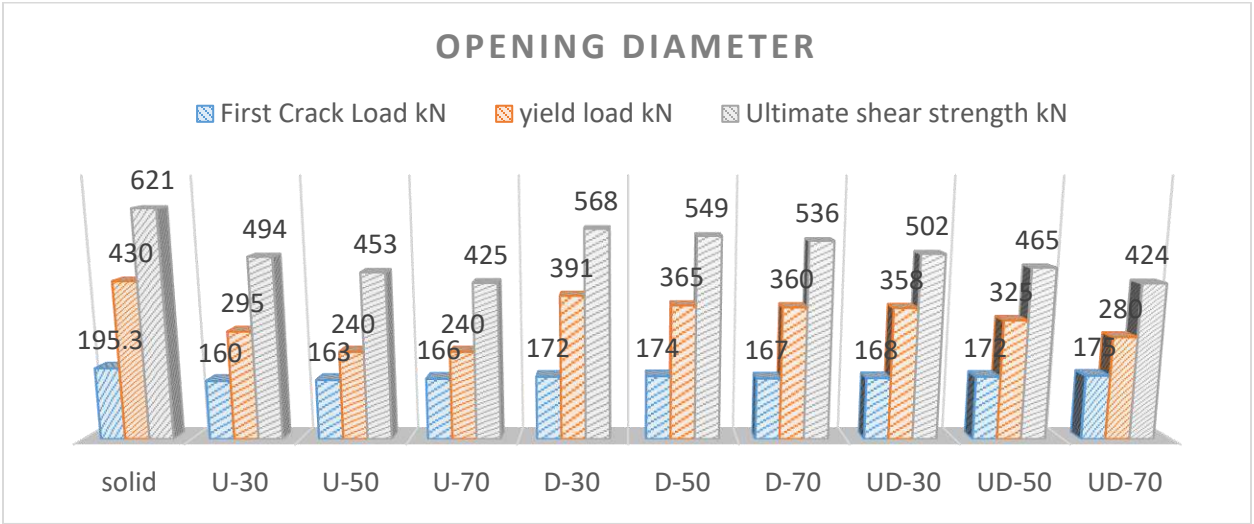

Figure 4.20 Results analysis: Opening Diameter Effect.

Table 4.8 Results analysis: a/d ratio Effect.

Beam ID	Opening Diameter (mm)	First Crack Load (kN)	Ultimate Shear Load (kN)	Ultimate Deflection mm	Splitting tensile (MPa)	Ductility Index	Failure Mode
Solid	-	195.3	621.2	21.8	498	7.27	Shear
U-30	**30**	160.5	494.2	17.1	7.8	6.58	Shear
U-50	**50**	163.0	453.1	15.4	7.9	6.16	Shear
U-70	**70**	166.5	425.3	14.3	6.9	5.72	Shear
D-30	**30**	171.9	567.7	20.6	9.0	6.87	Shear
D-50	**50**	173.5	549.1	19.6	9.3	6.76	Shear
D-70	**70**	167.2	536.1	15.4	8.4	5.50	Shear
UD-30	**30**	168.3	501.9	17.3	8.2	6.41	Shear
UD-50 (STD)	**50**	172.0	465.4	17.6	9.4	6.07	Shear
UD-70	**70**	175.0	423.9	14.5	7.4	6.04	Shear

Beam ID	Opening Diameter (mm)	Yield Load (kN)	Deflection Yield (mm)	Diagonal Strain	Max Shear Stress (MPa)	Energy Absorption (kN.mm)	Initial Stiffness (kN/mm)
Solid	-	430	3	0.0036	498	1699	143
U-30	**30**	295	2.6	0.0032	493	974	113
U-50	**50**	240	2.5	0.0047	492	791	96
U-70	**70**	240	2.5	0.0035	491	662	96
D-30	**30**	391	3	0.0035	497	1417	130
D-50	**50**	365	2.9	0.0041	497	1273	126
D-70	**70**	360	2.8	0.0035	495	829	129
UD-30	**30**	358	2.7	0.0038	494	995	133
UD-50 (STD)	**50**	325	2.9	0.0048	492	913	112
UD-70	**70**	280	2.4	0.0041	491	628	117

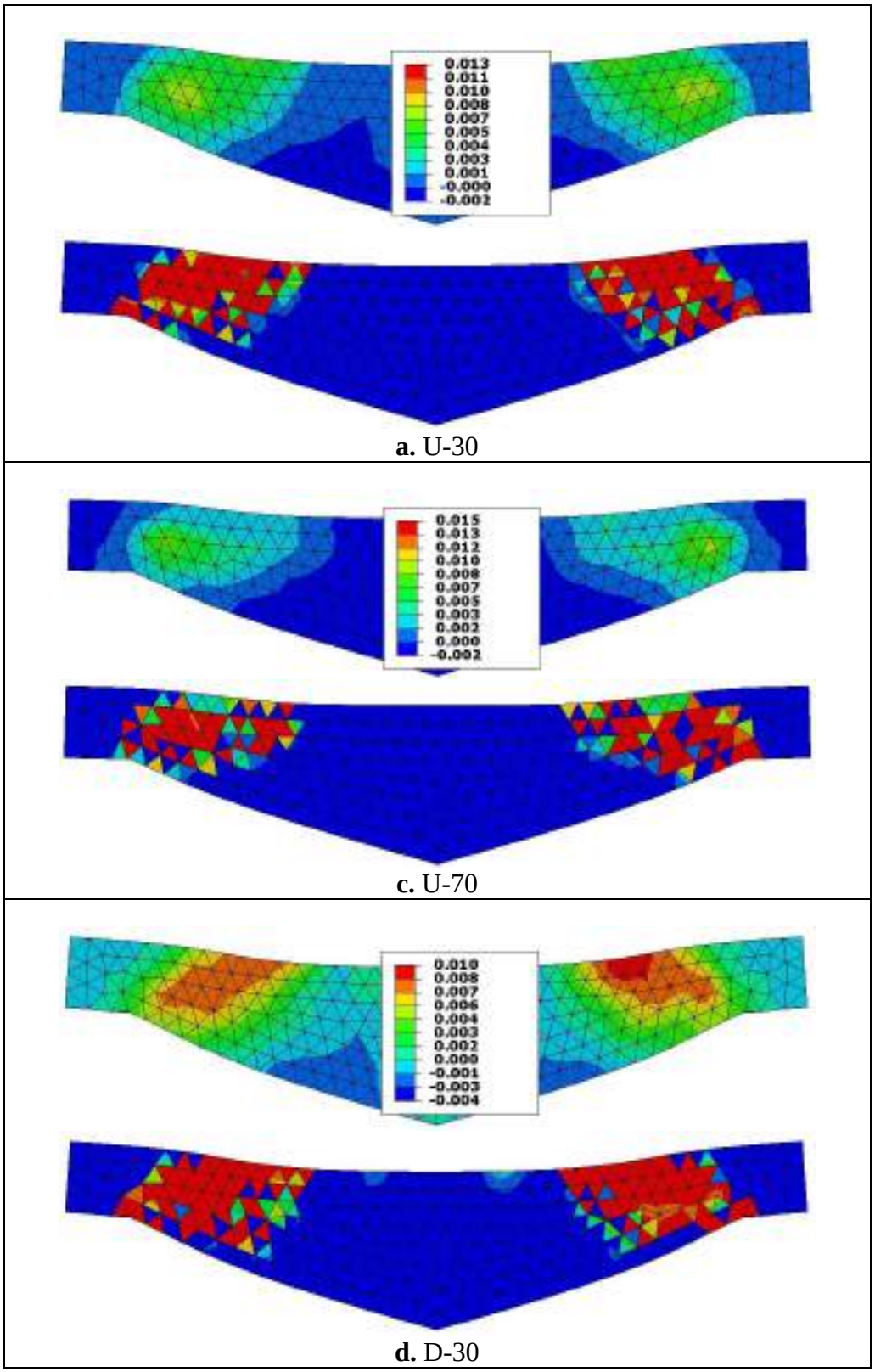

a. U-30

c. U-70

d. D-30

Figure 4.21 Failure modes (crack patterns) and total Strain distribution of FE model by effect of Opening Diameter.

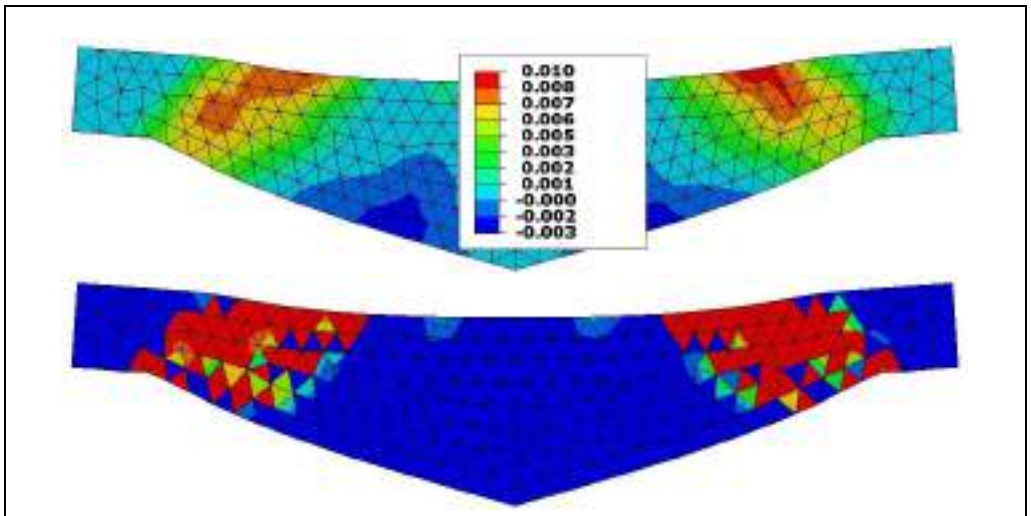

e. D-50

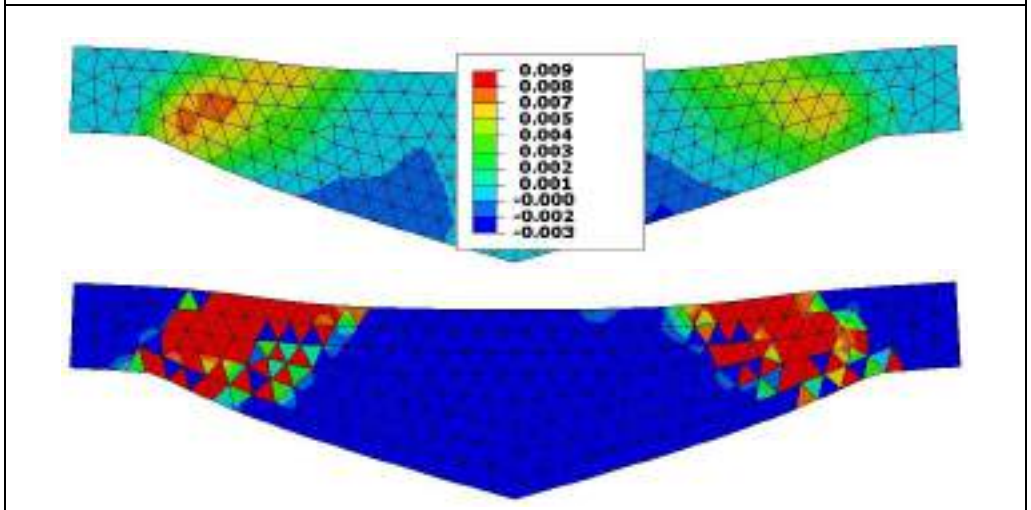

f. D-70

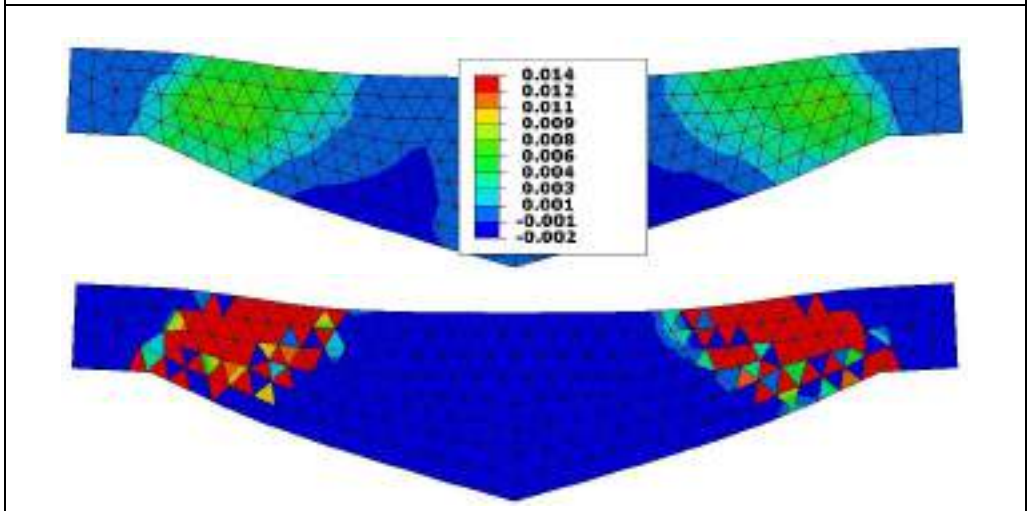

g. UD-30

Figure 4.22. Continue.

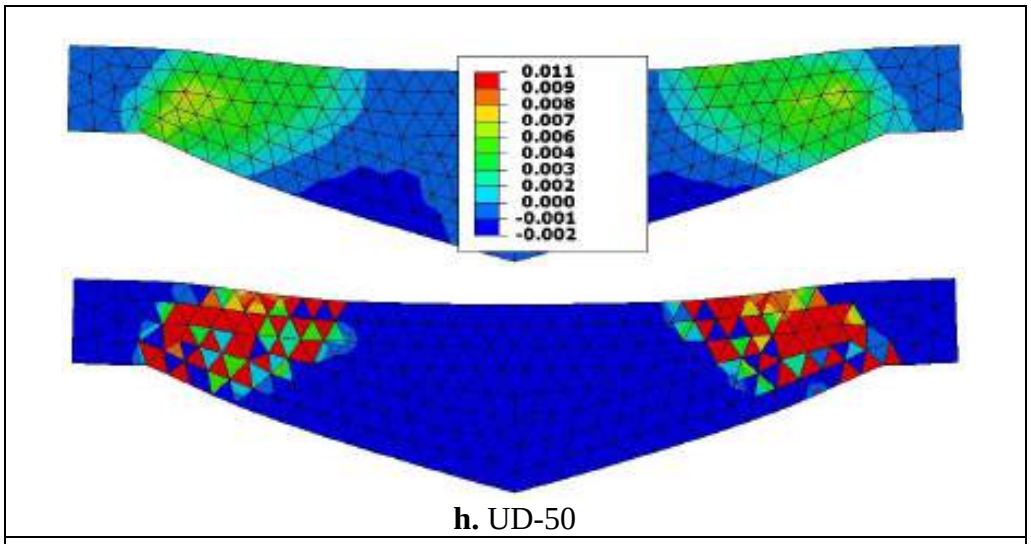

h. UD-50

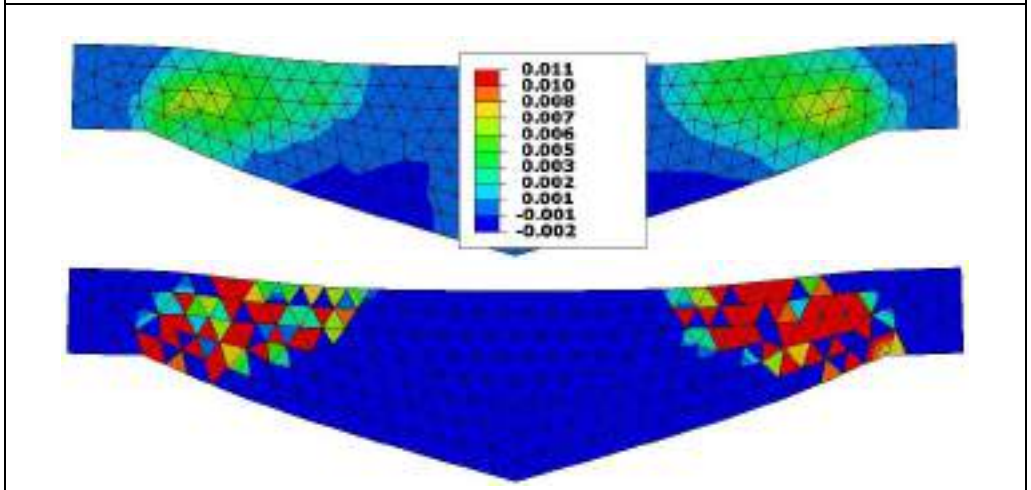

i. UD-70

Figure 4.22. Continue.

4.10 Reinforcement Ratio

4.10.1 Transvers Reinforcement Effect

The study was to verify the amount of transverse reinforcement using Ultra High-Performance Concrete with the addition of 2% fiber steel. The addition of transverse reinforcement in three phases with the same diameter of 8mm bar and at different spacings 850mm, 200mm, and 120mm is shown in Table 4.23. The results revealed that increased the amount of reinforcement led to 28% and 44%; respectively more in load capacity compared to the standard model TB-TR845

above. There is a significant effect on the mid-span deflection as the increase was observed by 79% and 148% on taking over compared to the model TB-TR845 the results are clear in Figure 4.23 as the pattern of Failure Turns Into flexural-shear failure mode. The models were designed for shear strength failure so the models were designed without stirrups and then after adding stirrups, the shear strength became higher than the flexural failure. Tensile strength increases by increasing the first crack load and decreases when the number and width of the cracks increase. As illustrated in Figure 4.24. Figure 4.25 shows the related crack patterns and strain distribution.

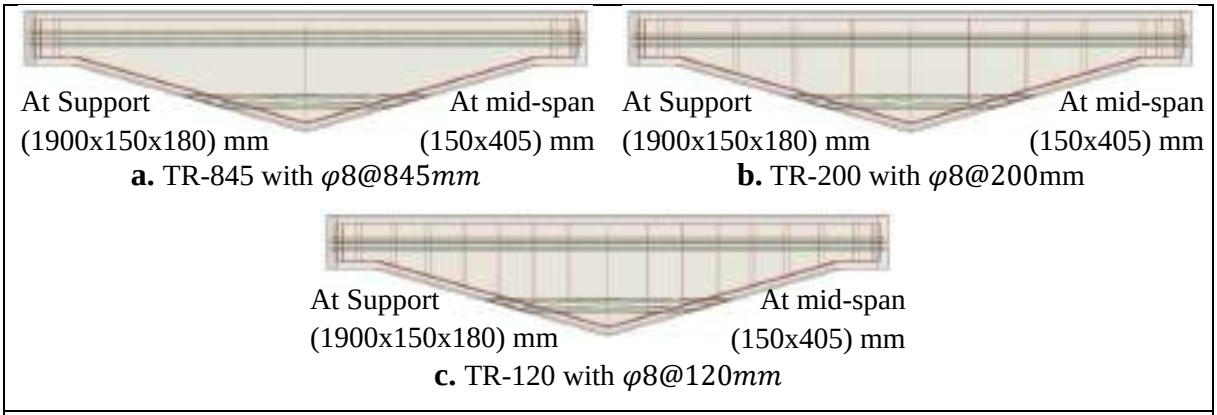

a. TR-845 with $\varphi 8@845mm$ **b.** TR-200 with $\varphi 8@200$mm

c. TR-120 with $\varphi 8@120mm$

Note: Compresstion Reinforcment: $2\varphi 8$, Tensile Reinforcement: $2\varphi 25$, Inclination angle: 15.9°, a/d Ratio:2.73, Grometry Daimention: (Length x width x depth).

Figure 4.22 Specimens' Modeling Details.

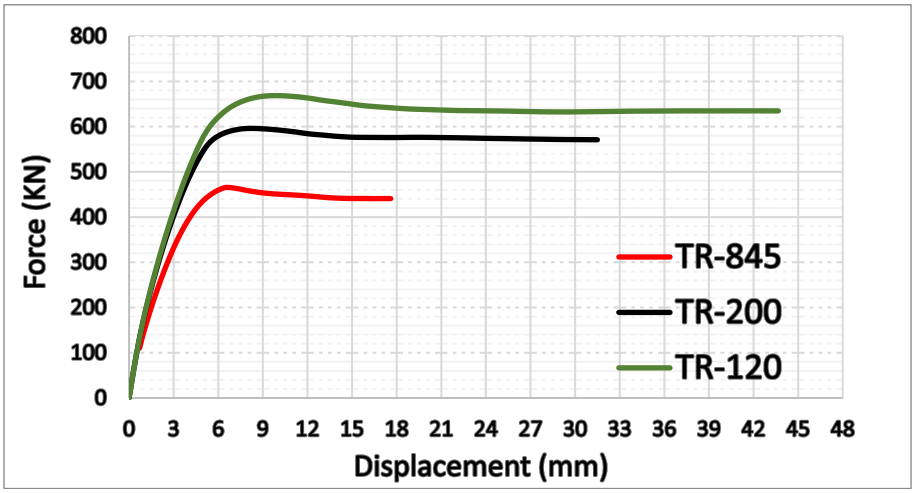

Figure 4.23 Results analysis: Transvers Reinforcement Effect.

Table 4.9 Results analysis: Transvers Reinforcement Effect.

Beam ID	Transvers Reinforcement	First Crack Load (kN)	Ultimate Shear Load (kN)	Ultimate Deflection mm	Splitting tensile (Mpa)	Ductility Index	Failure Mode
TR-120	**φ8@120**	187.8	668.4	43.7	14.40	12.5	Shear-flexural
TR-200	**φ8@200**	178.3	596.0	31.5	10.9	8.5	Shear-flexural
TR-845 (STD)	**φ8@845**	172.0	465.4	17.6	9.4	6.1	Shear

Beam ID	Transvers Reinforcement	Yield Load (kN)	Deflection Yield (mm)	Diagonal Strain	Max Shear Stress (Mpa)	Energy Absorption (kN.mm)	Initial Stiffness (kN/mm)
TR-120	**φ8@120**	498	3.5	0.0030	522	4770	142
TR-200	**φ8@200**	480	3.7	0.0031	507	2834	130
TR-845 (STD)	**φ8@845**	325	2.9	0.0048	492	913	112

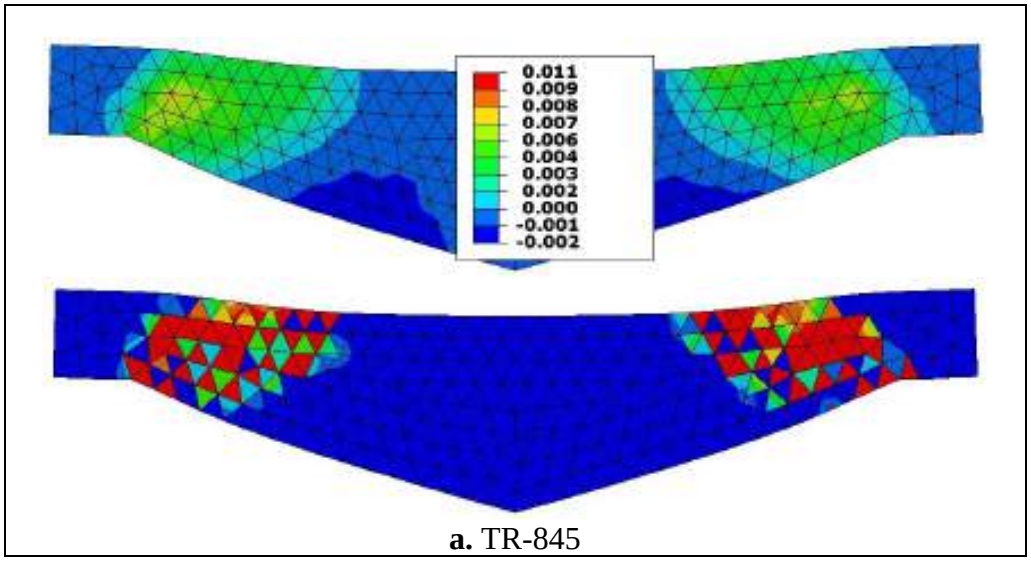

a. TR-845

Figure 4.24 Failure modes (crack patterns) and total Strain distribution of FE model by effect of Transvers Reinforcement.

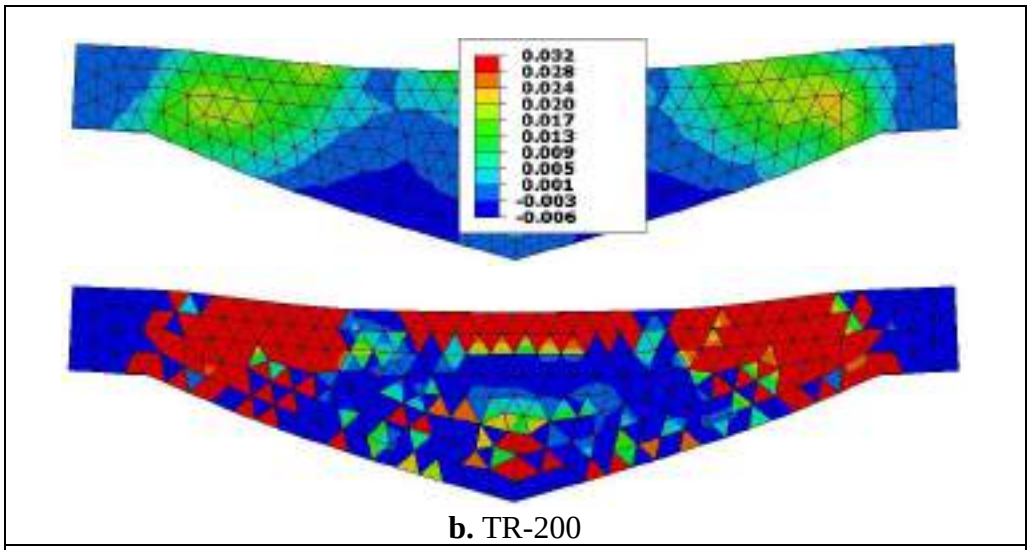

b. TR-200

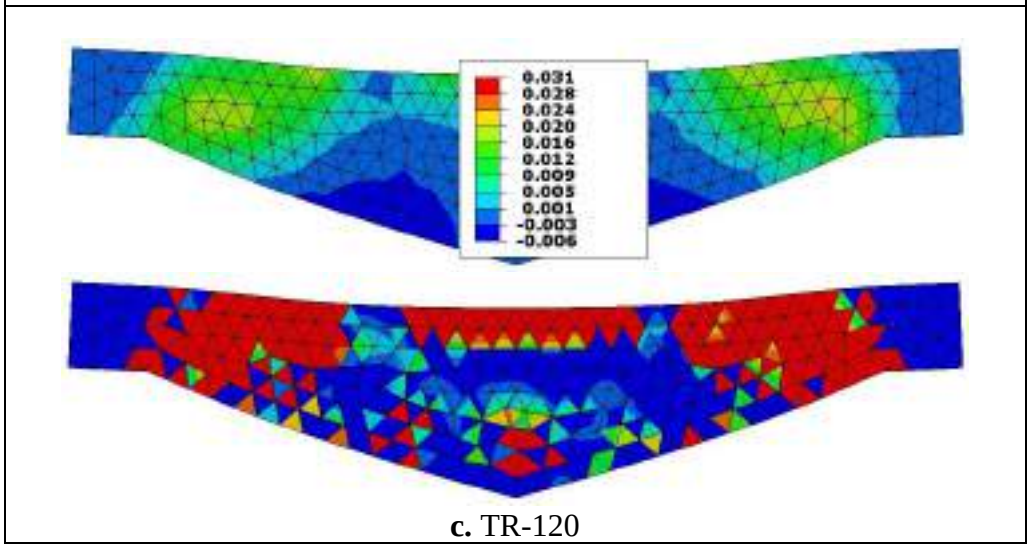

c. TR-120

Figure 4.26 Continue.

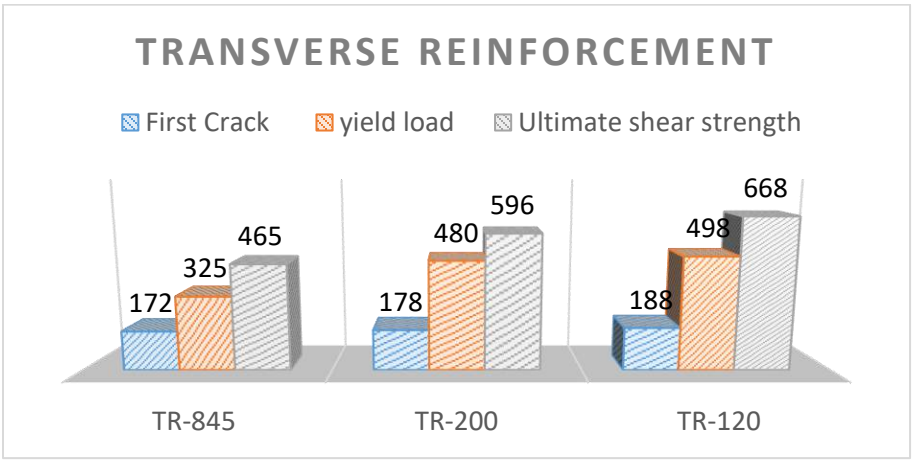

Figure 4.25 Results analysis: Transvers Reinforcement Effect.

4.10.2 Longitudinal Reinforcement Effect

The effect of longitudinal steel ratio within ductility limits, on the section as a shear response is considered and attainted in specimens (LR-2.24, LR-2.73, LR-3.01). The related specimens' modeling details are shown in Table 4. The numerical results were summarized in Table 7. The section strength is improved from 501 kN to 532 kN as the steel ratio changes from ρ=0.022 to ρ= 0.030 which are within ductility limit, the over-reinforcement section (ρ= 0.039), turns the section to over-reinforcement with brittle failure mode. Figure 4.28 shows the observed failure modes in the scope of crack patterns total Strain distribution. Results revealed that the ultimate shear strengths increase with increasing longitudinal reinforcement ratio. The increase in longitudinal reinforcement ratio from LR-2.73 to LR-3.01 results in a 14% increase in ultimate shear strength. This may be due to increased dowel action component and therefore increased shear strength. Figure 4.26 clearly illustrates the normalizing results of ultimate strength related to steel ratios.

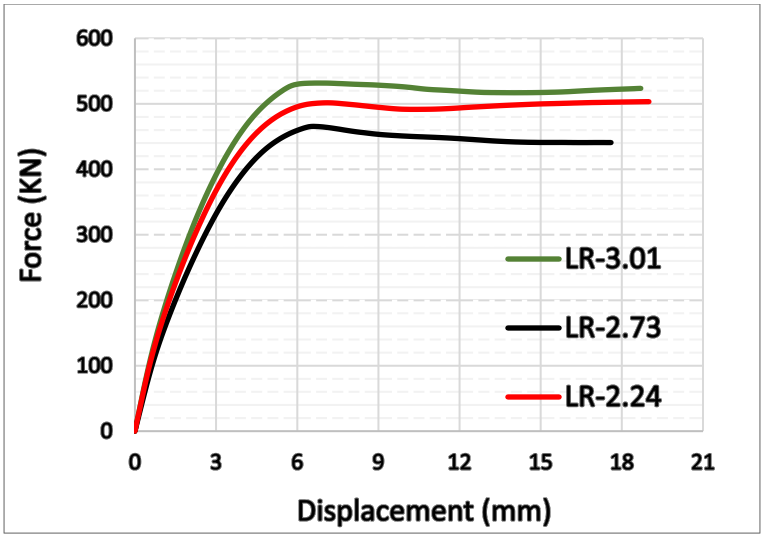

Figure 4.26 Results analysis: Longitudinal Reinforcement Effect.

Table 4.10a Results analysis: Longitudinal Reinforcement Effect.

Beam ID	Reinforcement Ratio	First Crack Load (kN)	Ultimate Shear Load (kN)	Ultimate Deflection mm	Splitting tensile (Mpa)	Ductility Index	Failure Mode
LR-2.24	$4\varphi16$	162.6	501.5	19	6.33	5.94	Shear
LR-2.73 (STD)	$2\varphi25$	172.0	465.4	17.6	6.29	6.07	Shear
LR-3.01	$2\varphi25 + 2\varphi8$	170.7	531.7	18.7	5.84	6.03	Shear

Beam ID	Reinforcement Ratio	Yield Load (kN)	Deflection Yield (mm)	Diagonal Strain	Max Shear Stress (Mpa)	Energy Absorption (kN.mm)	Initial Stiffness (kN/mm)
LR-2.24	$4\varphi16$	398	3	0.0033	561	1156	124
LR-2.73 (STD)	$2\varphi25$	325	2.8	0.0048	492	913	112
LR-3.01	$2\varphi25 + 2\varphi8$	425	3.2	0.0032	495	1198	137

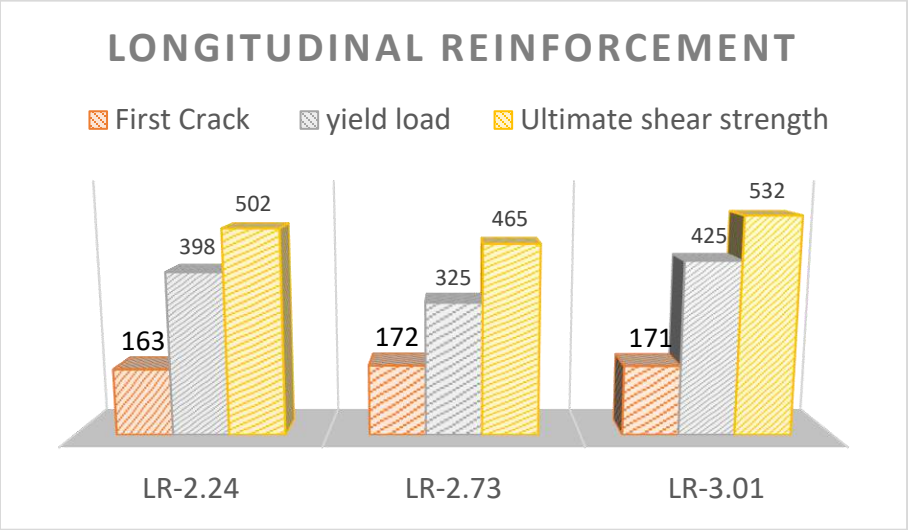

Figure 4.27 Results analysis: Longitudinal Reinforcement Effect.

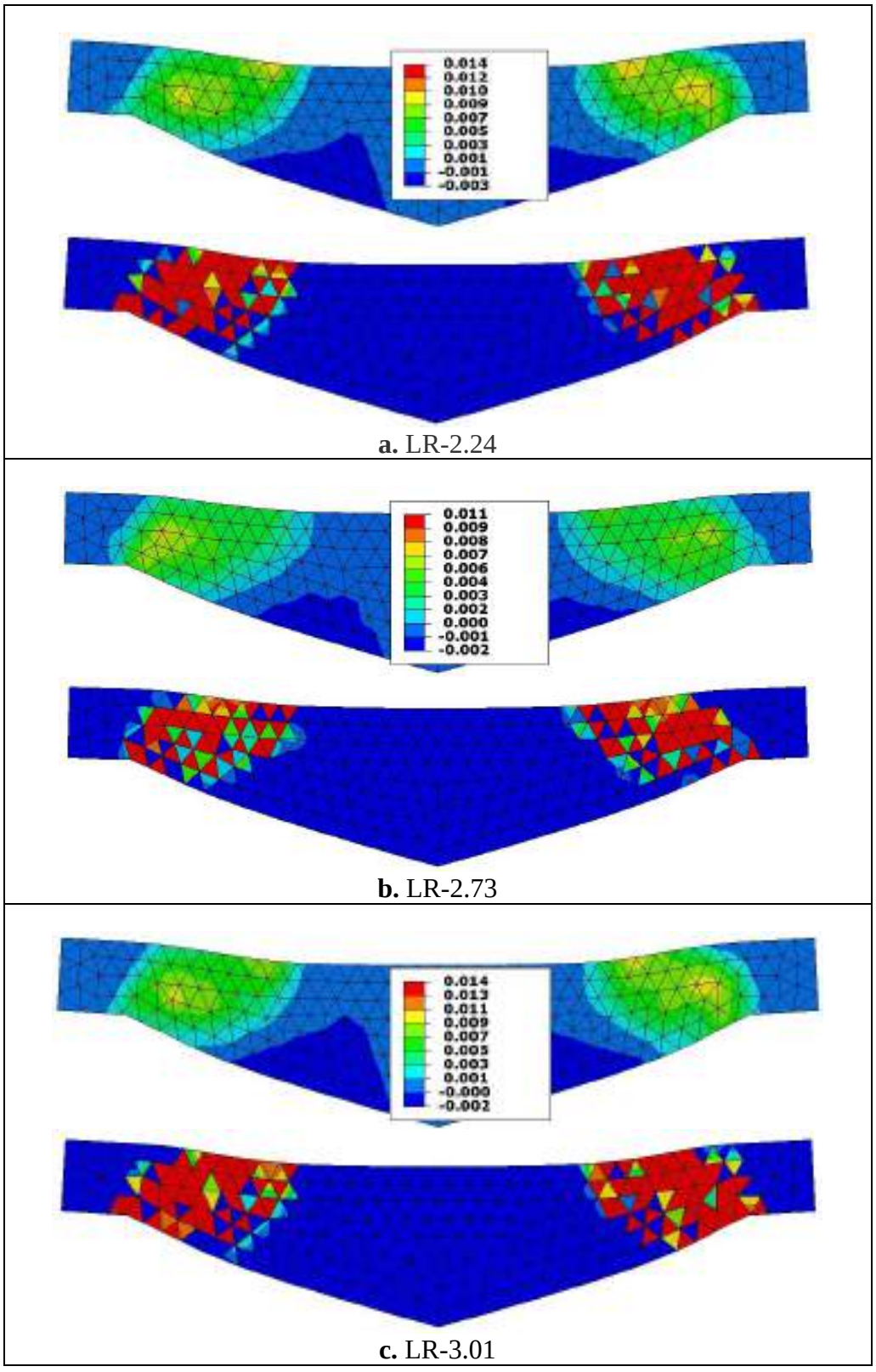

a. LR-2.24

b. LR-2.73

c. LR-3.01

Figure 4.28 Failure modes (crack patterns) and total Strain distribution of FE model by effect of Longitudinal Reinforcement.

4.11 Boundary Conditions Effect

Different boundary condition are considered their effect on strength, ductility of the developed tapered beam. Hinge-Roller, fully fixed boundary condition state are geometry details of adopted specimens which are indicated in the Table 4.2, while Table 4.10 exhibits the related results. Analysis the simply supported Hinge-Roller state concerned with a specified state that constrained the bottom face of section web in support the region only, while the fully fixed state relates to constrain the overall cross section within support region. Fig. 4.30 clearly depicts the various aspects of boundary conditions on shear load deflection response, the fixed state was more than simply supported shear load by 9%, and deflection decreased by 6%. Very close shear strength estimation is obtained in the case of simply supported and fixed conditions. As illustrated in Figure 4.31., while Figure 4.32 show the related crack patterns and strain distribution.

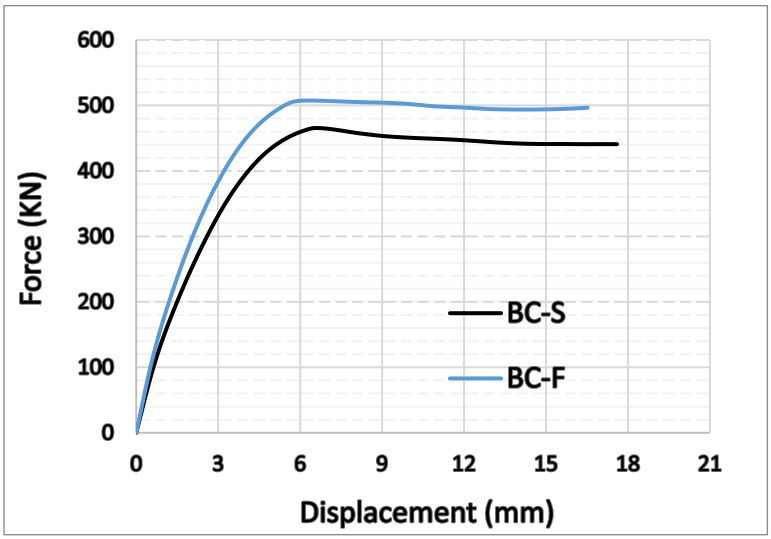

Figure 4.29 Results analysis: Boundary Conditions Effect.

Table 4.11 Results analysis: Longitudinal Reinforcement Effect.

Beam ID	Boundary Condition	First Crack Load (kN)	Ultimate Shear Load (kN)	Ultimate Deflection mm	Splitting tensile (MPa)	Ductility Index	Failure Mode
BC-S (STD)	**Simply Supported**	172	465.4	17.6	9.4	6.1	Shear
BC-F	**Fixed Supported**	170	507.5	16.5	7.7	5.3	Shear

Beam ID	Boundary Condition	Yield Load (kN)	Deflection Yield (mm)	Diagonal Strain	Max Shear Stress (MPa)	Energy Absorption (kN.mm)	Initial Stiffness (kN/mm)
BC-S (STD)	**Simply Supported**	325	2.9	0.0048	492	913	112
BC-F	**Fixed Supported**	410	3.1	0.0034	492	958	132

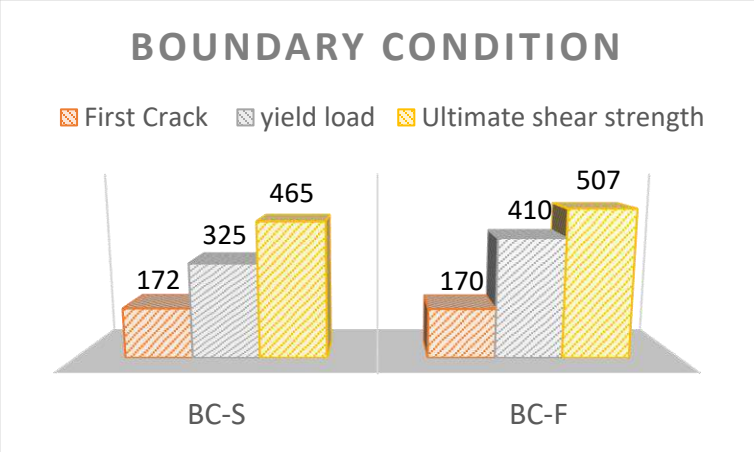

Figure 4.30 Results analysis: Boundary Condition Effect.

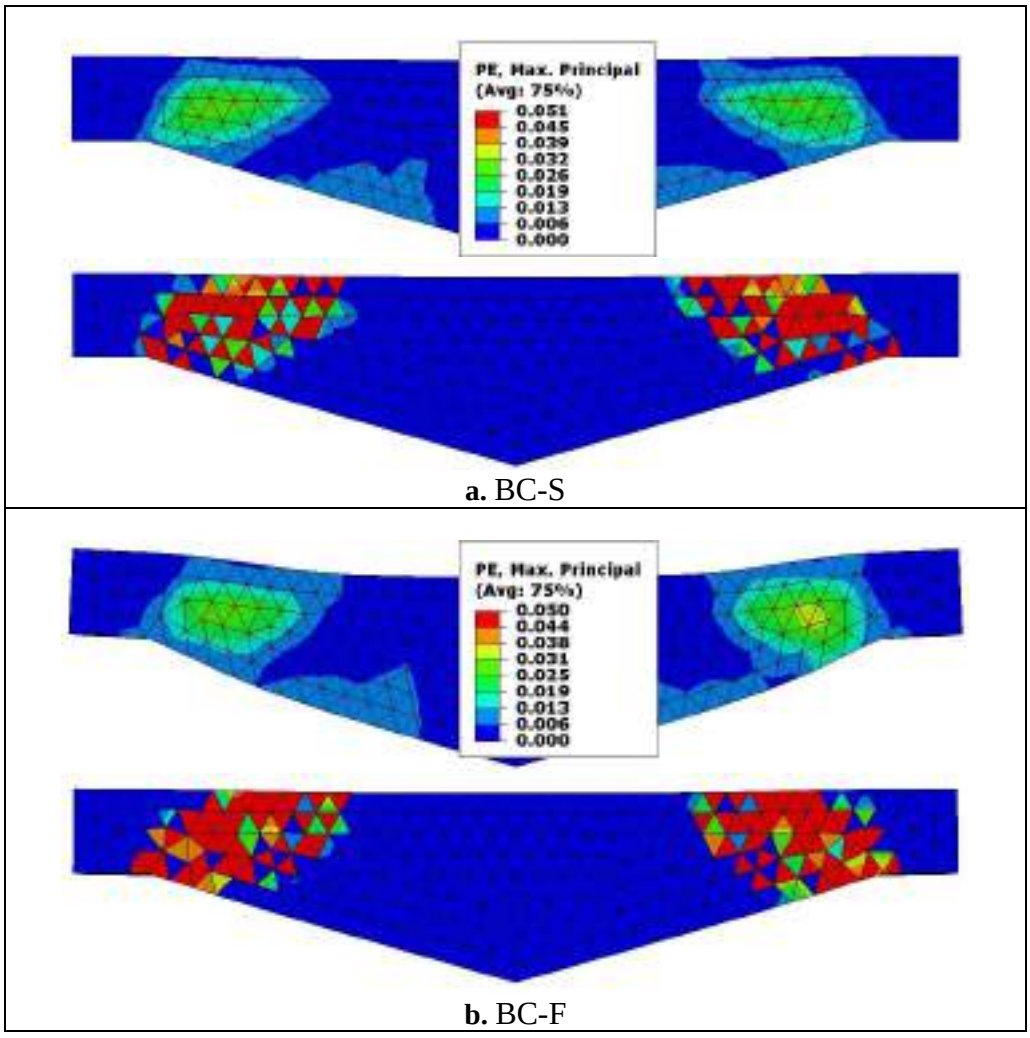

a. BC-S

b. BC-F

Figure 4.31 Failure modes (crack patterns) and total Strain distribution of FE model by effect of Boundary Condition.

CHAPTER FIVE:CONCLUSION AND RECOMMENDATIONS

5.1 Conclusion

The present numerical study is focused on the behavior of reinforced concrete Tapered beams. Based on the results obtained from the FEM by using ABAQUS program. Many factors have a significant effect on the general behavior of the beam at failure and these effects can be summarized as follows:

1. The comparison of nine numerical models with experimental results in the previous study approximately predicted the structural behaviors of UHPC beams models and showed a very good compatibility ranging from 0.96 to 1.07.
2. The shear resistance of a non-prismatic beam is stabilized and higher when longitudinal openings are at the bottom and its diameter is increased, compared to having the same openings at the top or having openings at both the top and bottom. This may be because the compression zone affects the shear resistance, which remains intact because the longitudinal opening is in the tensile zone and does not significantly impact its presence.
3. Increasing the size of the upper hole has no significant impact on shear resistance and can result in material savings while maintaining the same level of resistance.
4. The shear force of tapered beams is lower than other hollow beams when the hole is contained within the stress block. Using two circular holes in beams reduces weight while maintaining resistance and deflections, achieving higher optimization with two openings in the beam's area and diameter.
5. The a/d ratio has a direct impact on the shear strength of a beam. Consequently, a higher a/d ratio leads to a decrease in shear strength. This change in behavior can be attributed to the presence of a direct compression strut between the load

and support, as well as the arch action that occurs when the a/d ratio is less than 2.

6. An increase in shear strength was observed when the scale factor 2.4 was increased, resulting in a 348% increase. The concrete volume representation with semi-scale dimensions allows the concrete to resist greater compression force.
7. The crown's length is increased from 0 to 200 mm, and the shear strength is increased by 10%. Then, there is a slight increase after increasing the crown length from 200-500 mm.
8. The fixed support had a 9% higher shear load and a 6% decrease in deflection. The shear strength estimation is similar for simply supported and fixed conditions.
9. The shear strengths increase with increasing reinforcement ratio. This may be due to the increase of the dowel action component and therefore increased shear strength.
10. The higher the transverse reinforcement ratio, the more cracks formed with smaller openings. The increased shear reinforcement ratio enhanced the shear strength of the beams, leading to shear cracking under higher load. With an increase in shear reinforcement, the typical combined shear-flexural failure mode occurred.

5.2 Recommendations for Future Works

Extra investigation to understand the basic behavior of RC beams is required. The following suggestions are recommended:

1. Investigation of shear strength for the non-prismatic behavior when strengthened with CFRP bar and GFRP sheet.
2. Investigation of shear strength behavior in hybrid strength reinforced concrete beams of non-prismatic section.
3. Numerical analysis for transverse openings with strength system.
4. Numerical analysis for flexural strength of tapered beam.

REFERENCES

1. Nampalli, P. and P. Sangave, *Linear and Non-Linear Analysis of Reinforced Concrete Frames with Members of Varying Inertia*. IOSR Journal of Mechanical and Civil Engineering, 2015.

2. Ibrahim, S.K. and M.M. Rad. *Numerical Plastic Analysis of Non-Prismatic Reinforced Concrete Beams Strengthened by Carbon Fiber Reinforced Polymers*. in *Proc. of the 13th fib International PhD Symposium in Civil Engineering*. 2020. Marne-la-Vallée Paris France.

3. Toshniwal, S., *Shear Analysis of Non-Prismatic Concrete Beams.* 2019.

4. Tena-Colunga, A., H.I. Archundia-Aranda, and Ó.M. González-Cuevas, *Behavior of reinforced concrete haunched beams subjected to static shear loading.* Engineering Structures, 2008. **30**(2): p. 478-492.

5. Jaafer, A.A. and A.W. Abdulghani. *Nonlinear finite element analysis for reinforced concrete haunched beams with opening*. in *IOP Conference Series: Materials Science and Engineering*. 2018. IOP Publishing.

6. CODE, A., *318-14: Building Code Requirements for Structural Concrete and Commentary.* American Concrete Institute: Farmington Hills, MI, USA, 2014.

7. Nimnim, H.T., A.T. Jassim, and A.A. Abdul Mohsen, *Structural behavior of reinforced reactive powder concrete tapered beams.* Practice Periodical on Structural Design and Construction, 2019. **24**(2): p. 04019002.

8. Shooshtari, A. and R. Khajavi, *An efficient procedure to find shape functions and stiffness matrices of nonprismatic Euler–Bernoulli and Timoshenko beam elements.* European Journal of Mechanics-A/Solids, 2010. **29**(5): p. 826-836.
9. Ozay, G. and A. Topcu, *Analysis of frames with non-prismatic members.* Canadian Journal of Civil Engineering, 2000. **27**(1): p. 17-25.

10. El-Mezaini, N., C. Balkaya, and E. Çitipitio g ˘ lu, *Analysis of frames with nonprismatic members.* Journal of Structural Engineering, 1991. **117**(6): p. 1573-1592.

11. Tan, K.H., *Design of non-prismatic RC beams using strut-and-tie models.* Journal of Advanced Concrete Technology, 2004. **2**(2): p. 249-256.

12. El-Niema, E., *Investigation of concrete haunched T-beams under shear*. Journal of Structural Engineering, 1988. **114**(4): p. 917-930.

13. Adeline, R. *Design and Behavior of the Sherbrooke footbridge*. in *International Symposium of High Performance Concrete, Sherbrooke*. 1998.

14. Tayeh, B.A., L.K. Askar, and B.A. Bakar, *Ultra-High-Performance Concrete (UHPC)-Applications Worldwide: A State-of-the-Art Review.* Journal of Engineering Research and Technology, 2023. **10**(1).

15. Deem, S., *Concrete Attraction–Something new on the French menu—concrete.* Popular Mechanics, 2002.

16. Dere, Y. and M.A. Koroglu, *Nonlinear FE modeling of reinforced concrete.* International Journal of Structural and Civil Engineering Research, 2017. **6**(1): p. 71-74.

17. George, J., et al., *Behavior of plain concrete beam subjected to three point bending using concrete damaged plasticity (CDP) model.* Materials Today: Proceedings, 2017. **4**(9): p. 9742-9746.

18. Rašeta, A., et al. *Use of Finite Element Method for Simulation of RC Beam Nonlinear Behavior*. in *5th Int. Conf. Contemporary Achievements Civ. Eng.* 2017.

19. Miehe, C., M. Hofacker, and F. Welschinger, *A phase field model for rate-independent crack propagation: Robust algorithmic implementation based on operator splits.* Computer Methods in Applied Mechanics and Engineering, 2010. **199**(45-48): p. 2765-2778.

20. Rokugo, K., et al., *Applications and recommendations of high performance fiber reinforced cement composites with multiple fine cracking (HPFRCC) in Japan.* Materials and structures, 2009. **42**(9): p. 1197-1208.

21. Richard, P. and M.H. Cheyrezy, *Reactive powder concretes with high ductility and 200-800 MPa compressive strength.* Special Publication, 1994. **144**: p. 507-518.

22. Hamoda, A., et al., *Experimental and numerical assessment of reinforced concrete beams with disturbed depth.* International Journal of Concrete Structures and Materials, 2019. **13**(1): p. 1-28.

23. Sada, M.J. *Comparative Experimental Investigation of Flexure and Shear Strength in Hybrid-Trapezoidal Reinforced Concrete Sections*. in *IOP Conference Series: Materials Science and Engineering*. 2021. IOP Publishing.

24. Mahzuz, H., A. Ahmed, and M. Yusuf, *Use of stone powder in concrete and mortar as an alternative of sand.* African Journal of Environmental Science and Technology, 2011. **5**(5): p. 381-388.

25. Khalil, A.H., M. Nabil, and M. Mohamed, *Shear Behavior of Trapezoidal Beams.* Journal of Al-Azhar University Engineering Sector, 2017. **12**(42): p. 37-53.

26. Aaleti, S. and S. Sritharan, *Investigation of a suitable shear friction interface between UHPC and normal strength concrete for bridge deck applications*. 2017.

27. Prabha, S.L., et al., *Study on stress-strain properties of reactive powder concrete under uniaxial compression.* International Journal of Engineering Science and Technology, 2010. **2**(11): p. 6408-6416.

28. Collepardi, S., et al., *The influence of the fiber type on the performance of RPC.* INDUSTRIA ITALIANA DEL CEMENTO, 2003: p. 334-341.

29. Gowripalan, N. and R. Gilbert, *Design guidelines for ductal prestressed concrete beams. Design guide.* Civil & Environmental Engineering School, University of NSW, Sydney, Australia, 2000.

30. Santos, S.P., J.A. Barros, and L. Lourenço, *Steel fibres for the shear resistance of high strength concrete beams.* 2008.

31. Committee, A. *Building code requirements for structural concrete (ACI 318-08) and commentary*. 2008. American Concrete Institute.

32. Graybeal, B.A., *Material property characterization of ultra-high performance concrete*. 2006, United States. Federal Highway Administration. Office of Infrastructure.

33. Russell, H.G., et al., *State-of-the-art report on high-strength concrete.* ACI Committee, 1997. **363**: p. 92.

34. Allen, T., et al., *A new working stress method for prediction of reinforcement loads in geosynthetic walls.* Canadian Geotechnical Journal, 2003. **40**(5): p. 976-994.

35. Resplendino, J. *First recommendations for Ultra-High-Performance Concretes and examples of application*. in *International Symposium on Ultra High Performance Concrete*. 2004.

36. Maroliya, M., *Bond strength of reactive powder concrete containing steel fibre and silica fume.* International Journal of Emerging Technology & Advanced Engineering, 2012. **2**(10): p. 66-68.

37. Habeeb, G.M., M.B. Dawood, and A.H. Adheem, *FLEXURAL BEHAVIOR OF PRECAST-PRESTRESSED CONCRETE BEAM WITH REACTIVE POWDER CONCRETE SLAB.*

38. Ridha, M.M., I.A. Al-Shaarbaf, and K.F. Sarsam, *Experimental study on shear resistance of reactive powder concrete beams without stirrups.* Mechanics of Advanced Materials and Structures, 2020. **27**(12): p. 1006-1018.

39. Kotsovos, M., *Shear failure of reinforced concrete beams.* Engineering Structures, 1987. **9**(1): p. 32-38.

40. Bazant, Z.P. and M.T. Kazemi, *Size effect on diagonal shear failure of beams without stirrups.* ACI Structural journal, 1991. **88**(3): p. 268-276.

41. Słowik, M., *Shear failure mechanism in concrete beams.* Procedia materials science, 2014. **3**: p. 1977-1982.

42. Kristiawan, S., et al. *Shear failure of patched reinforced concrete beam without web reinforcements*. in *Key engineering materials*. 2017. Trans Tech Publ.

43. Słowik, M., *The analysis of failure in concrete and reinforced concrete beams with different reinforcement ratio.* Archive of applied mechanics, 2019. **89**: p. 885-895.

44. Ashour, S.A., G.S. Hasanain, and F.F. Wafa, *Shear behavior of high-strength fiber reinforced concrete beams.* Structural Journal, 1992. **89**(2): p. 176-184.

45. Orr, J., et al., *The shear behaviour of non-prismatic reinforced concrete beams determined using digital image correlation.* 2013.

46. Park, R. and T. Paulay, *Reinforced Concrete Structures, John Wiley & Sons.* NY, USA, 1975.

47. Al-Maliki, H.N.G.M., *Experimental behavior of hollow non-prismatic reinforced concrete beams retrofit with CFRP sheets.* Journal of Engineering and Sustainable Development, 2013. **17**(5): p. 224-237.

48. Balaji, G. and R. Vetturayasudharsanan, *Experimental investigation on flexural behaviour of RC hollow beams.* Materials today: proceedings, 2020. **21**: p. 351-356.

49. Abdulrahman, M.B. and S.M. Mahmood, *Strength of reinforced reactive powder concrete hollow beams.* Tikrit Journal of Engineering Sciences, 2019. **26**(2): p. 15-22.

50. Murugesan, A. and A. Narayanan, *Influence of a longitudinal circular hole on flexural strength of reinforced concrete beams.* Practice Periodical on Structural Design and Construction, 2017. **22**(2): p. 04016021.

51. Abbass, A.A., et al. *Flexural response of hollow high strength concrete beams considering different size reductions*. in *Structures*. 2020. Elsevier.

52. Alshimmeri, A.J.H. and H.N.G. Al-Maliki, *Structural behavior of reinforced concrete hollow beams under partial uniformly distributed load.* Journal of Engineering, 2014. **20**(07): p. 130-145.

53. Chaudhari, S. and M. Chakrabarti, *Modeling of concrete for nonlinear analysis using finite element code ABAQUS.* International Journal of Computer Applications, 2012. **44**(7): p. 14-18.

54. Sinaei, H., et al., *Evaluation of reinforced concrete beam behaviour using finite element analysis by ABAQUS.* Scientific Research and Essays, 2012. **7**(21): p. 2002-2009.

55. Słowik, M. and T. Nowicki, *The analysis of diagonal crack propagation in concrete beams.* Computational Materials Science, 2012. **52**(1): p. 261-267.

56. Rao, C.K., P.P. Raju, and T.N.S. Babu, *Comparative study on analysis of plain and rc beam using ABAQUS.* Int J Civil Eng Technol (IJCIET), 2017. **8**(4): p. 1531-1538.

57. Kalyana Rama, J., et al., *Fracture properties of concrete using damaged plasticity model-A parametric study.* Structural engineering and mechanics: An international journal, 2017. **64**(1): p. 59-69.

58. Giner, E., et al., *An Abaqus implementation of the extended finite element method.* Engineering fracture mechanics, 2009. **76**(3): p. 347-368.

59. Tejaswini, T. and M. Raju, *Analysis of RCC Beams using ABAQUS.* International journal of Innovations in Engineering and Technology (IJIET), 2015. **5**(3).

60. Hansen-Dörr, A.C., et al., *Phase-field modelling of fracture in heterogeneous materials.* PAMM, 2018. **18**(1): p. e201800082.

61. Rombach, G.A. and A. Faron, *Numerical analysis of shear crack propagation in a concrete beam without transverse reinforcement.* Procedia structural integrity, 2019. **17**: p. 766-773.

62. Kriaa, Y., H. Hentati, and B. Zouari, *Applying the phase-field approach for brittle fracture prediction: Numerical implementation and experimental validation.* Mechanics of Advanced Materials and Structures, 2022. **29**(6): p. 828-839.

63. Board, N.T.S., *Collapse of I-35W highway bridge, Minneapolis, Minnesota, August 1, 2007.* Accident Report NTSB/HAR-08/03, PB2008916203, 2008.

64. Eftekhari, M., S.H. Ardakani, and S. Mohammadi, *An XFEM multiscale approach for fracture analysis of carbon nanotube reinforced concrete.* Theoretical and Applied Fracture Mechanics, 2014. **72**: p. 64-75.

65. Deng, S., Z. Qie, and L. Wang. *Nonlinear analysis of reinforced concrete beam bending failure experimentation based on ABAQUS*. in *First International Conference on Information Sciences, Machinery, Materials and Energy*. 2015. Atlantis Press.

66. Bažant, Z.P. and T.-P. Chang, *Nonlocal finite element analysis of strain-softening solids.* Journal of engineering mechanics, 1987. **113**(1): p. 89-105.

67. Park, R. and T. Paulay, *Reinforced concrete structures*. 1991: John Wiley & Sons.

68. Kmiecik, P. and M. Kamiński, *Modelling of reinforced concrete structures and composite structures with concrete strength degradation taken into consideration.* Archives of civil and mechanical engineering, 2011. **11**(3): p. 623-636.

69. Code, P. *Eurocode 2: Design of Concrete Structures. Part 1-1: General Rules and Rules for Buildings. British Standard Institution; London, UK: 2004*. in *12th Asia-Oceania Symposium on Fire Science and Technology*. 2021.

70. Stoner, J., *Finite element modelling of GFRP reinforced concrete beams*. 2015, University of Waterloo.

71. Tu'ma, N.H., M.R. Aziz, and H.J.J. Barry, *Residual Tensile Stress Estimation for Shear Strength of UHPC Nonprismatic Beams.* Civil and Environmental Engineering, 2021. **17**(1): p. 164-177.

72. Nguyen, H.T. and S.E. Kim, *Finite element modeling of push-out tests for large stud shear connectors.* Journal of Constructional Steel Research, 2009. **65**(10-11): p. 1909-1920.

73. Najafgholipour, M., et al., *Finite element analysis of reinforced concrete beam-column connections with governing joint shear failure mode.* Latin American Journal of Solids and Structures, 2017. **14**: p. 1200-1225.

74. Karlsson, B. and E. Sorensen, *ABAQUS Analysis User's Guide Volume IV: Elements.* Hibbitt Publication: Pawtucket, RI, USA, 2006.

75. Lateef, H.A., R.M. Laftah, and N.A. Jasim, *Study on the Shear Failure of Reinforced Concrete Beams Using Extended Finite Element Method (XFEM).* Basrah Journal for Engineering Sciences, 2021. **21**(3): p. 55-65.

76. Jasim, N.A. and M.S.M. Abd Al-baqer, *Analysis of Composite Panels of Profiled Steel Sheet with Ferrocement by Using Finite Element Method.* Univesity of Thi-Qar Journal, 2019. **14**(4).

77. Rakhshanimehr, M., et al., *Flexural ductility of reinforced concrete beams with lap-spliced bars.* Canadian Journal of Civil Engineering, 2014. **41**(7): p. 594-604.

78. Abdulraheem, M.S., *Experimental investigation of fire effects on ductility and stiffness of reinforced reactive powder concrete columns under axial compression.* Journal of Building Engineering, 2018. **20**: p. 750-761.

79. Othman, H. and H. Marzouk, *Applicability of damage plasticity constitutive model for ultra-high performance fibre-reinforced concrete under impact loads.* International Journal of Impact Engineering, 2018. **114**: p. 20-31.

80. Chen, L. and B.A. Graybeal, *Modeling structural performance of ultrahigh performance concrete I-girders.* Journal of Bridge Engineering, 2012. **17**(5): p. 754-764.

81. Zhang, Y., H. Xin, and J.A. Correia, *Fracture evaluation of ultra-high-performance fiber reinforced concrete (UHPFRC).* Engineering Failure Analysis, 2021. **120**: p. 105076

APPENDIX A

A.1 Introduction

ABAQUS is a powerful finite element package vastly used in civil engineering practice. Particularly used for modeling the reinforced concrete structure. Concrete damaged plasticity is one of the most appropriate models that deals with concrete behavior considering possible failure modes; the tensile cracking and compressive crashing. A program input of concrete and steel reinforcement modelling for the specimens with 155 MPa compressive strength is given as an example for material modeling and all special definitions about the property of elements are described below.

A.2 Material Properties Modeling

A.2.1 Material properties

All parameters for the material models were illustrated in Tables. (A-3) to (A-8). ABAQUS element needs some properties for proper entities which are elastic and plastic properties. The stress-strain curve of the concrete that obtained from the equations (3.1), (3.13) and (3.14) is used in the modeling of the nonlinear behavior.

Table (A-1): Elastic properties of concrete.

Type	Youngs Modulus (MPa)	Poisson's Ratio
Isotropic	50000	0.2

Table (A-2): Plastic properties of concrete.

Dilation Angle (ψ)	**Eccentricity (ϵ)**	**Strength ratio (σ_{b0}/σ_{c0})**	***Kc***	**Viscosity parameter (ŋ)**
39	0.1	1.16	0.667	0.0001

Table (A-3): Concrete compressive behavior.

Yield stress (MPa)	**Inelastic strain**	***dc***
116.83	0	0
124.28	0.000025	0
137.37	0.000155	0
147.85	0.000331	0
153.28	0.000543	0
155	0.000755	0
153.76	0.001179	0.008
152.3	0.001391	0.017
150.26	0.001603	0.031
147.69	0.001815	0.047
145.15	0.002027	0.064
142.51	0.002239	0.081
139.93	0.002451	0.097
137.31	0.002663	0.114
134.75	0.002874	0.131
132.15	0.003086	0.147
129.56	0.003298	0.164
126.97	0.00351	0.181
124.38	0.003722	0.198
121.83	0.003934	0.214
119.23	0.004146	0.231
116.64	0.004358	0.247
114.07	0.00457	0.264

Table (A-4): Concrete tensile behavior.

Yield stress (MPa)	Inelastic strain	dt
8.0	0.00000	0.00000
7.8	0.00028	0.03150
6.6	0.00043	0.17290
7.1	0.00098	0.11640
6.6	0.00133	0.18030
6.1	0.00168	0.23450
5.7	0.00203	0.28810
5.3	0.00238	0.34050
4.9	0.00269	0.38270

Table (A-5): Material properties for Ø8 rebar (longitudinal reinforcement for top and stirrups).

Elastic properties			
Type	**Youngs Modulus (MPa)**	**Poisson's Ratio**	**Density (tonne/mm^3)**
Isotropic	200000	0.3	7890
Plastic properties			
Hardening		**Yield stress (MPa)**	**Plastic strain**
Isotropic		423.5	0
		526.4	0.288

Table (A-6): Material properties for ∅12 rebar (longitudinal reinforcement for bottom).

Elastic properties			
Type	**Youngs Modulus (MPa)**	**Poisson's Ratio**	**Density (tonne/mm^3)**
Isotropic	200000	0.3	7890
Plastic properties			
Hardening		**Yield stress (MPa)**	**Plastic strain**
Isotropic		577.6	0
		653.0	0.116

Table (A-7): Material properties for ∅16 rebar (longitudinal reinforcement for bottom).

Elastic properties			
Type	**Youngs Modulus (MPa)**	**Poisson's Ratio**	**Density (tonne/mm^3)**
Isotropic	200000	0.3	7890
Plastic properties			
Hardening		Yield stress (MPa)	Plastic strain
Isotropic		551.6	0
		655.0	0.102

Table (A-8): Material properties for ∅25 rebar (longitudinal reinforcement for bottom).

Elastic properties			
Type	**Youngs Modulus (MPa)**	**Poisson's Ratio**	**Density (tonne/mm^3)**
Isotropic	200000	0.3	7890
Plastic properties			
Hardening		Yield stress (MPa)	Plastic strain
Isotropic		481.3	0
		671.6	0.133

APPENDIX B

B.1 Introduction

In this appendix, the simulation of tapered beams made of UHPC, which was simulated by experimental method is discussed. Different samples in different categories have been simulated in this research, 8 samples out of 4 categories presented in this research (category 1 to 4) have been simulated in Abaqus software. In the following, the details of the simulation are presented in full.

B.2 Modeling geometry

The geometry of the modeling is different in different samples, but generally a schematic of the models analyzed in category 1 to 4 is presented below.

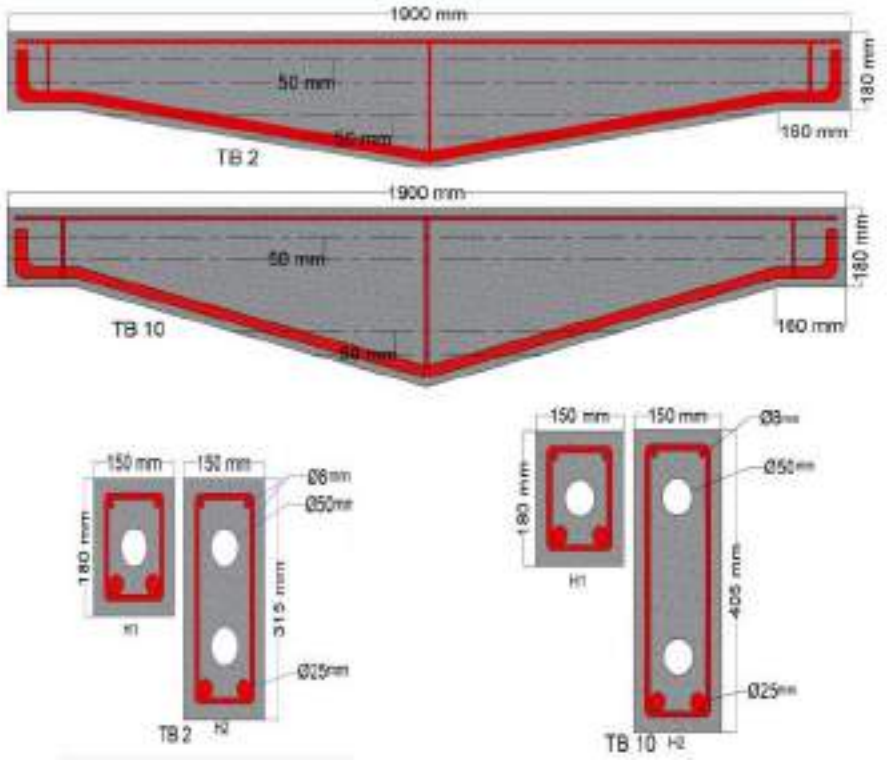

Figure 1: Geometry and specifications of the first category sample.

From the samples presented in the first category, the variable of which is the length of the tapered area, samples TB2 and TB10 have been simulated, and in all

samples, the length of the beam is 1.9 meters and its effective length is 1.6 meters, and the thickness of all samples is It was 150 mm. The length of the non- tapered part under the beam on both sides is 160 mm, and the height of the tapered sample in the first category is 315 mm in the first sample and 405 mm in the TB10 sample. Two reinforcements with a diameter of 8 mm are placed on the top and two tapered reinforcements with a diameter of 25 mm are placed in the lower part. Two holes with a diameter of 50 mm are placed in the upper and lower parts of the samples. A schematic of the concrete part and reinforcement in the TB10 sample is presented in Figures 2 and 3, and the assembled sample of the TB2 model is also presented in Figure 4.

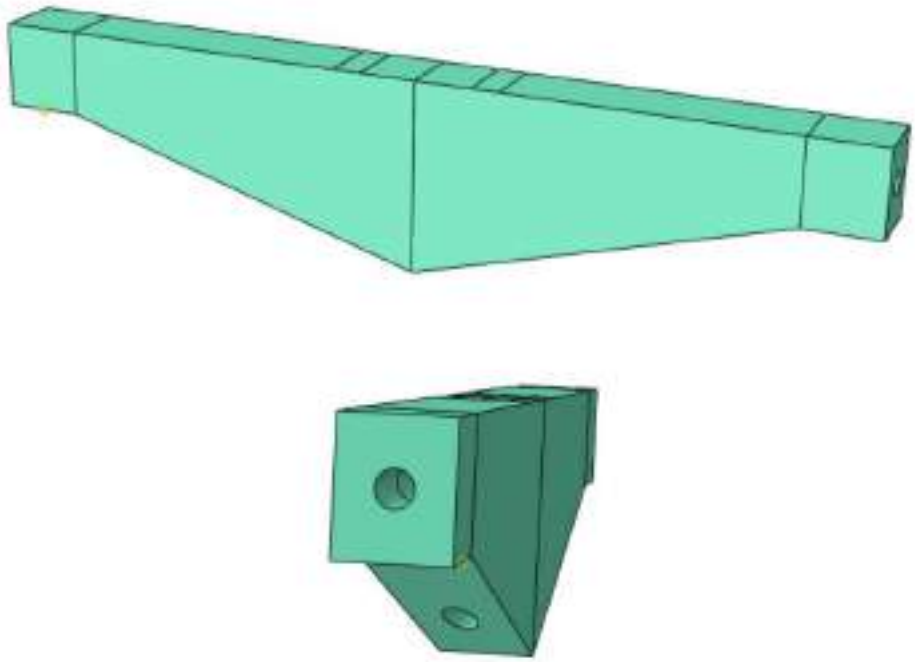

Figure 2: Concrete beam geometry in TB10 model.

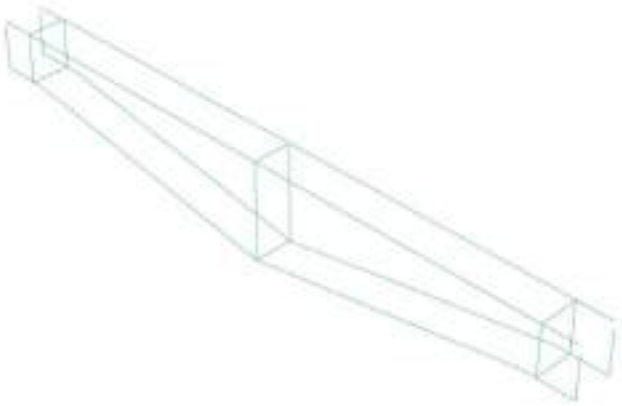

Figure 3: Reinforcement geometry in TB10 model.

The geometry of the samples analyzed in the second category is presented in Figure 4. From this category, TB5 and TB6 samples have been analyzed and the variable of this category is the location of the hole, which is at the top in the TB5 model and at the bottom in the TB6 model. Other specifications of the sample are similar to TB10 sample.

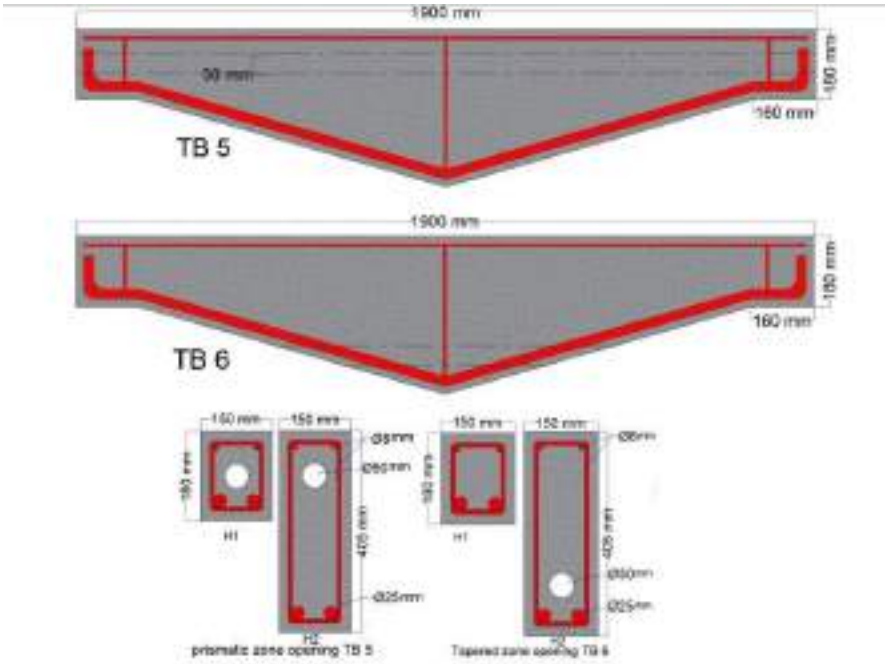

Figure 4: The geometry of the samples analyzed in the second category.

A schematic of the samples analyzed in the second category, which is related to samples TB5 and TB6, is presented in Figures 5 and 6.

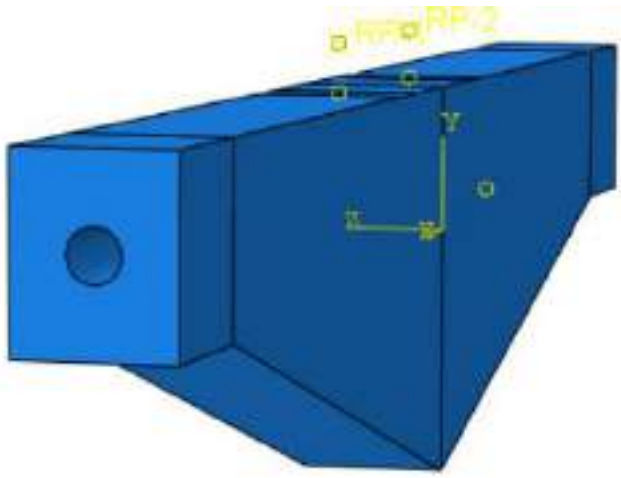

Figure 5: Concrete section geometry of sample TB5 with a hole at the top.

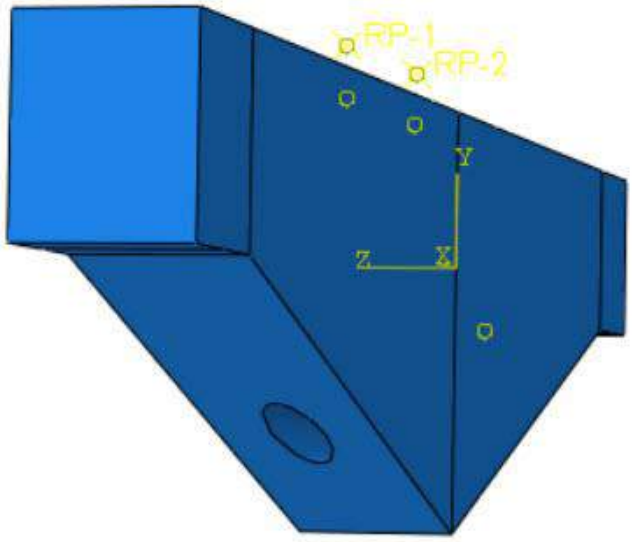

Figure 6: Concrete section geometry of specimen TB6 with a hole at the top.

The geometry of the samples analyzed in the third category is presented in Figure 7. From this category, TB7 and TB8 samples have been analyzed and the variable of this category is the type and number of rebars, in the TB7 model, there are two 16 diameter rebars and two 12 diameter rebars in the tensile part, and in the TB8 model, there are two 16 diameter rebars at the bottom. Other specifications of the sample are similar to TB10 sample.

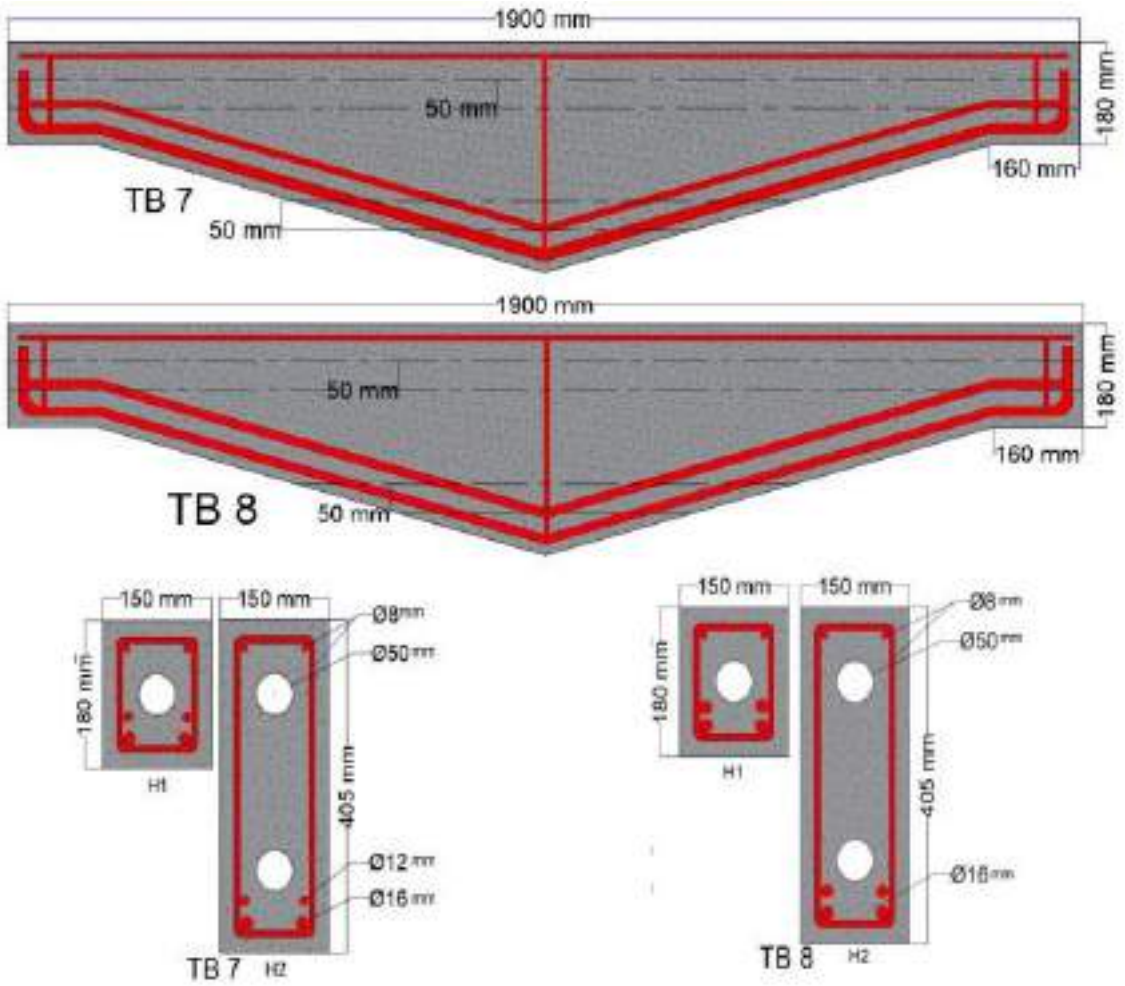

Figure 7: Schematic of TB7 and TB8 models analyzed in the third category.

A schematic of the reinforcement used in the two models analyzed in the third category is presented in Figure 8.

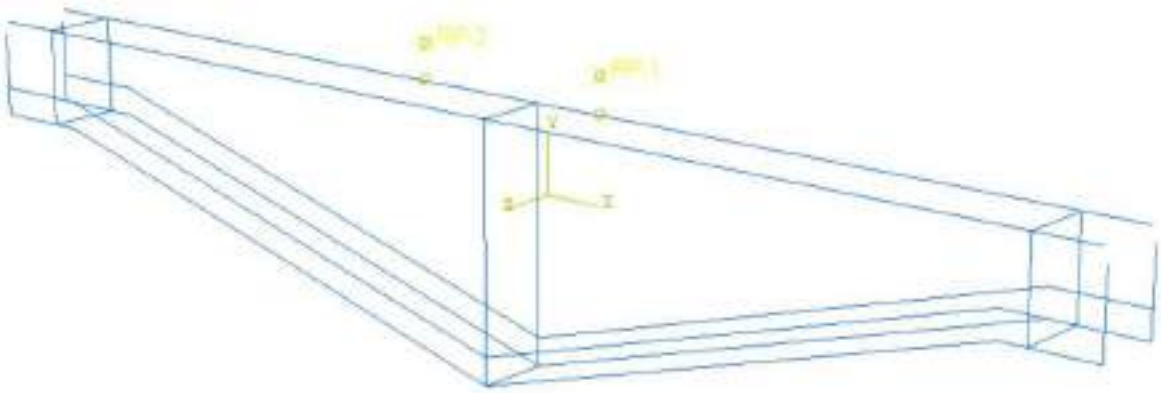

Figure 8: Schematic of the reinforcement used in the third category of analysis.

The geometry of the samples analyzed in the fourth category is presented in Figure 9. From this category, TB9 and TB1 samples have been analyzed and the variable of this category is the distance of the load application, in the TB9 model, the distance between the jaws is 500 mm, and in the TB model, this distance is equal to 200 mm. The rest of the sample characteristics are similar. The sample is TB10. A schematic of the models of this category is presented in Figures 9 to 11.

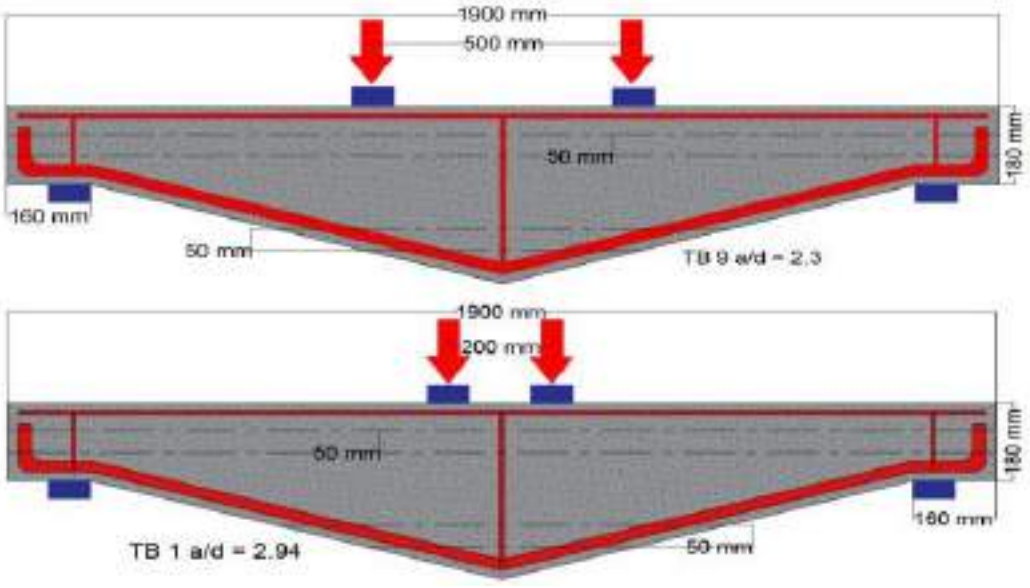

Figure 8: Schematic of the samples analyzed in the fourth category of analyzes (samples TB9 and TB1).

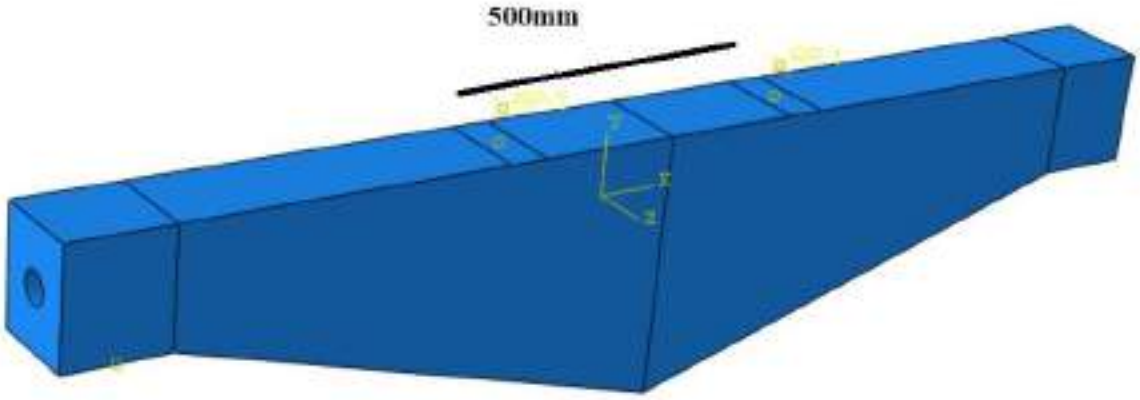

Figure 9: Schematic of TB9 model with 500 mm loading distance.

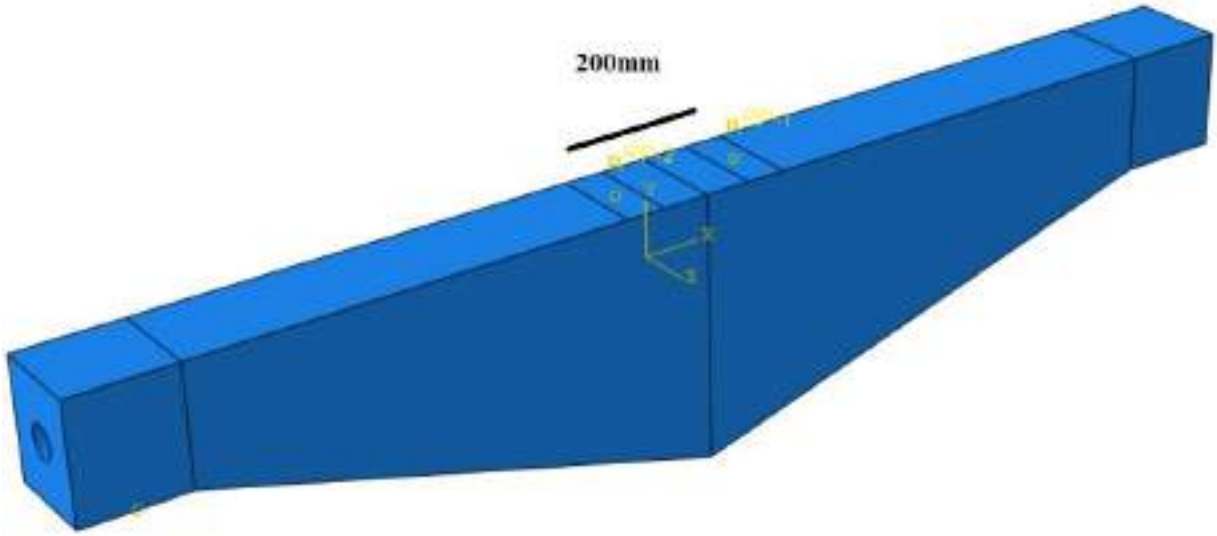

Figure 10: Schematic of TB1 model with 200 mm loading distance.

B.3 Material properties

The steel used in different sections has a modulus of elasticity of 200 GPa and a Poisson's ratio of 0.3 and has diameters of 8, 12, 16 and 25 mm, and other specifications of these reinforcements are presented in Appendix A.

The concrete used in the research was ultra-high-strength concrete (UHPC), with the highest compressive strength of 153 MPa, for its simulation, the CDP model

was used in Abaqus software. To define material properties in Abaqus software according to Figure 10, enter the menu of defining material properties and according to Figures 11 to 13, density, elastic and plastic properties are defined for steel.

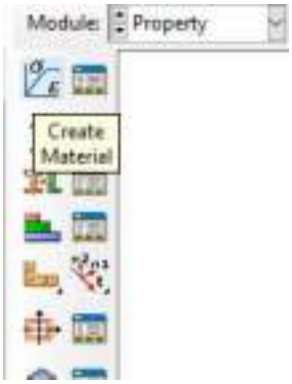

Figure 10: Material properties definition menu in Abaqus software.

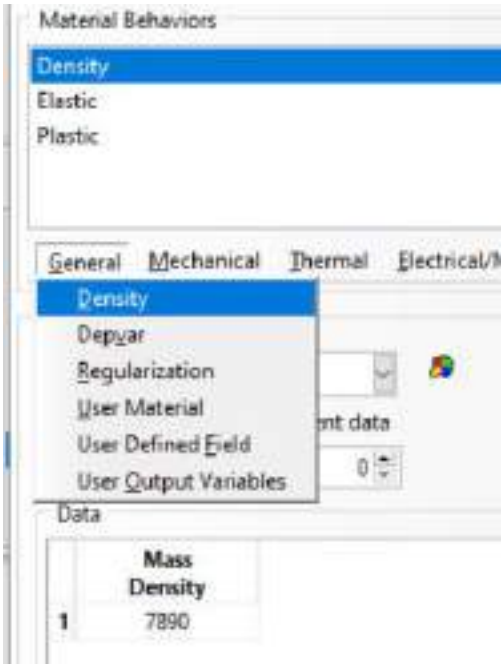

Figure 11: Definition of density in Abaqus software.

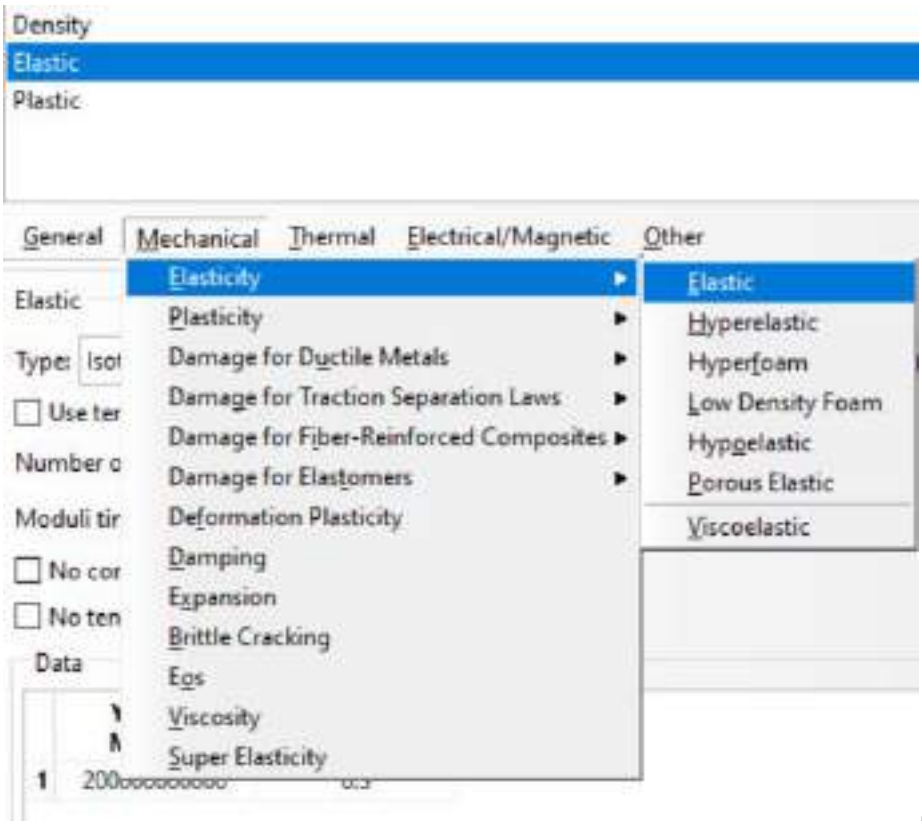

Figure 12: Definition of elastic properties in Abaqus software.

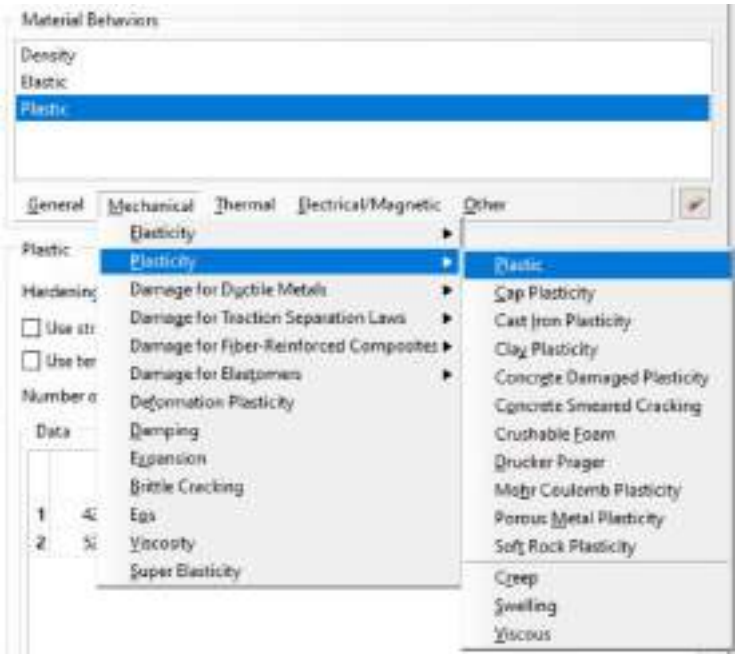

Figure 13: Definition of plastic properties in Abaqus software.

To define concrete properties, elastic properties are defined similar to the case of steel, and for plastic properties, the CDP model according to Figure 14 is used.

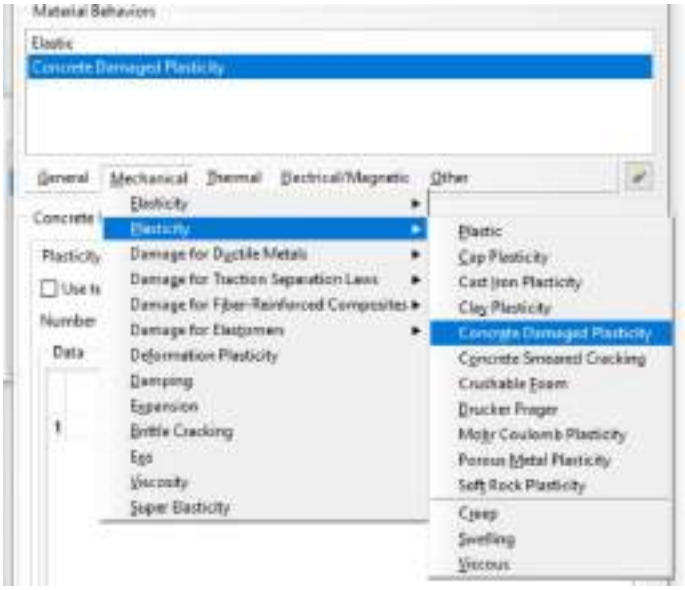

Figure 14: Selection of the CDP model to define the plastic properties of concrete.

After defining the properties of the materials, the distribution of the properties of the materials for concrete is similar to Figure 15, homogeneously, and for rebars and reinforcements, as shown in Figure 16, in the form of a truss and by defining the cross section for each diameter of the rebar, it is selected and allocate.

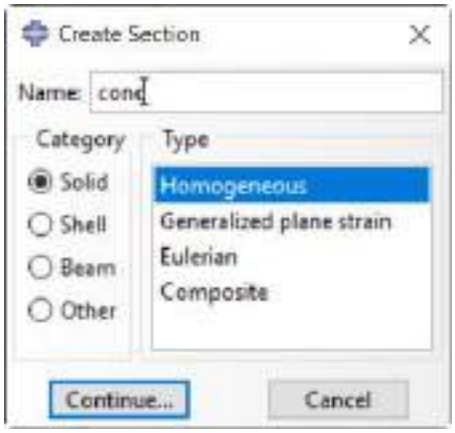

Figure 15: Homogeneous distribution of concrete properties.

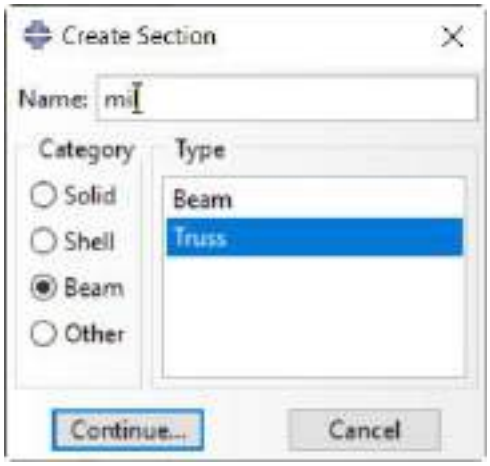

Figure 16: Determining the distribution of material properties for reinforcements in the form of trusses.

B.4 Determining the type of solution

The type of solution is considered statically and considering large deformations similar to Figure 17.

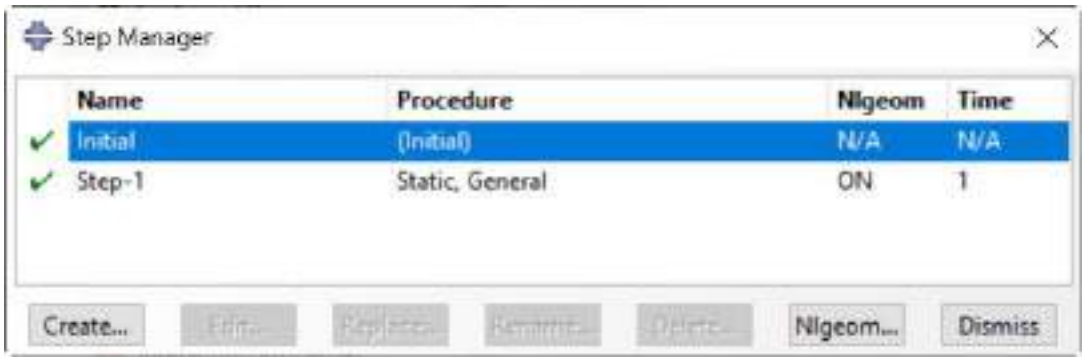

Figure 17: Determine the solution type static.

B.5 Determining the Limitations Used in The Simulation

The first constraint used is the coupling constraint to apply the compressive load to the upper part of the beam, which is used for the models in accordance with Figures 18 and 19 .

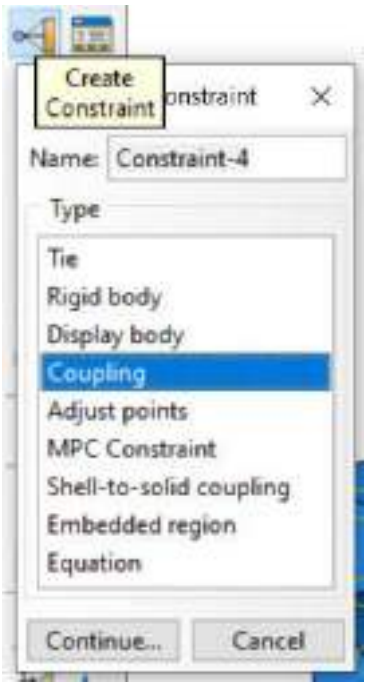

Figure 18: Coupling constraint selection in Abaqus.

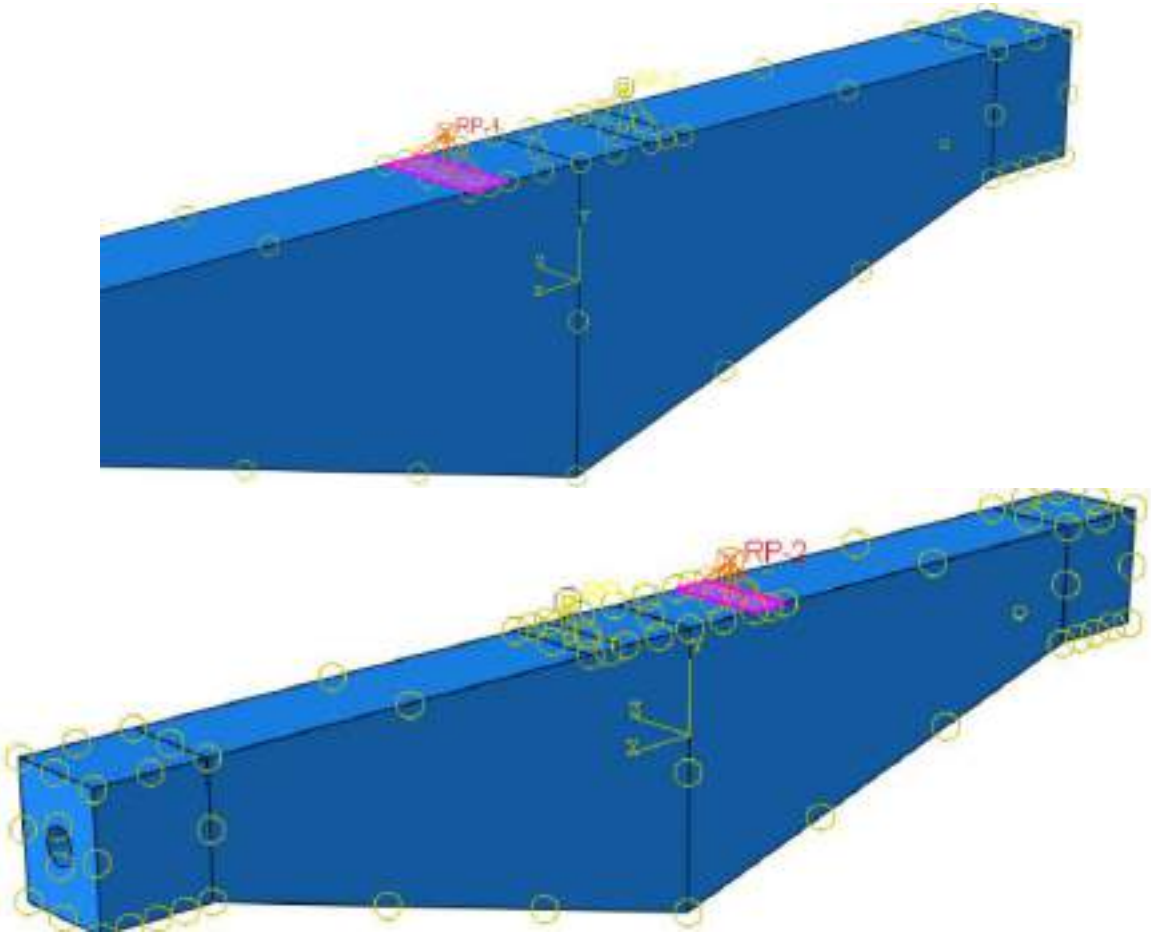

Figure 19: Applying the coupling constraint to apply the load to the model.

The next constraint used is the Embedded Region constraint, which is used for burying rebars and reinforcements inside the concrete according to Figures 20 and 21.

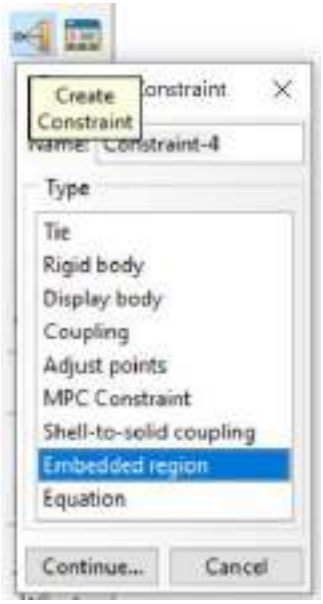

Figure 20: Selecting the Embedded Region constraint.

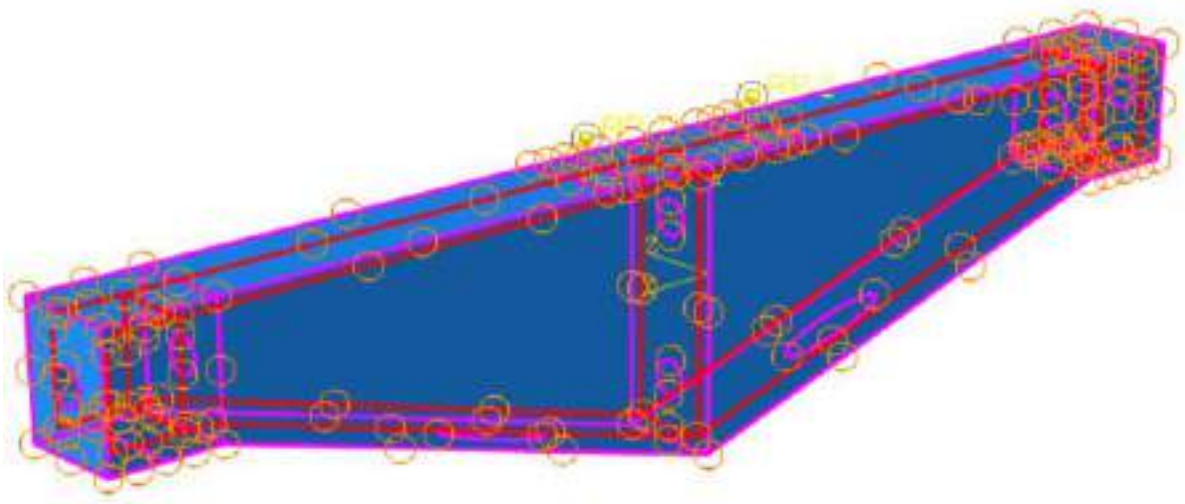

Figure 21: Using the Embedded Region constraint to bury rebars in concrete.

B.6 Loading and boundary conditions

The loading and boundary conditions used in this research are presented in this section. The loading and boundary conditions used in this research have been done on the models according to Figure 22. That is, the two lower parts are completely bound according to Figure 23, and the load is applied to the upper two parts of the model according to Figure 24.

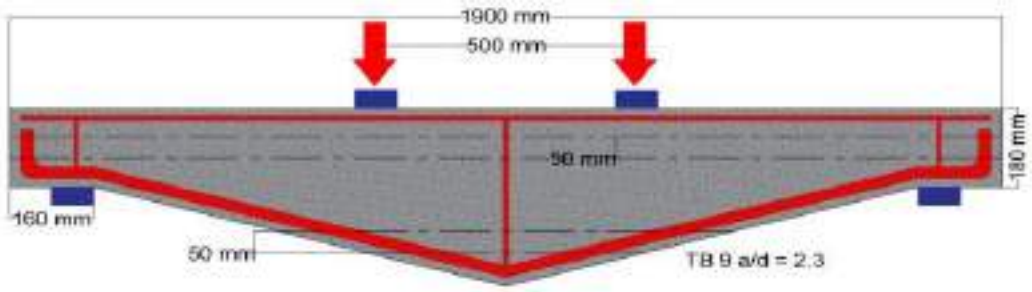

Figure 22: Schematic of loading and boundary conditions used in the model.

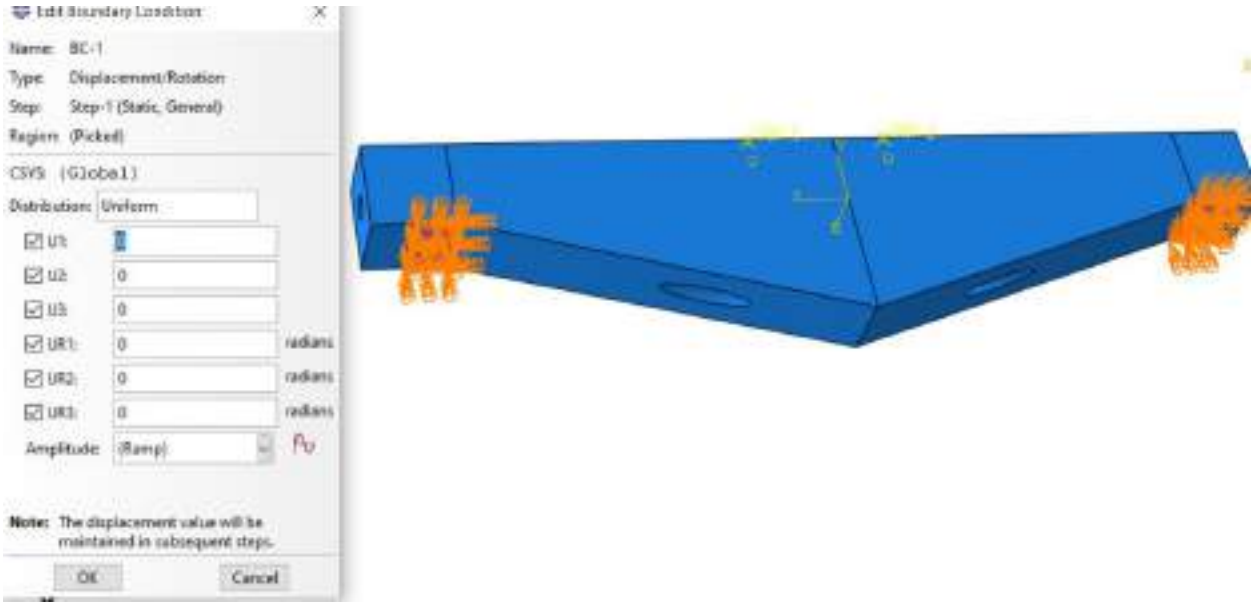

Figure 23: Boundary conditions of the lower parts of the model.

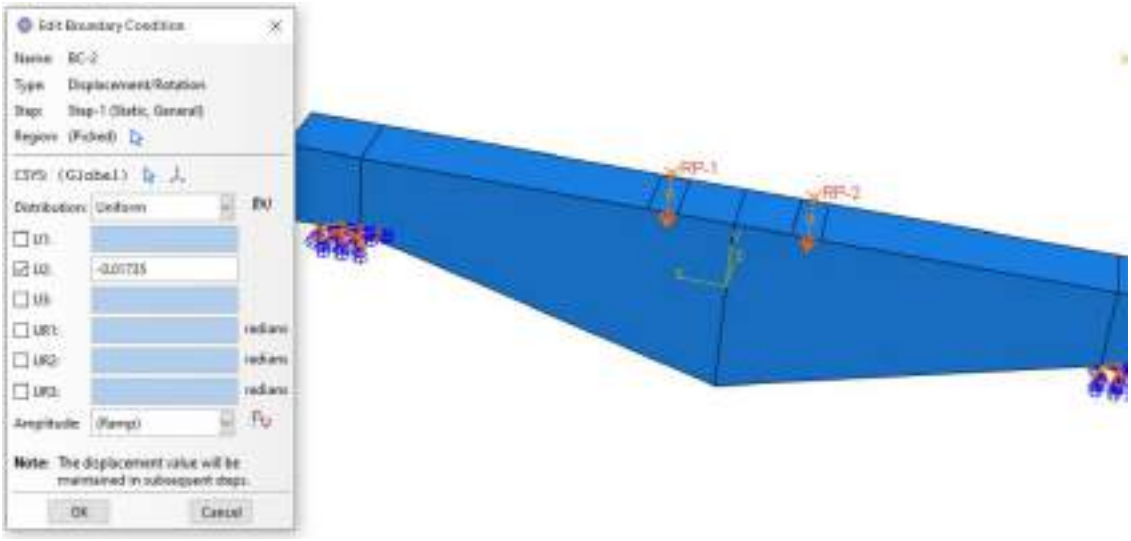

Figure 24: Load applied to the upper part of the model.

1.7 Model Meshing

The meshes used for the concrete part are triangular mesh of C3D4 type, which is a three-dimensional 4-node mesh with a grain size of 5 cm, and the meshes used for the reinforcements are truss mesh with a grain size of 5 cm.

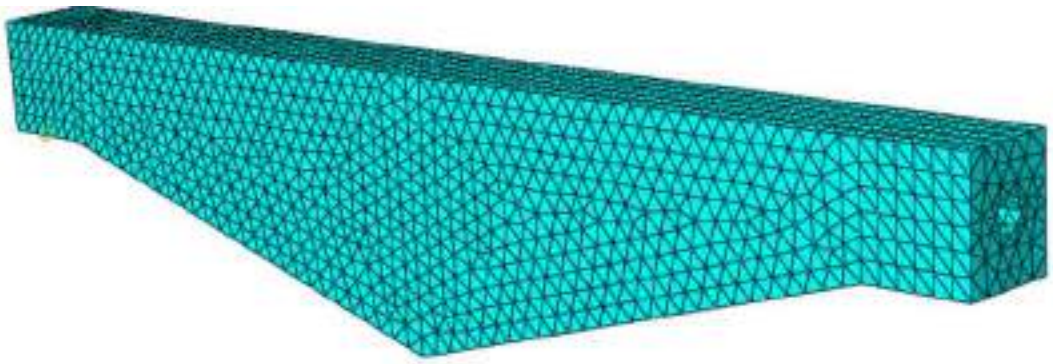

Figure 25: Meshing of the concrete section.

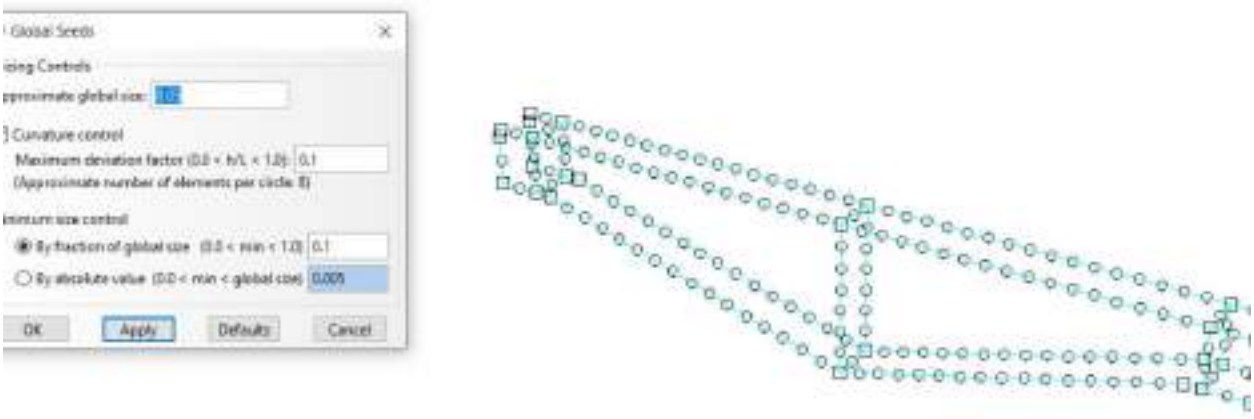

Figure 26: Schematic of meshing of rebars and reinforcements.

APPENDIX C

C.1 Irregular shape beam Method

Ec = 5000 MPa
H1 = 180 mm
H2 = 225 mm
d = 364.3 mm
b =150 mm
Overhang length = 0.16 m
Load gap = 0.3 m
fc' = 130 MPa
Max. L.L. = 329 kN
PD = 0.75912853
Assume Z = 311.4 mm
As = 896.4713 mm^2
α = 0.65
εcu = 0.003
Es = 200000 MPa
β = 0.65

Ht = 405 mm
Cover = 20 mm
bar 1 = 16 mm
bar 2 = 8 mm
Lt = 1.9 m
Ln = 1.58 m
Shear Span (a) = 0.64 m
fy = 420 MPa
wD = 1.99423077 kN/m
Mu = 105.5229 kN
$\emptyset$ = 0.9 Factor

The Main Reinforcement
4Ø16

Two Point Loads
Theoretical FLAXURAL Failure's Load = 329 kN
Experimental SHEAR Failure's Load = 446 kN
Numerical SHEAR Failure's Load = 456 kN

Find the Value of (c) from C = T

C = α.fc'.b − 0.5 × (α.fc')^2 .b/(Ec × εcu) + 0.4 × √(f_c') × b) × (C)^2
T = (− 0.4 × √(f_c') × b.H + As.Es.εcu) × (C) − As.Es.εcu.d
A = α.fc'.b − 0.5 × (α.fc')^2 .b/(Ec × εcu) + 0.4 × √(f_c') × b) = 13359.1
B = (− 0.4 × √(f_c') × b.H + As.Es.εcu) = 350467.2911
D = − As.Es.εcu.d = −217125352.1
c1 = −141.2774 *Neglect*
c2 = 115.043 *OK*
a =74.7779 mm
y° = a/2 = 37.38899
Z = d − y° = 308611 mm
Cycle 2, Recycle with Z = 308.611 mm
As = 904.57 mm^2

Rectangular Shape
< Assume Z = 311.4 mm

$A = \alpha.fc'.b - 0.5 \times (\alpha.fc')^2 .b/(Ec \times \varepsilon cu) + 0.4 \times \sqrt{(fc')} \times b) = 13359.1$

$B = (- 0.4 \times \sqrt{(fc')} \times b.H + As.Es.\varepsilon cu) = 356138.44$

$D = - As.Es.\varepsilon cu.d = -219087569.7$

$c1 = -142.08$ Neglect

$c2 = 115.424$ OK

$a = 75.025$ mm

$y° = a/2 = 37.51$ Rectangular Shape

$Z = d - y° = 308.487$ mm $< Z = 311.4$ mm

Cycle 3, Recycle with $Z = 308.487$ mm

$As = 904.9363$ mm^2

$A = \alpha.fc'.b - 0.5 \times (\alpha.fc')^2 .b/(Ec \times \varepsilon cu) + 0.4 \times \sqrt{(fc')} \times b) = 13359.1$

$B = (- 0.4 \times \sqrt{(fc')} \times b.H + As.Es.\varepsilon cu) = 356392.8104$

$D = - As.Es.\varepsilon cu.d = -219175581.8$

$c1 = -142.1193199$ Neglect

$c2 = 115.44$ OK

$a = 75.0369$ mm

$y° = a/2 = 37.5184$ Rectangular Shape

$Z = d - y° = 308.48$ mm $= Z = 308.487$ mm, ∴ OK

$As\ (min)\ 1 = (1.4/fy) \times (Ac\ of\ depth = d) = 173$

$As\ (min)\ 2 = (0.25 \times \sqrt{(fc')}\ /fy) \times (Ac\ of\ depth = d) = 352.23$

$As = 904.936$ mm^2 $>$ As (min)1 & As (min)1, ∴ OK

$c = 115.44$ As use 1013.4 mm^2

$\varepsilon t = 0.003 \times (dt - c)/c = 0.0059$ $0.004 < \varepsilon t < 0.005$

$\emptyset = 0.9$ as assumed we have to check it

$\emptyset = 0.75 + 0.15 \times (\varepsilon t - \varepsilon y) / 0.005 - \varepsilon y) = 0.9495$

check $\emptyset Mn$

$\emptyset Mn = \emptyset As \times fy \times (d-y°) = 111.333 > Mu = 105.5229$ OK

C.2 Dr. Nasser's Method

The Depth at Failure Position (H) = 266.86 mm
Effective Depth (ds) = 207.86 mm
Total Thickness (H total) = 405 mm
Compressive Strength (fc') = 150 MPa
Beam Width (b)= 150 mm
Concrete Modulus Of Elasticity (Ec)= 5000 MPa
ratio of $\alpha 1$ to $\gamma \rightarrow \alpha$ = 0.65
Ratio Of Average Concrete Stress to fc' $\rightarrow \alpha 1$ = 0.85
Concrete Cover (C) =20 mm
Diameter Of Main Reinforcement = Ø16
Effective Depth at Mid Span (d) = 346 mm
(a/d) (d at support) = 3.07899
Modulus Of Elasticity Of Steel (Es) = 20000 MPa
Ultimate Concrete Strain (εcu) = 0.0035
Overhang Length = 0.16 m
Load Gap = 0.3 m
Shear Span (a) = 0.64 m
Length Beam (L) = 1.9 m
Ø of stirrups = 8 mm
tan (θ) = 0.2848
Yield Stress (fy) = 420 MPa
Failure's Angle = 32.797°
Inclination Angle (θ) = 15.9°
Span Length (L) = 1.58m
Quantity = 0.07796
Ln/2 = 790
As (4Ø16) = 804.22 mm^2
H2 = 225 mm

For Prismatic Solid Section

c = 117.819
A = α.fc'.b − 0.5 × (α.fc')^2 .b/(Ec × εcu) + 0.4 × √(fc') × b) = 10298.998
B = (− 0.4 × √(fc') × b.H + As.Es.εcu) = 439817.8541
D = − As.Es.εcu.d = −194783052.8
C = [α.fc'.b − 0.5 × (α.fc')^2 .b/(Ec × εcu) + 0.4 × √(fc') × b)] × (C)^2 = 133.4677 kN.m
T = 0.4 × √(fc') × b.H × C −0.4 × √(fc') × b × C^2 + As.Es.εcu − As.Es.εcu.d × C = 133.4677 kN.m

For Tapered Hollow Section

$I = (bh^3 / 12) \times (1 + x / 2L)^3$ $\quad \beta = 0.65$ $\quad a = 76.5824$ $\quad c = 117.819$

$hx = h(1 + x / 2L)$ $\quad r = (\varepsilon cu - \alpha.fc'/Ec) \times (c / \varepsilon cu) = 60.03$

$C1 = \alpha.fc'.b.r/10^6 = 0.772279$

$C2 = 0.5\ \alpha.fc'\ (b \times (c-r) - \pi\ 25^2)/ 10^6 = 0.27758$

$T1 = 0.4\ \sqrt{(fc')}\ (b \times (h-c) - \pi\ 25^2)/ 10^6 = 0.03358$

$T2 = (As.Es.\ \varepsilon cu\ (d/c-1) = 1.090$

Calculation of tensile strain (εt) & stress (fpf) of steel bar

$\varepsilon s = \varepsilon cu.(d-c) / c = 0.006778$

$fs = 1355.69257 > fy = 420$ Not OK $\quad$ use $fy = 420$ MPa

Calculation Of Flexural Strength (Mn) :-

Inclination angle of reinforcement (ζ) = 11.8667

$\emptyset\ 8\ (As2)\ \pi\ ((8^2) / 4\ ) \times 2 = 100.53088$

$Mn1 = C1\ (c-r/2)$	$= 67.462$	
$Mn2 = C2 \times 2/3 \times (c-r)$	$= 10.5277$	
$Mn3 = T1 \times (h-c)/2$	$= 1.04411$	use fy for stirrups = 420 MPa
$Mn4 = As \times fs \times (d-c)$	$= 77.0735$	
	$= 156.107$	

$Vc = (0.18 \times \sqrt{(fc')} \times (b.ds - (3.14159 \times 25^2)) / M11) / 1000$	$= 46.12264$
$Vf = ((0.4 \times \sqrt{(fc')} \times 0.9 \times (b.ds - \pi\ 25^2) / M11) / (\tan(32.79 \times 3.14159/180))) / 1000$	$= 143.15$
$Vs = (0.9 \times (As2 / 800 \times fy.ds /1.3) / 1000$	$=0$
$Vda = 0.2 \times As.fy.\sin(\zeta)$	$= 13.8916$
	$= 203.167$

M D.L of beam self-weight = ((b × H - 50 × 50) ×G12 10^6 + (0.5 × L × 120 × b - ((L+840)/2) ×50×50))/10^9 × M12 × L^2 / 8) /2 = 0.146

M (total) = (Pu.f × shear span)/2 = 155.9 *Pu.f = (2 × M) /a = 487.37* *Vt = 406.33*

Theorical Failure's Load = 406.3 kN

Experimental Failure's Load = 446 kN *Pu.f > Vt* *Shear Dominate*

Numerical Failure's Load = 456 kN

الخلاصة

عتبة خرسانية مسلحة متغيرة المقطع هي عتبة مثالية ولها اهمية خاصة. العتبة الخرسانية غير الموشورية هي الية محدده ويمكن استخدامها في الهندسة الانشائية للحصول على الاستثمار الانسب للمواد. تم تقديم هذه الدراسة للتحقق من الثقة الهيكلية للعتبة الخرسانية متغيرة المقطع التي تم تطويرها مؤخرًا بأشكال هندسية جديدة باستخدام التحليل الرقمي بواسطة برنامج (ABAQUS) والذي تضمن مجموعة واسعة من المتغيرات التي تتعلق بالجوانب الهيكلية المختلفة.

مقارنة النتائج العددية بالنتائج التجريبية المتاحة ، في نطاق قوة القص النهائية ، والعلاقات بين الحمل والإزاحة ؛ أظهر اتفاقا جيدا. تراوحت المعدلات المقترحة من 0.96 إلى 1.07. علاوة على ذلك ، تهتم الدراسة البارامترية بالعديد من المعلمات الهيكلية مثل طول التاج، ومحاكاة الحزمة المدببة بعامل مقياس متعدد، وقوة التعزيز الفولاذي، ونسبة الفولاذ (الطولية والمستعرضة)، وتأثير امتداد القص، والفتحات الطولية (الموقع والحجم).

تبحث الدراسة الحالية في العتبات متغيرة المقطع للخرسانة فائقة الأداء باستخدام 2٪ من الألياف الفولاذية من حيث الحجم. قدمت هذه العتبات متغيرة المقطع نهجًا جديدًا لإنتاج الخرسانة فائقة الأداء لاستخدامها كبديل للخرسانة التقليدية مع وجود فتحات على طول العتبة. نظرًا للعديد من العوامل التي تؤثر على السلوك الخرساني عالي الأداء وبسبب وجود الألياف الفولاذية وأنماط الفشل المختلفة ، بالإضافة إلى آلية العمل داخل المصفوفة الخرسانية ، يلعب شد الخرسانة دورًا مهمًا في تحسين المقاومة ، وخاصة قوة القص. تم تصميم العتبات متغيرة المقطع بأبعاد يبلغ طولها 1900 ملم وعرضها 150 ملم وعمقها عند المسند 180 ملم وفي منتصف العتبة 405 ملم. أشارت النتائج التي تم الحصول عليها من النمذجة العددية إلى انخفاض كبير في الوزن مع وجود الفتحات الطولية. تمت دراسة ست نسب مختلفة من طول فضاء القص إلى العمق الفعال، مع تنبؤ نظري بأن زيادة نسبة طول فضاء القص إلى العمق الفعال يقلل من القوة. بالنسبة للمساند، يُظهر حالة الاسناد البسيط أنه يتم الحصول على تقدير متقارب جدًا لقوة القص في حالة الاسناد البسيط والاسناد الثابت. وأشارت إلى أن الزيادة في نسبة التعزيز الطولي تؤدي إلى زيادة بنسبة 14٪ في قوة القص النهائية. قد يكون هذا بسبب زيادة عنصر (dowel action) و بالتالي زيادة قوة القص. أسفر اختبار القص على عتبات

الخرسانة الفولاذية مع نسبة الألياف الفولاذية 2٪ من حيث الحجم عن نتائج إيجابية من حيث تأثير نسبة تعزيز القص على قوة القص. كلما زادت نسبة التعزيز العرضي، لوحظ حدوث المزيد من الشقوق بعرض فتحات أصغر. عند زيادة نسبة التعزيز العرضي، يكون هناك تأثير كبير على انحراف منتصف الامتداد حيث لوحظت الزيادة بنسبة 79٪ و148٪ على تولي المسؤولية مقارنة بالنموذج TB-TR845. لقد تم تحول نمط فشل القص إلى النمط المركب فشل القص-الانثناء. تم تصميم النماذج لفشل قوة القص لذلك تم تصميم النماذج بدون ركاب. تزداد قوة الشد بزيادة حمل الشقوق الأول وتقل بزيادة عدد وعرض الشقوق. أيضا، عندما تم زيادة عامل القياس 2.4، لوحظت زيادة في قوة القص بنسبة 348٪. في حين أن زيادة طول التاج من 0 إلى 200 ملم أدى إلى زيادة قوة القص بنسبة 10%.

جمهورية العراق

وزارة التعليم العالي والبحث العلمي

كلية الهندسة/ جامعة ميسان

قسم الهندسة المدنية

التحليل العددي لقوة القص لعتبات خرسانية متغيرة المقطع فائقة الأداء

من قبل

عقيل عبدالرضا جبارة

رسالة

مقدمة الى كلية الهندسة في جامعة ميسان

كجزء من متطلبات الحصول على درجة الماجستير في علوم الهندسة المدنية/الانشاءات

آب 2023

بأشراف

الاستاذ المساعد الدكتور: ناصر حكيم طعمة